THE BUCKLING OF CLAMPED SHALLOW SPHERICAL SHELLS UNDER UNIFORM PRESSURE

Thesis by

Robert Reid Parmerter

In Partial Fulfillment of the Requirements

For the Degree of

Doctor of Philosophy

California Institute of Technology

Pasadena, California

1964

ACKNOWLEDGMENT

The author is deeply indebted to Dr. Y. C. Fung for guidance and support received during the course of this investigation. The helpful suggestions of Dr. E. E. Sechler during the experimental phase of the investigation is gratefully acknowledged. The technical assistance of Dr. C. D. Babcock and Dr. L. V. Schmidt, and numerous discussions with these and other members of the Aeronautics staff has left an indelible mark on this work.

The success of the experimental program rests in no small part on the skills of C. A. Bartsch, G. F. Carlson, and T. Johnson of the Aeronautics shop. The suggestions which they made, and the care which they exercised during the manufacture of the wax forms is sincerely appreciated. Thanks are also due Miss Helen Burrus who typed the manuscript, for her patience, skill, and helpful suggestions.

Portions of the investigation were sponsored by the Air Force Office of Scientific Research, United States Air Force. This assistance, and the financial support of the Ford Foundation, is gratefully acknowledged.

Finally, the author is indebted to his wife and children, who have silently borne the burdens imposed by his graduate study, and without whose continuing encouragement, the work might not have been undertaken.

ABSTRACT

In view of the wide discrepancy between previous theoretical and experimental results the problem of the buckling of clamped spherical shells under uniform external pressure is reexamined.

A theoretical study is carried out to determine if asymmetrical modes participate in the snap-through process. It is shown that asymmetrical buckling does occur in a certain range of a geometric parameter, at loads which are significantly less than those predicted from symmetrical theory. Additional effects can be expected if the shell has symmetrical or asymmetrical imperfections, however, the present study considers only the perfect shell.

Experiments were carried out with copper shells fabricated by an electroforming process. The initial imperfections in the test specimens were of the order of 1/10 of the thickness. The buckling loads of these shells exceeded the loads which have previously been reported by as much as a factor of two at higher values of the geometrical parameter λ.

Good agreement is found between theory and experiment, and with the recently published asymmetrical theory of Huang.

TABLE OF CONTENTS

LIST OF FIGURES

LIST OF FIGURES (Cont'd)

LIST OF TABLES

NOTATION

List of Symbols

b	Radius of spherical segment
E	Young's modulus
$F(r,\theta)$	Stress function
$G(r)$	Symmetrical component of F
$H(r)$	Radial dependence of the asymmetrical component of F
h	Center rise of shell
m	Wave number in assumed form of $U(r)$
N	Number of terms in assumed form of $U(r)$
n	Wave number in assumed form of $V(r,\theta)$
$N_r, N_\theta, N_{r\theta}$	Membrane stress resultants
p	Pressure
q	$(\frac{R}{t})^2 \frac{\sqrt{3(1-\nu^2)}}{2E} p$
R	Spherical radius of shell
r,θ	Polar coordinates
t	Thickness
$U(r)$	Symmetrical component of W
U_i	Coefficients of assumed form of $U(r)$
$V(r,\theta)$	Asymmetrical component of W
$V(r)$	Radial dependence of $V(r,\theta)$
V_1	Coefficient of assumed form of $V(r)$
$W^*(r,\theta)$	Final deviation of middle surface from the r,θ plane
$W_0(r,\theta)$	Initial deviation of middle surface from r,θ plane
$W(r,\theta)$	$W^* - W_0$

x, y	Rectangular coordinates
η	Inplane radial displacement
λ	$\left[\frac{12(1-\nu^2)}{R^2t^2} b^4\right]^{1/4}$
ξ	Inplane tangential displacement
μ	Density
ν	Poisson's ratio
ρ	$\frac{\pi}{b} r$
ϕ	Angle between center of segment and edge, measured at spherical center

Non-Dimensional Quantities

A bar over a quantity indicates it has been non-dimensionalized as indicated on page 15

I. INTRODUCTION

The stability of thin elastic shells which are shallow and have a spherical shape and clamped edges, will be considered in this thesis. It is well known that for finite deformations, the equations governing a thin shell are nonlinear. This nonlinearity arises from the nonlinear strain displacement relationship, although the strain itself may be infinitesimal so that the stress-strain law remains linear.

The criterion of buckling must be defined, since there is no unique definition of instability for a nonlinear system (Ref. 1). The definitions which follow have been adopted from reference 2.

1. Snap Buckling: Let the configuration of the shell, under a uniform pressure load p, be specified by $W(r,\theta,p)$, where W is the deflection of the mid-surface normal to the r,θ plane (Fig. 1). If an approximate solution for $W(r,\theta,p)$ is carried out using a Ritz or Galerkin procedure, the function $W(r,\theta,p)$ can be made to depend upon a finite number of parameters $U_i (i = 1, 2, \ldots, N)$ through the assumption

$$W(r,\theta,p) = \sum_{i=1}^{N} U_i(p)\, f_i(r,\theta)$$

where the $f_i(r,\theta)$ are chosen functions of r and θ. Thus the configuration can be represented by a point in an N dimensional space with coordinates $(U_1, U_2, \ldots, U_N)$. The potential energy Ψ can be

written as a function of these parameters and the load p, $\Psi = \Psi(U_1, U_2, \ldots, U_N, p)$, and the N equilibrium conditions $\frac{\partial \Psi}{\partial U_i} = 0$ can then be used to define equilibrium paths in the N dimensional configuration space. Each point along an equilibrium path is associated with a unique pressure p, although the inverse association is not necessarily unique.

Consider the path which passes through the origin, and unfolds in the direction corresponding to an initial increase in p(path A, Fig. 2a). Denoting arc length between the origin and a point P on the curve by $S(P)$, we can consider the pressure p as a function of S (Fig. 2b). If p is not a monotonic function of S, then the first maximum of p, which occurs at $S = S_s$, will be called the "snap buckling load" p_s. Any attempt to increase the pressure to $p = p_s + \Delta p$ will lead to a finite change in configuration, since no adjacent static equilibrium configuration exists for $p = p_s + \Delta p$.

2. Bifurcation Buckling: A second equilibrium path may intersect the path which passes through the origin (Fig. 2a). A change in stability can occur at this intersection (Ref. 2), and the shell displacements may jump to non-adjacent values. The pressure corresponding to this intersection will be called the "bifurcation buckling load" p_b, provided the corresponding arc length S_b satisfies the condition $0 \leq S_b \leq S_s$.

In these definitions, stability of the static equilibrium configurations with respect to adjacent static configurations, is considered. Static theory has proven entirely adequate for predicting the buckling of many types of structures. However Ziegler (Ref. 3) has given examples

where static considerations do not suffice. Hoff and Bruce (Ref. 4) have studied the stability of an arch under a dynamic definition of buckling. They find that the arch, which exhibits features analogous to a spherical shell, has identical buckling loads under static and dynamic buckling criteria. In this thesis it will be shown that a theory of buckling based on definitions 1) and 2) is in reasonable agreement with experiments conducted with near perfect shells. It is unlikely, therefore, that theories based on other definitions of buckling will add significantly to the understanding of this particular problem.

1.1 Brief Review of Previous Work.

The problem of the instability of a shallow spherical shell, clamped along its boundary, and subjected to a uniform pressure p (Fig. 1), has been the subject of many papers in recent years (Refs. 5-16 inc.). Initially the problem was studied in conjunction with the buckling of a complete sphere (Ref. 5). In their classic work von Karman and Tsien showed the importance of nonlinear effects in the problem. More recently, the basic differences between perfect complete shells, and perfect shallow shells, have been pointed out, and the shallow shell has been studied in its own right.

With the exception of Refs. 13-16, the shell has been constrained to deflect in a radially symmetrical manner. Three of the papers (Refs. 10-12) find buckling loads which agree with each other, and are now generally believed to be correct for an analysis based on symmetrical equations (curve 4 of Fig. 3). Four recent papers have attempted to remove the constraint of symmetry (Refs. 13-16). The first of these

does not present buckling data. The second is of little interest due to the crudeness of the assumptions, and the third and fourth are in disagreement with each other, and with the existing experimental data to varying degrees (Fig. 4).

The existing buckling data (Refs. 7, 17, and 18) leaves a good deal to be desired from the standpoint of consistency (Fig. 3). The experimental techniques which have been employed are questionable (see Experimental Section) and the shells which have been tested have had significant imperfections. Thus there is some question if the existing test data is suitable for comparison with theory, if the object of the comparison is to judge the validity of the buckling theory of perfect shells.

In view of these facts, the question of the stability of shallow spherical shells appears far from closed. The following experimental work was undertaken in an effort to improve upon the test data and to substantiate or refute the various theoretical results.

It might be noted in passing that the idea of considering asymmetrical modes of buckling apparently arose quite independently in various quarters, the present theoretical work (Section II) having been initiated some time before the aforementioned works on asymmetrical buckling were published.

II. THE MATHEMATICAL PROBLEM

2.1 Preliminary Remarks about Symmetry.

In many of the papers which were discussed in the previous section, the deflections of the shell were assumed to be symmetrical. In view of the fact that the shell exhibits radial symmetry, the boundary is clamped symmetrically, and the load is uniform, this may seem to be a reasonable assumption. If the stability of the shell with respect to small perturbations is of interest, however, these symmetry arguments do not rule out asymmetrical perturbations. Only the stable equilibrium positions can be expected to exhibit radial symmetry.

In order to crystallize this idea, it is instructive to consider a well known buckling problem, the problem of a perfectly straight column subjected to axial end load.

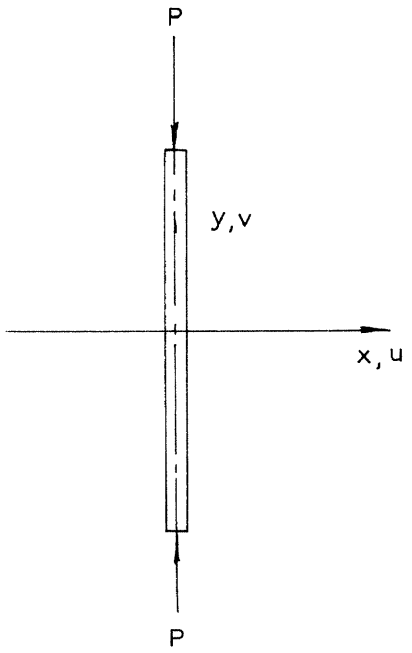

Symmetry dictates that the displacement in the x direction will be zero

$$u = 0$$

and the equations of elasticity reduce to

$$\epsilon_y = \frac{dv}{dy} = -\frac{P}{EA}$$

$$v = -\frac{Py}{EA}\,, \tag{1}$$

a uniform contraction in the y direction. This solution, based on equations derived from symmetry considerations, shows no instability.

If non-symmetrical deflections, u, are considered, they will be governed by the beam column equation

$$\frac{d^2u}{dx^2} + \frac{P}{EI} \qquad u = \text{function (transverse forces and moments)} \tag{2}$$

Now the transverse forces and moments are zero, so the equation is homogeneous and has the solution $u = 0$, which is in agreement with the assumption of symmetry. However, the solution based on symmetry did not suggest that an asymmetrical deflection could be coupled to the symmetrical load system through the coupling term $\frac{P}{EI}$ u! The presence of this term casts an entirely new light on the question of stability, because it opens up the possibility of non-trivial solutions to the asymmetrical equations for certain special values of P.

This is of course, well known, but it focuses attention on the dubious nature of conclusions which are drawn about buckling, from equations which have been simplified by assumptions based on symmetry. The assumption of symmetrical deflections places a constraint upon the theoretical problem which is not placed on the experiment, and may entirely mask the phenomenon of bifurcation buckling.

In the course of this thesis it will be shown that an entirely analogous coupling exists between the symmetrical pressure loading on a spherical shell, and the asymmetrical deflections of the form $V(r) \cos n\theta$. Because of this coupling, certain symmetrical configurations permit non-trivial solutions for asymmetrical deflections to exist. This bifurcation in the symmetrical solution opens up the possibility that bifurcation buckling may occur before snap buckling, which can bring about changes in the stability curve shown in Fig. 3.

2.2 The Nonlinear Equations of Shallow Shells

Simplifications can be introduced into the theory of shells, as a consequence of its thinness. The classical approach introduced by Kirchhoff is to make the following assumptions:

a. Lines perpendicular to the mid-surface of the shell remain perpendicular during deformation.

b. Stresses normal to the surface are neglected.

Additional simplifications can be made by assuming that the shell is "shallow". If the deflection normal to the x-y plane is denoted by W, and the "rise" of the shell above the x-y plane is denoted by W_o, then the "shallowness assumption" is

$$\left(\frac{\partial W_o}{\partial x}\right)^2 \ll 1, \qquad \left(\frac{\partial W_o}{\partial y}\right)^2 \ll 1, \qquad \left(\frac{\partial W}{\partial x}\right)^2 \ll 1, \qquad \left(\frac{\partial W}{\partial y}\right)^2 \ll 1$$

In particular, it is common practice to restrict the term "shallow spherical shell" to shells for which

$$h < b/8$$

so that

$$\left(\frac{\partial W_o}{\partial x}\right)^2_{max} = \left(\frac{\partial W_o}{\partial y}\right)^2_{max} \approx 1/16$$

The nonlinear equations of shallow shells have been derived by Marguerre using these assumptions. They can also be obtained by a slight extension of von Kármán's large deflection equations for the flat plate (Ref. 1). The Marguerre equations are:

$$\nabla^4 W = \frac{1}{D}\left[p + \frac{\partial^2 F}{\partial y^2}\frac{\partial^2 (W + W_o)}{\partial x^2} - 2\frac{\partial^2 F}{\partial x \partial y}\frac{\partial^2 (W + W_o)}{\partial x\, \partial y} + \frac{\partial^2 F}{\partial x^2}\frac{\partial^2 (W + W_o)}{\partial y^2}\right]$$

$$\nabla^4 F = Et\left[\left(\frac{\partial^2 W}{\partial x \partial y}\right)^2 - \frac{\partial^2 W}{\partial x^2}\frac{\partial^2 W}{\partial y^2} - \frac{\partial^2 W}{\partial x^2}\frac{\partial^2 W_o}{\partial y^2} - \frac{\partial^2 W}{\partial y^2}\frac{\partial^2 W_o}{\partial x^2} + 2\frac{\partial^2 W}{\partial x \partial y}\frac{\partial^2 W_o}{\partial x \partial y}\right] \tag{3}$$

where the stress function F is defined by

$$N_x = \frac{\partial^2 F}{\partial y^2}, \qquad N_y = \frac{\partial^2 F}{\partial x^2}, \qquad N_{xy} = -\frac{\partial^2 F}{\partial x \partial y}$$

and the membrane stress resultants are defined as follows:

$$N_x = \int_{-t/2}^{t/2} \sigma_x \, dz \qquad N_y = \int_{-t/2}^{t/2} \sigma_y \, dz$$

$$N_{xy} = \int_{-t/2}^{t/2} \sigma_{xy} \, dz$$

The nonlinear terms which appear on the right hand side of equations (3) arise from the non-linear terms which involve W in the strain displacement relationship. In other words, these equations are not limited to infinitesimal displacements perpendicular to the x-y plane.

Using the shallowness assumption, the initial spherical shape of the shell can be written

$$W_o(r) = \frac{1}{2R} (r^2 - b^2)$$

Substituting $W_o(r)$ into equation (3), and transforming to cylindrical coordinates, the equations of a shallow spherical shell are obtained.

$$D\ \nabla^4 W = p + \frac{1}{r} F_{rr} W_r + \frac{1}{r^2} F_{rr} W_{\theta\theta}$$

$$+ \frac{1}{r} F_r W_{rr} + \frac{1}{r^2} F_{\theta\theta} W_{rr} - \frac{2}{r^2} F_{r\theta} W_{r\theta}$$

$$+ \frac{2}{r^3} F_{r\theta} W_\theta + \frac{2}{r^3} F_\theta W_{r\theta} - \frac{2}{r^4} F_\theta W_\theta$$

$$+ \frac{1}{R} F_{rr} + \frac{1}{Rr} F_r + \frac{1}{Rr^2} F_{\theta\theta} \qquad (4)$$

$$\frac{1}{Et} \nabla^4 F = \frac{1}{r^2} W_{r\theta}^2 - \frac{2}{r^3} W_{r\theta} W_\theta + \frac{1}{r^4} W_\theta^2$$

$$- \frac{1}{r} W_{rr} W_r - \frac{1}{r^2} W_{rr} W_\theta - \frac{1}{Rr} W_r$$

$$- \frac{1}{Rr^2} W_{\theta\theta} - \frac{1}{R} W_{rr}$$

where

$$\nabla^4 = \frac{\partial^4}{\partial r^4} + \frac{2}{r} \frac{\partial^3}{\partial r^3} - \frac{1}{r^2} \frac{\partial^2}{\partial r^2} + \frac{1}{r^3} \frac{\partial}{\partial r} + \frac{4}{r^4} \frac{\partial^2}{\partial \theta^2}$$

$$- \frac{2}{r^3} \frac{\partial^3}{\partial r \partial \theta^2} + \frac{2}{r^2} \frac{\partial^4}{\partial r^2 \partial \theta^2} + \frac{1}{r^4} \frac{\partial^4}{\partial \theta^4}$$

$$N_r = \frac{1}{r} \frac{\partial F}{\partial r} + \frac{1}{r^2} \frac{\partial^2 F}{\partial \theta^2}$$

$$N_{r\theta} = - \frac{\partial}{\partial r} \left[\frac{1}{r} \frac{\partial F}{\partial \theta} \right]$$

$$N_\theta = \frac{\partial^2 F}{\partial r^2}$$

If the in-plane displacements (Fig. 1) in the r and θ directions are denoted by η and ξ respectively, and nonlinear terms in W are retained, the strain displacement relations are

$$\epsilon_{rr} = \frac{\partial \eta}{\partial r} + \frac{1}{2}\left[\frac{\partial W}{\partial r}\right]^2$$

$$\epsilon_{\theta\theta} = \frac{\eta}{r} + \frac{1}{r}\frac{\partial \xi}{\partial \theta} + \frac{1}{2r^2}\left[\frac{\partial W}{\partial \theta}\right]^2 \qquad (5)$$

$$\epsilon_{r\theta} = \frac{\partial \xi}{\partial r} + \frac{1}{r}\frac{\partial \eta}{\partial \theta} - \frac{1}{r}\eta + \frac{1}{r}\frac{\partial W}{\partial r}\frac{\partial W}{\partial \theta}$$

The relationship between mid-surface strain and the stress function F can be obtained from Hooke's law, and the definitions of stress resultants and stress function.

$$\epsilon_{rr} = \frac{1}{Et}(N_r - \nu N_\theta)$$

$$\epsilon_{\theta\theta} = \frac{1}{Et}(N_\theta - \nu N_r)$$

$$\epsilon_{r\theta} = \frac{2(1+\nu)}{Et} N_{r\theta}$$

so that

$$\epsilon_{rr} = \frac{1}{Et}\left[\frac{1}{r}\frac{\partial F}{\partial r} + \frac{1}{r^2}\frac{\partial^2 F}{\partial \theta^2} - \nu\frac{\partial^2 F}{\partial r^2}\right]$$

$$\epsilon_{\theta\theta} = \frac{1}{Et}\left[\frac{\partial^2 F}{\partial r^2} - \nu\left(\frac{1}{r}\frac{\partial F}{\partial r} + \frac{1}{r^2}\frac{\partial^2 F}{\partial \theta^2}\right)\right] \qquad (6)$$

$$\epsilon_{r\theta} = \frac{2(1+\nu)}{Et}\left[-\frac{\partial}{\partial r}\left(\frac{1}{r}\frac{\partial F}{\partial \theta}\right)\right]$$

In the next section, equations (4) will be used to find the non-linear equations of a symmetrical deformation, and the homogeneous equations which govern asymmetrical perturbations around this symmetrical state. These equations will be analogous to equation (2) in the Euler buckling problem.

2.3 Reduction of the General Equations.

The equations of a symmetrical deformation of the shell can be obtained from equations (4) by assuming W and F to be independent of θ. Since the equations governing small asymmetrical perturbations are also required, however, the entire set can be generated from (4) by assuming:

$$W(r,\theta) = U(r) + \tilde{V}(r,\theta)$$

$$F(r,\theta) = G(r) + \hat{H}(r,\theta)$$

where

$$\left.\begin{array}{l} \left|\hat{V}(r,\theta)\right|_{max} \ll \left|U(r)\right|_{max} \\ \left|\hat{H}(r,\theta)\right|_{max} \ll \left|G(r)\right|_{max} \end{array}\right\} \quad \begin{array}{lll} 0 & r & b \\ 0 & \theta & 2\pi \end{array}$$

In order to simplify the problem further, only perturbations of the form

$$\begin{aligned} \hat{V}(r,\theta) &= V(r) \cos n\theta \\ \hat{H}(r,\theta) &= H(r) \cos n\theta \end{aligned} \tag{7}$$

will be considered. This restriction on the asymmetrical perturbations has also been assumed in Refs. 13-16. When equations (7) are substituted into equations (4), and the resultant equations separated into the parts dependent on θ and independent of θ, the following four equations are obtained:

$$\text{(a)} \quad D\nabla_r^4 U = p + \frac{1}{r}(G_{rr}U_r + G_r U_{rr}) + \frac{1}{R}(G_{rr} + \frac{1}{r} G_r)$$

$$\text{(b)} \quad \frac{1}{Et}\nabla_r^4 G = -\frac{1}{r} U_r U_{rr} - \frac{1}{Rr} U_r - \frac{1}{R} U_{rr}$$

$$\text{(c)} \quad D\nabla_\theta^4 V = \frac{1}{r}(U_r H_{rr} + V_r G_{rr} + H_r U_{rr} + V_{rr} G_r + \frac{1}{R} H_r) + \frac{1}{r^2}(-G_{rr} V - H U_{rr} - \frac{1}{R} H) + \frac{1}{R} H_{rr}$$

$$\text{(d)} \quad \frac{1}{Et}\nabla_\theta^4 H = -\frac{1}{r}(U_r V_{rr} + U_{rr} V_r + \frac{1}{R} V_r) + \frac{1}{r^2}(U_{rr} V + \frac{1}{R} V) - \frac{1}{R} V_{rr}$$

(8)

where

$$\nabla_r^4 = \frac{d^4}{dr^4} + \frac{2}{r}\frac{d^3}{dr^3} - \frac{1}{r^2}\frac{d^2}{dr^2} + \frac{1}{r^3}\frac{d}{dr}$$

$$\nabla_\theta^4 = \frac{d^4}{dr^4} + \frac{2}{r}\frac{d^3}{dr^3} - \frac{1+2n^2}{r^2}\frac{d^2}{dr^2} + \frac{1+2n^2}{r^3}\frac{d}{dr} + \frac{n^2(n^2-4)}{r^4}$$

Second order terms in the small quantities V and H have been eliminated from equations (8c) and (8d).

Equations (8a) and (8b) are the usual nonlinear equations of the shell for symmetrical deflections. Equations (8c) and (8d) which govern the asymmetrical perturbations V(r) and H(r) are homogeneous as expected. The presence of the functions U and G on the right hand side of these equations shows that the asymmetrical deformations are coupled to the symmetrical load (U(r) and G(r) can be looked upon as functions of p upon inverting equations (8a) and (8b)) so bifurcation buckling analogous to Euler column buckling can occur for certain values of p.

These four equations can be written in non-dimensional form by defining the following non-dimensional quantities

$$\rho = \frac{\pi}{b} r \qquad \overline{V} = \left(\frac{\lambda}{b}\right)^2 \pi^2 RV$$

$$\overline{U} = \left(\frac{\lambda}{b}\right)^2 \pi^2 RU \qquad \overline{H} = \frac{12(1-\nu^2)}{Et^3} H$$

$$\overline{G} = \frac{12(1-\nu^2)}{Et^3} G \qquad \overline{\eta} = \left(\frac{\lambda}{b}\right)^2 \pi^2 R\eta$$

$$q = \left(\frac{R}{t}\right)^2 \frac{\sqrt{3(1-\nu^2)}}{2E} p \qquad \overline{\xi} = \left(\frac{\lambda}{b}\right)^2 \pi^2 R\xi$$

$$\lambda^4 = \frac{12(1-\nu^2)\, b^4}{R^2 t^2}$$

Equations (8) then become

$$\text{(a)} \quad \nabla_\rho^4 \overline{U} = \frac{4}{\pi^2} \lambda^4 q + \frac{1}{\rho}\left[\overline{G}_{\rho\rho}\overline{U}_\rho + \overline{G}_\rho \overline{U}_{\rho\rho}\right] + \lambda^2\left[\overline{G}_{\rho\rho} + \frac{1}{\rho}\overline{G}_\rho\right]$$

$$\text{(b)} \quad \nabla_\rho^4 \overline{G} = -\frac{1}{\pi^4}\left[\frac{\overline{U}_\rho \overline{U}_{\rho\rho}}{\rho} + \lambda^2\left(\frac{\overline{U}_\rho}{\rho} + \overline{U}_{\rho\rho}\right)\right]$$

$$\text{(c)} \quad \nabla_\theta^4 \overline{V} = \frac{1}{\rho}\left[\overline{U}_\rho \overline{H}_{\rho\rho} + \overline{V}_\rho \overline{G}_{\rho\rho} + \overline{H}_\rho \overline{U}_{\rho\rho} + \overline{V}_{\rho\rho}\overline{G}_\rho + \lambda^2 \overline{H}_\rho\right]$$

$$+ \lambda^2 \overline{H}_{\rho\rho} - \frac{n^2}{\rho^2}\left[\overline{G}_{\rho\rho}\overline{V} + \overline{H}\,\overline{U}_{\rho\rho} + \lambda^2 \overline{H}\right] \qquad (9)$$

$$\text{(d)} \quad \nabla_\theta^4 \overline{H} = \frac{1}{\pi^4}\left[-\frac{1}{\rho}\left[\overline{U}_{\rho\rho}\overline{V}_\rho + \overline{V}_{\rho\rho}\overline{U}_\rho\right] + \frac{n^2}{\rho^2}\overline{U}_{\rho\rho}\overline{V}\right.$$

$$\left. + \lambda^2\left[-\frac{\overline{V}_\rho}{\rho} + \frac{n^2\overline{V}}{\rho} - \overline{V}_{\rho\rho}\right]\right]$$

where

$$\nabla_\rho^4 = \frac{d^4}{d\rho^4} + \frac{2}{\rho}\frac{d^3}{d\rho^3} - \frac{1}{\rho^2}\frac{d^2}{d\rho^2} + \frac{1}{\rho^3}\frac{d}{d\rho}$$

$$\nabla_\theta^4 = \frac{d^4}{d\rho^4} + \frac{2}{\rho}\frac{d^3}{d\rho^3} - \frac{1+2n^2}{\rho^2}\frac{d^2}{d\rho^2} + \frac{1+2n^2}{\rho^3}\frac{d}{d\rho} + \frac{n^2(n^2-4)}{\rho^4}$$

Notice that the non-dimensional displacement $\bar{U}$ is a function only of the non-dimensional parameters q and λ. Thus the non-dimensional buckling pressure q_{crit} will be a function of the geometrical parameter λ, and Poisson's ratio ν, which enters through the boundary conditions.

The non-dimensional parameter q is simply the pressure normalized by the classical buckling load of a complete sphere of the same radius and thickness:

$$p_{crit} = \frac{2E}{\sqrt{3(1-\nu^2)}}\left(\frac{t}{R}\right)^2 \qquad \text{(complete sphere)}$$

Thus a buckling pressure $q_{crit} = 1$ will indicate a shallow spherical shell which buckles at the same pressure as that predicted for a complete spherical shell of similar geometry.

Under the assumption of shallowness, λ can be expressed in the form

$$\lambda = \sqrt[4]{48(1 - \nu^2)\left[\frac{h}{t}\right]^2}$$

Thus a wide range of λ is possible without violating the shallowness assumption. Vastly different shells of the same λ will be expected to buckle at the same value of q, provided they are sufficiently shallow.

For shells which do not satisfy the shallowness assumption, there is no reason to expect that q_{crit} depends only on λ and ν. Thus it is advisable in experiments to increase λ by decreasing t, rather than increasing h, whenever possible, if the object of the experiments is to check conclusions drawn from equations (9).

The method of solution can now be outlined:

1. Equations (9a) and (9b) are to be used to obtain $\overline{U}(\rho)$ and $\overline{G}(\rho)$ as functions of q. This solution will define equilibrium curve A of Fig. 2a, and snap buckling loads can be located.

2. $\overline{U}(\rho)$ and $\overline{G}(\rho)$ from step 1) are to be substituted into equations (9c) and (9d). These linearized equations describe the behavior of asymmetrical equilibrium paths of the form $\overline{V}(\rho) \cos n\theta$, along the symmetrical equilibrium path A. Thus points where the paths intersect can be located.

2.4 Solution of the Symmetrical Equations.

The first step is to solve equations (9a) and (9b) for $\overline{U}(\rho)$ and $\overline{G}(\rho)$. The following scheme will be used. First, $\overline{U}(\rho)$ is approximated by the expression

$$\overline{U}(\rho) = \sum_{i=1}^{N} \overline{U}_i \, f_i(\rho)$$

where the functions $f_i(\rho)$ and the number N are choosen to give an adequate representation of $\overline{U}(\rho)$, and the magnitudes $\overline{U}_i$ are to be determined by Galerkin's method. This approximation to $\overline{U}(\rho)$ will then be substituted into the right hand side of (9b), and the resulting linear equation will be solved for a $\overline{G}(\rho)$ which is compatible with the assumed $\overline{U}(\rho)$. $\overline{G}(\rho)$ and $\overline{U}(\rho)$ will then be substituted into (9a), and equation (9a) will be approximately satisfied in the Galerkin sense by the choice of $\overline{U}_i$. In other words, the N algebraic equations

$$\int_0^{\pi} K\left[\, \overline{G}(\rho),\ \overline{U}(\rho) \,\right] \cdot f_i(\rho) \cdot 2\pi\rho \cdot d\rho = 0 \qquad (i = 1,\ 2,\ \ldots N)$$

where

$$K\left[\overline{G},\ \overline{U}\right] = \frac{4}{\pi^2} \lambda^4 q + \frac{1}{\rho}\left[\, \overline{G}_{\rho\rho}\, \overline{U}_{\rho} + \overline{G}_{\rho}\, \overline{U}_{\rho\rho} \,\right]$$

$$+ \lambda^2 \left[\, \overline{G}_{\rho\rho} + \frac{1}{\rho}\, \overline{G}_{\rho} \,\right] - \nabla_{\rho}^4 \overline{U}$$

will be solved for the N unknowns $\bar{U}_i$. In this manner, the operator $K\ \bar{G}, \bar{U}$, which is zero everywhere in the domain of the shell for the exact solutions, is made zero in a weighted average sense in this domain.

The functions $f_i(\rho)$ must be chosen so that they are capable of representing $\bar{U}(\rho)$, and must satisfy the boundary conditions on $\bar{U}(\rho)$, namely

$$\frac{\partial \bar{U}}{\partial \rho}\Big|_{\rho=\pi} = \bar{U}\Big|_{\rho=\pi} = 0 \quad \text{(clamped at } \rho = \pi)$$

$$\frac{\partial \bar{U}}{\partial \rho}\Big|_{\rho=o} = 0 \quad \text{(symmetry)}$$

Assuming that the deflections of the exact solution agree with experiment, the choice of $f_i(\rho)$ can be based on the measured deflections. Experimental results show that the deflection shape is wavy, and that it becomes increasingly wavy with increased λ (Fig. 5). Thus the experiments suggest the choice

$$f_m(\rho) = 1 + (-1)^{m+1} \cos m\rho$$

The term $m = 1$ will dominate for $\lambda < 5$, $m = 1$ and $m = 2$ will be important in the region $5 < \lambda < 7$, and $m = 3$ will be required to represent the mode shapes for $7 < \lambda < 10$. For $\lambda > 10$, the terms $m = 4$ etc. will become increasingly important. In view of this, terms up to and including $m = 3$ have been included in this analysis. Thus, the deflection is assumed to be

$$\bar{U}(\rho) = \bar{U}_1(1 + \cos\rho) + \bar{U}_2(1 - \cos 2\rho) + \bar{U}_3(1 + \cos 3\rho) \qquad (10)$$

On substituting this expression into the right hand side of equation (b) the following equation in $\bar{G}(\rho)$ is obtained

$$\nabla_\rho^4 \bar{G} = -\frac{1}{\pi^4}\left[\sum_{m=1}^{3}\sum_{n=1}^{3}(-1)^{m+n}\frac{mn^2 \sin m\rho \cos n\rho}{\rho}\bar{U}_m\bar{U}_n\right.$$

$$\left. + \lambda^2 \sum_{m=1}^{3}(-1)^m \bar{U}_m\left[m^2\cos m\rho + \frac{m\sin m\rho}{\rho}\right]\right]$$

The solution is straightforward, but lengthy. It has the form

$$\bar{G}(\rho) = \sum_{m=1}^{3}\sum_{n=1}^{3}\xi_{1,n,m}(\rho)\ \bar{U}_n + \xi_{2,m}(\rho)\ \bar{U}_m$$

In other words, $\bar{G}(\rho)$ is quadratic in $\bar{U}_i$ and also contains terms of first order in $\bar{U}_i$

$$\bar{G}(\rho) = \xi_3(\bar{U}_i^2, \bar{U}_i)$$

The solutions to the homogeneous equation $\nabla_\rho^4 \bar{G} = 0$ are added to satisfy boundary conditions. The boundary conditions appropriate to this problem are:

1. Stresses finite as $\rho \to 0$
2. The radial in-plane displacement $\bar{\eta}(\rho)$ must be zero at the edge, since the edge is clamped.

The homogeneous solution is

$$\bar{G}(\rho) = A\rho^2 + B \log \rho + C \rho^2 \log \rho + D$$

Now, since $\bar{G}$ plays the role of a stress potential, and is related to the physical problem only through its derivatives, D can be chosen arbitrarily, say $D = 0$. B and C are determined so that condition 2) is satisfied.

Using equations (5) and (6),

$$\frac{\eta}{r} = -\frac{1}{r}\frac{\partial \xi}{\partial \theta} - \frac{1}{2r^2}\left(\frac{\partial W}{\partial \theta}\right)^2 + \frac{1}{Et}\left[\frac{\partial^2 F}{\partial r^2} - \nu\left[\frac{1}{r}\frac{\partial F}{\partial r} + \frac{1}{r^2}\frac{\partial^2 F}{\partial \theta^2}\right]\right]$$

In this symmetrical problem we have

$$W = U(r) \qquad F = G(r) \qquad \xi = 0$$

so that

$$\frac{\eta(r)}{r} = \frac{1}{Et}\left[\frac{\partial^2 G}{\partial r^2} - \frac{\nu}{r}\frac{\partial G}{\partial r}\right]$$

Transforming to the non-dimensional variables, and setting $\eta = 0$ at the boundary $\rho = \pi$ the equation

$$\bar{G}_{\rho\rho}(\pi) - \frac{\bar{G}_{\rho}(\pi)}{\pi} = 0 \tag{11}$$

is obtained. This equation determines A.

The solution for $\bar{G}(\rho)$ can now be substituted into equation (9a), and the three algebraic equations of Galerkin's method can be obtained by integration as previously outlined. It will be noted that since $\bar{G}$ is quadratic in $\bar{U}_i$ and equation (9a) contains terms of the form $\bar{U} \cdot \bar{G}$, the resultant equations will be cubic in $\bar{U}_i$. The load, q, however, appears linearly. Thus three equations of the form

$$\begin{aligned}
&A_1\bar{U}_1^3 + A_2\bar{U}_1^2\,\bar{U}_2 + A_3\,\bar{U}_1^2\,\bar{U}_3 + A_4\,\bar{U}_2^3 + A_5\,\bar{U}_2^2\,\bar{U}_1 + \\
&A_6\,\bar{U}_2^2\,\bar{U}_3 + A_7\,\bar{U}_3^3 + A_8\,\bar{U}_3^2\,\bar{U}_1 + A_9\,\bar{U}_3^2\,\bar{U}_2 + A_{10}\,\lambda^2\,\bar{U}_1^2 + \\
&A_{11}\,\lambda^2\,\bar{U}_2^2 + A_{12}\,\lambda^2\,\bar{U}_3^2 + A_{13}\,\lambda^2\,\bar{U}_1\,\bar{U}_2 + A_{14}\,\lambda^2\,\bar{U}_1\,\bar{U}_3 + \\
&A_{15}\,\lambda^2\,\bar{U}_2\,\bar{U}_3 + (A_{16} + \lambda^4 A_{17})\bar{U}_1 + (A_{18} + \lambda^4 A_{19})\,\bar{U}_2 + \\
&(A_{20} + \lambda^4 A_{21})\,\bar{U}_3 + A_{22}\,\lambda^4\,q = \bar{\Phi}(\bar{U}_i, q) = 0
\end{aligned} \tag{12}$$

are obtained. Given q and λ, these three equations determine U_1, U_2, U_3. The deflection of the shell can then be determined from equation (10).

2.5 Solution of the Asymmetrical Equations.

The procedure which is followed to find a solution to the asymmetrical equations is similar to the procedure which was used in the previous section. Referring again to the four basic equations, it will be noted that if $\overline{V}(\rho)$ is assumed, and $\overline{U}(\rho)$ and $\overline{G}(\rho)$ have been determined by the symmetrical solution, equation (9d) can be solved for $\overline{H}(\rho)$. $\overline{H}(\rho)$ and $\overline{U}(\rho)$ can then be substituted into equation (9c), and this equation can be satisfied in the Galerkin sense.

The functional form of $\overline{V}(\rho)$ must satisfy certain boundary conditions. First, it must satisfy

$$\overline{V}\Big|_{\rho=\pi} = \frac{d\overline{V}}{d\rho}\Big|_{\rho=\pi} = 0$$

since any admissible perturbation must leave the shell clamped at its edge. Secondly, since the complete asymmetrical shape is given by

$$\overline{V}(\rho)\cos n\theta$$

conditions of continuity and smoothness at $\rho = 0$ require that

$$\overline{V}\Big|_{\rho=o} = \frac{d\overline{V}}{d\rho}\Big|_{\rho=o} = 0$$

Note that the condition

$$\frac{d\overline{V}}{d\rho}\Big|_{\rho=o} = 0$$

is not required for $n = 1$. Applying it in this case places an unnecessary constraint upon V. However, the effect on the buckling loads is of minor importance.

In view of these boundary conditions, $\overline{V}(\rho)$ has been chosen in the form

$$\overline{V}(\rho) = \overline{V}_1 \left[\rho^4 - 2\pi \rho^3 + \pi^2 \rho^2 \right]$$

where $\overline{V}_1$ is an undetermined amplitude.

Substituting this assumption into equation (9d), the following equation for $\overline{H}(\rho)$ is obtained

$$\frac{\nabla_\theta^4 \overline{H}}{\overline{V}_1} = \sum_{m=1}^{3} \frac{(-1)^m}{\pi^4} \left[m^2 \cos m\rho \left[(n^2 - 4)\rho^2 - 2(n^2 - 3)\pi\rho + (n^2 - 2)\pi^2 \right] - m \sin m\rho \left[12\rho - 12\pi + \frac{2\pi^2}{\rho} \right] \right] \overline{U}_m + \frac{\lambda^2}{\pi^4} \left[(n^2 - 16)\rho^2 - 2(n^2 - 9)\pi\rho + (n^2 - 4)\pi^2 \right]$$

so that $\overline{H}(\rho)$ will be linear in $\overline{U}_m$ and linear and homogeneous in $\overline{V}_1$. The homogeneous solution is

$$\overline{H}(\rho) = A\rho^{n+2} + B\rho^n + C\rho^{2-n} + D\rho^{-n} \qquad n \neq 1$$

$$\text{or} \quad \overline{H}(\rho) = A\rho^3 + B\rho + C\rho \, \ell n \rho + \frac{D}{\rho} \qquad n = 1$$

The constants A, B, C, and D are chosen by the following boundary conditions

1. All stresses finite at $\rho = 0$
2. $\bar{\eta}(\pi) = 0$
3. $\bar{\xi}(\pi) = 0$

where $\bar{\xi}(\rho)$ is the in-plane tangential displacement, which is not identically zero, as it was in the symmetrical case, because of the θ dependence of the solution.

The first condition determines C and D for all values of n, while the second and third conditions are used to determine A and B. From equations (5) and (6)

$$\frac{\eta}{r} + \frac{1}{r}\frac{\partial \xi}{\partial \theta} + \frac{1}{2r^2}\left(\frac{\partial W}{\partial \theta}\right)^2 = \frac{1}{Et}\left[\frac{\partial^2 F}{\partial r^2} - \nu\left[\frac{1}{r}\frac{\partial F}{\partial r} + \frac{1}{r^2}\frac{\partial^2 F}{\partial \theta^2}\right]\right]$$

$$\frac{\partial \eta}{\partial r} + \frac{1}{2}\left(\frac{\partial W}{\partial r}\right)^2 = \frac{1}{Et}\left[\frac{1}{r}\frac{\partial F}{\partial r} + \frac{1}{r^2}\frac{\partial^2 F}{\partial \theta^2} - \nu\frac{\partial^2 F}{\partial r^2}\right]$$

On substituting

$$W = U(r) + V(r)\cos n\theta$$

$$F = G(r) + H(r)\cos n\theta$$

and using equations (8a) and (11), the in-plane displacement boundary conditions can be written

$$\frac{\bar{H}(\pi)}{\pi} + (1 - n^2)\int_0^{\pi} \frac{\bar{H}(\rho)}{\rho}\, d\rho - \left.\frac{d\bar{H}}{d\rho}\right|_{\rho=\pi}$$

$$+ \frac{2}{\pi^4}\int_0^{\pi} \bar{V}(\rho)d\rho - \frac{1}{\pi^4}\int_0^{\pi} \frac{d\bar{U}}{d\rho}\frac{d\bar{V}}{d\rho}\, d\rho = 0$$

$$\pi \left.\frac{d^2\bar{H}}{d\rho^2}\right|_{\rho=\pi} - \nu \left(\left.\frac{d\bar{H}}{d\rho}\right|_{\rho=\pi} - \left.\frac{n^2\bar{H}}{\pi}\right|_{\rho=\pi}\right) = 0$$

When $\bar{H}(\rho)$ and $\bar{V}(\rho)$ are substituted into equation (9c) and the Galerkin integration is carried out, an equation of the following form is obtained for each n.

$$\bar{V}_1 \left[f_n(\bar{U}_i^2, \bar{U}_i) \right] = 0$$

with solutions

$$\bar{V}_1 = 0 \quad \text{or} \quad f_n(\bar{U}_i^2, \bar{U}_i) = 0$$

The first solution is trivial and tells us that no equilibrium perturbation of the assumed asymmetrical form is possible under clamped boundary conditions. The second solution gives a condition on the $\bar{U}_i$, which may be satisfied at certain points by the solutions to the three cubic equations given in the previous section. At these exceptional

points, bifurcation of the symmetrical solution occurs, and buckling involving nth mode asymmetrical forms may occur.

This procedure has been carried out for $n = 1, 2, \ldots, 6$, so that information can be obtained for buckling in any of the first six asymmetrical modes. In detail, the equations have the form

$$B_1 \bar{U}_1^2 + B_2 \bar{U}_1 \bar{U}_2 + B_3 \bar{U}_1 \bar{U}_3 + B_4 \bar{U}_2^2 + B_5 \bar{U}_2 U_3 + B_6 \bar{U}_3^2 + \lambda^2 \left[B_7 \bar{U}_1 + B_8 \bar{U}_2 + B_9 \bar{U}_3 \right] + \lambda^4 B_{10} + B_{11} = f_n(\bar{U}_i^2, \bar{U}_i) = 0 \tag{13}$$

2.6 Solution of the Algebraic Equations.

The solution of the symmetrical problem has been reduced to the solution of three cubic equations. The bifurcation of this solution in an asymmetrical mode $\bar{V}(\rho) \cos n\theta$ has been reduced to a quadratic side condition for each n. Now solutions to these algebraic equations must be found.

The branch of solutions which is sought among the many possible solutions $\bar{U}_1, \bar{U}_2, \bar{U}_3$ for a given q is the path which passes through the point $\bar{U}_1 = \bar{U}_2 = \bar{U}_3 = 0$ for $q = 0$. The solution can be extended step by step from (0, 0, 0) by making an initial guess at an adjacent solution, and then improving upon this guess with an iteration procedure which is analogous to the single variable Newton's method.

Assume that the solution $(\bar{U}_1^o, \bar{U}_2^o, \bar{U}_3^o)$ corresponding to pressure q_o has been found. The solution for an adjacent point

$(\bar{U}_1, \bar{U}_2, \bar{U}_3) = (\bar{U}_1^o + \Delta\bar{U}_1, \bar{U}_2^o + \Delta\bar{U}_2, \bar{U}_3^o + \Delta\bar{U}_3)$ corresponding to $q = q_o + \Delta q$ (see Figs. 6 and 7) is sought. The solution could be extended by using the three equations (equation 12), and assuming $\Delta\bar{U}_1 = \Delta\bar{U}_2 = \Delta\bar{U}_3 = 0$, $\Delta q = \delta$, where δ is some small, pre-assigned step. It could also be extended by assuming a step in any one of the $\bar{U}_i$, say $\Delta\bar{U}_m = \delta$, $\Delta\bar{U}_i = 0$ $i = m$, $\Delta q = 0$. Having chosen one of these procedures, some iteration procedure could then be used to find the corresponding changes required in the other three variables in order to satisfy equations (12). This is not a satisfactory procedure, however, since there is no assurance that either q, or any of the $\bar{U}_i$, will be monotonic functions of arc length along the path (Fig. 6) beginning at $(0, 0, 0, 0)$. These thoughts suggest the following procedure. The solution can be extended by proceeding from one solution to the next in steps of arc length. To apply this method, the equations must be rewritten so that a new solution can be easily specified by a step in arc length. First, the parameter q can be eliminated from the equations. The load enters each of the three equations (12)

$$\bar{\Phi}_k(\bar{U}_1, \bar{U}_2, \bar{U}_3, q) = 0 \qquad k = 1, 2, 3$$

linearly. Thus linear combinations can be formed from these three equations, and q can be eliminated. The new equations

$$\varphi_1(\bar{U}_1, \bar{U}_2, \bar{U}_3) = \bar{\Phi}_1 - C_1 \bar{\Phi}_2 = 0$$

$$\varphi_2(\bar{U}_1, \bar{U}_2, \bar{U}_3) = \bar{\Phi}_1 - C_2 \bar{\Phi}_3 = 0$$

are obtained, where the C_i are chosen so that q will be eliminated. These two equations are satisfied by every point along the equilibrium path. Once a solution $\bar{U}_i^o$ has been found, the path is extended by seeking a new solution $\bar{U}_i$ such that

$$\Delta\bar{U}_1^2 + \Delta\bar{U}_2^2 + \Delta\bar{U}_3^2 - \delta^2 = \varphi_3(\bar{U}_1, \bar{U}_2, \bar{U}_3) = 0$$

$$\Delta\bar{U}_i = \bar{U}_i - \bar{U}_i^o$$

where δ is a pre-assigned constant. In other words, the next solution is constrained to lie an arc length δ from the given solution $(\bar{U}_1^o, \bar{U}_2^o, \bar{U}_3^o)$ (see Fig. 7). This does not uniquely define the next solution however, since there are at least two adjacent solutions which satisfy this condition. The solution corresponding to a retrogression in arc length is eliminated by making a good initial guess at $\Delta\bar{U}_1$, $\Delta\bar{U}_2$ and $\Delta\bar{U}_3$. This first approximation is obtained by extrapolating the previous four solutions.

The three equations

$$\varphi_k = 0 \qquad k = 1, 2, 3 \tag{14}$$

are used to improve the solution. Let $(\bar{U}_1^{(1)}, \bar{U}_2^{(1)}, \bar{U}_3^{(1)}) = (\bar{U}_1^o + \Delta\bar{U}_1^{(1)}, \bar{U}_2^o + \Delta\bar{U}_2^{(1)}, \bar{U}_3^o + \Delta\bar{U}_3^{(1)})$ be the initial guess. This first approximation does not in general satisfy equations (14), so a second approximation is sought, which more nearly satisfies the equations.

$$(\bar{U}_1^{(2)},\ \bar{U}_2^{(2)},\ \bar{U}_3^{(2)}) = (\bar{U}_1^{(1)} + \epsilon_1,\ \bar{U}_2^{(1)} + \epsilon_2,\ \bar{U}_3^{(1)} + \epsilon_3)$$

In order to determine the effect that a change ϵ_i has on the value of φ_k, φ_k is expanded in Taylor's series.

$$\varphi_k(\bar{U}_1^{(2)},\ \bar{U}_2^{(2)},\ \bar{U}_3^{(2)}) \approx \varphi_k\Big|_{\bar{U}_j=\bar{U}_j^{(1)}} + \sum_{j=1}^{3} \frac{\partial \varphi_k}{\partial \bar{U}_j}\Big|_{\bar{U}_j=\bar{U}_j^{(1)}} \epsilon_j$$

The second approximation $\bar{U}_i^{(2)}$ should make $\varphi_k = 0$ so the linear equations

$$\frac{\partial \varphi_k}{\partial U_1}\Big|_{U_1=U_1^{(1)}} \epsilon_1 + \frac{\partial \varphi_k}{\partial U_2}\Big|_{U_2=U_2^{(1)}} \epsilon_2 + \frac{\partial \varphi_k}{\partial U_3}\Big|_{U_3=U_3^{(1)}} \epsilon_3 = -\varphi_k\Big|_{U_j=U_j^{(1)}} \qquad k = 1,\ 2,\ 3$$

for determining ϵ_i are obtained. By replacing the first approximation by the second approximation, the procedure can be repeated to obtain a third approximation and so on until the successive approximations to $\bar{U}_i$ converge. The value of q corresponding to a solution $\bar{U}_i$ can be evaluated from any one of the three equations $\bar{\Phi}_k = 0$.

In this manner, the equilibrium configurations extending from the unloaded state to the snap buckling point (1st local max. in q), and beyond, can be found.

As each triple $(\bar{U}_1,\ \bar{U}_2,\ \bar{U}_3)$ is found along this curve, it is tested in each of the six quadratic side conditions (equation 13). For certain ranges of λ, one or more of the expressions may change sign

in passing from one solution to the next. When this occurs, the quadratic surface $f_n(\bar{U}_i^2, \bar{U}_i) = 0$ has been intersected by the symmetrical equilibrium path (see Fig. 7). Denote the pressures corresponding to these two adjacent solutions by q_1 and q_2, where the first change of sign in the value of $f_n(\bar{U}_i^2, \bar{U}_i)$ was observed at the solution corresponding to q_2. The solution corresponding to q_1 is separated in configuration space from q_2 by an increment in arc length $-\delta$. A zero of $f_n(\bar{U}_i^2, \bar{U}_i)$ occurs at some point along the arc length δ, so the limits $q_1 \leqslant q_b^n \leqslant q_2$ are obtained for the nth mode bifurcation buckling load q_b^n.

The snap and bifurcation buckling points which have been found in this manner, are shown in Figs. 8-11 inclusive. No bifurcation points were found in the range of λ which was investigated, for $n = 5$ or $n = 6$. These results snould be compared with those of Huang (Ref. 16) and Weinitschke (Ref. 15) (Fig. 4). Except for the absence of solutions for $n = 5$ and $n = 6$, the results agree in general with those of Huang.

The present results cannot be expected to hold for $\lambda > 10$, and will be increasingly inaccurate as $\lambda \longrightarrow 10$, because the assumed form for $\bar{U}(\rho)$ is incapable of representing the experimental shapes for $\lambda > 10$. In view of this limitation, the present results do not conflict with those of Huang, although no confirmation can be offered for $\lambda > 8$.

2.7 The Effect of Poisson's Ratio on Buckling.

The non-dimensional differential equations do not contain Poisson's ratio ν, as it has been absorbed in the definitions of the non-dimensional parameters q and λ. However, ν occurs in the boundary conditions which are applied to both $G(\rho)$ and $H(\rho)$, so the solution for W and the curves q_{crit} vs. λ are not independent of ν.

In order to find out how strongly the occurrence of ν in the boundary conditions affects the solutions, the procedure has been carried out for $\nu = 0, 1/4, 1/3$, and $1/2$. The values of the coefficients of the three resulting cubic equations (12) are given in Table I for each value of ν. The coefficients of the quadratic expressions $f_n(\bar{U}_i^2, \bar{U}_i)$, which determine nth mode bifurcation (equation 13) are given in Table II for $n = 1, \ldots, 6$ and the above values of ν. Carrying out the solution of these equations $q_{crit}(\lambda)$ is found to vary with ν as indicated in Figs. 8, 9, 10, and 11.

III. EXPERIMENTS

3.1 Review of Previous Experiments

Experiments on shallow spherical shells have been reported by Kaplan and Fung (Ref. 7), Homewood, Brine and Johnson (Ref. 17), and Bellinfante (Ref. 18). The buckling loads are shown in Fig. 3. Note that the scatter band is fairly wide, and that the results tend to be in agreement, insofar as the data from the three sources overlaps throughout the scatter band.

Kaplan and Fung tested shells which were 8 inches in diameter and had nominal radii of curvature of 20" and 30", and varied in thickness from 0.032" to 0.102". The shells were spun hot from magnesium plates. This procedure probably resulted in thickness variations, however the magnitude is not given. The value of λ was calculated from the measured shell rise. Maximum variations from sphericity in a given shell ranged from 0.005" up to 0.020", resulting in initial imperfections as great as 40 $^{o}/o$ of the thickness. The shells were held between two rings which were bolted together to provide the clamped edge boundary condition during testing. Tests were conducted with both air and oil pressure loads (approximations to dead weight load and a rigid testing machine respectively), however, no significant variations were observed in the buckling loads obtained by the two methods.

The shells tested by Homewood, Brine and Johnson were 34" in diameter with nominal radii of curvature of 40" and 78". They varied in thickness from 0.067" to 0.260" and had average thickness variations of $\pm$ 4 $^{o}/o$. Unfortunately, the initial imperfections are not given in the

reference, nor is the method of determining λ indicated. The shells were spun from hot rolled steel or wrought aluminum alloy. The method of clamping and testing was similar to that of Kaplan and Fung. Based on the experiences reported by Kaplan and Fung with spun aluminum shells, it may be assumed that the residual stresses were high.

Bellinfante utilized a hydroforming technique to make shells with nominal radii of curvature of 23" and 8" from aluminum. He considered this process superior to spinning as thickness variations were reduced. The thicknesses of the shells varied from 0.028" to 0.251" and had typical thickness variations of $\pm$ 0.001. Initial imperfections, and the method of determining λ are not given. The shells were clamped between rings whose inside diameter was 10", and tested under oil pressure.

The 8" radius of curvature shells tested by Bellinfante violate the shallowness assumption h b/8. It is true, as he points out, that one can calculate λ for a non-shallow shell. However, it is likely that λ is not the only geometric correlation factor for a non-shallow shell, so comparing non-shallow shell data with shallow shell data of similar λ, is a questionable practice.

None of the papers referred to above have made any mention of:

1. How E and ν were determined (probably handbook values),
2. How t was determined or how rough was the surface,
3. How R and hence λ were determined (probably from nominal values).

In view of the crudeness of the results, perhaps refinements were not justified. However, attention to these details can be of primary importance in buckling experiments.

3.2 Basic Requirements of an Experiment to Compare with Theory.

The experimental problem can be simply stated: To build stress-free shallow shells which match the geometry of the theory, clamp them rigidly without inducing edge moments, and buckle them with a uniform, slowly increasing pressure. Once the shell has buckled, a corresponding point must be placed in the q_{crit} vs. λ plane for ν appropriate to the shell (see Figs. 8-11). From the definitions of these quantities

$$\lambda = \sqrt[4]{12(1-\nu)^2}\,\frac{b}{\sqrt{Rt}}$$

$$q_{crit} = \frac{\sqrt[2]{3(1-\nu^2)}}{2E}\,\frac{R^2}{t^2}\,p_{crit}$$

it is clear that the quantities b, r, t, ν, E, p_{crit} must be measured, to varing degrees of accuracy. Let $\xi = (1-\nu^2)$. Then the relative error in λ and q, as a function of the relative errors in b, R, t, E, p and ξ, will be

$$\left|\frac{\Delta\lambda}{\lambda}\right|_{max} = \frac{1}{4}\left|\frac{\Delta\xi}{\xi}\right| + \left|\frac{\Delta b}{b}\right| + \frac{1}{2}\left|\frac{\Delta R}{R}\right| + \frac{1}{2}\left|\frac{\Delta t}{t}\right|$$

$$\left|\frac{\Delta q_{crit}}{q_{crit}}\right|_{max} = \frac{1}{2}\left|\frac{\Delta\xi}{\xi}\right| + 2\left|\frac{\Delta R}{R}\right| + 2\left|\frac{\Delta t}{t}\right| + \left|\frac{\Delta E}{E}\right| + \left|\frac{\Delta p_{crit}}{p_{crit}}\right|$$

Note that the error in λ depends most heavily on b, which can be easily measured to high precision. The determination of q is much more difficult, due to the quadratic dependence on R and t.

If the accuracy with which the components of λ can be measured is considered, it becomes apparent that λ can be measured to 2 ^{o}/o or 3 ^{o}/o without much effort. The proper location of the experimental point in the q vs. λ plane hinges mainly on determining the value of t to use in evaluating q.

The error in t arises from two distinct sources: Error due to measurement of t, and error due to the "uncertainty" in t. The error in measurement is a clear concept, and can be reduced by diligent measurement. The "error of uncertainty" is fundamental to the experiment itself, and must be dealt with more carefully. The theoretical shell is uniform in thickness, and has a perfectly smooth surface. The experimental shell possesses neither of these virtues.

If the experimental shell has thickness variations from point to point of $\pm$ 3 ^{o}/o, values of q_{crit} can be calculated which differ by

as much as 12 $^{o}/o$, depending on whether the maximum or minimum thickness, or perhaps some intermediate value is used. No theoretical study suggests which, if any, of these thicknesses should correlate with the uniform thickness theory. Indeed, the answer is probably not defined without a detailed statement of the thickness distribution.

A rough surface on a shell leads to uncertainty in the thickness in still another way. The bending stiffness of the shell depends on Et^3, but how effective is a disconnected, random array of lumps on the surface, in resisting bending? The resistance to stretching depends on Et. It is perfectly conceivable that the effective thickness t_b in bending is not the same as the effective thickness in stretching t_s!

This conclusion leads one to reconsider the derivation of p_{class}, the classical buckling load of a complete sphere, which is used to normalize the present data. If the derivation of p_{class} is carried out assuming that $t_b \neq t_s$, then (Appendix I)

$$p_{class} = \frac{2E\, t_s^{1/2}\, t_b^{3/2}}{R^2\sqrt{3(1-\nu^2)}}$$

Young's modulus must also be measured for the material of the shell. The method which has been used in these experiments is a simple tension test, where the change $\delta \ell$ in the length of a specimen of length ℓ is observed as a function of the load L. Under these conditions

$$E = \frac{L\,\ell}{t_e \cdot a \cdot \delta\ell}$$

where a is the width, and t_e is the thickness, of the tension specimen. Unfortunately a test for E has not been devised which utilizes material from the spherical shell, so a third thickness must be measured. Substituting this expression for p_{class} into the normalization equation the following expression for q_{crit} is obtained.

$$q_{crit} = \frac{\sqrt{3(1-\nu^2)}}{2} \frac{R^2}{t_b^{3/2}\, t_s^{1/2}} \frac{t_e \cdot a \cdot \delta\ell}{L \cdot \ell}$$

This leads to the following expression for relative error

$$\left|\frac{\Delta q}{q}\right|_{max} = \frac{1}{2}\left|\frac{\Delta\xi}{\xi}\right| + 2\left|\frac{\Delta R}{R}\right| + \frac{3}{2}\left|\frac{\Delta t_B}{t_B}\right| + \frac{1}{2}\left|\frac{\Delta t_s}{t_s}\right|$$

$$+ \left|\frac{\Delta L}{L}\right| + \left|\frac{\Delta\delta\ell}{\delta\ell}\right| + \left|\frac{\Delta t_e}{t_e}\right| + \left|\frac{\Delta a}{a}\right| + \left|\frac{\Delta\ell}{\ell}\right|$$

Using the measuring techniques which have been developed for these experiments, the contributions to the error in q from the quantities R, L, $\delta\ell$, a and ℓ are negligible compared to the error arising from the thickness terms.

These considerations emphasize the necessity of minimizing thickness variations and surface roughness. Most of the tests have been run with shells whose RMS surface roughness (measured with a "Profilometer" made by Physicists Research Company) was about

60 micro inches, with typical thickness variations of $\pm 2\ ^{o}/o$ (see Table III).

The practice of bolting the shells between rings to obtain a clamped boundary condition is questionable. Past experience at GALCIT* has shown that this offers a very poor approximation to a clamped condition. Of even more importance, however, is the fact that this method of mounting almost inevitably will put random moments into the edge of the shell, which depend on how well the shell and the ring conform, and how much normal pressure is applied by the bolts. These moments could buckle the shell: At the very least they will introduce scatter into the value of pressure which is required for buckling.

A method of mounting the shells into the rings without inducing initial deflections via edge moments, which will simulate a true clamped condition to a high degree of approximation, appeared necessary before consistent buckling data could be obtained. The method used for this work shows considerable promise and is outlined in a later section.

Due to the fact that the deflections are governed by nonlinear equations, the effect of internal stress in the unloaded specimen is difficult to evaluate. Kaplan (Ref. 7) attempted to spin shells from aluminum before he turned to magnesium. He found the aluminum shells had high internal stresses and would, he reports, snap with very little external urging. Clearly internal stress should be avoided, and played a part in the choice of material for the present shells.

---

* Graduate Aeronautical Laboratories, California Institute of Technology.

3.3 The Electroforming Process.

Electroforming has been used by Babcock (Ref. 19) for several years to make highly successful cylindrical shells at GALCIT. The method is patterned after one used by Thompson (Ref. 20), to make complete spherical shells. The method is quite simple in concept. A wax form is cut to the desired shape, painted with a conducting paint, and placed in an electroplating tank. Current is passed between a metal anode and the silver coating, and metal is deposited. When the desired thickness is obtained, the wax is melted, leaving a thin shell.

Following Babcock, the plating was carried out in a Copper Fluoborate bath, and the shells were plated from copper. The choice of copper may seem surprising, due to its usual nonlinear stress-strain behavior, even at low stress levels. It was chosen for this work because it is easy to plate, and developes the lowest internal stress during plating of any of the materials considered (Ref. 21). Consistency of bath temperature also plays a role in freedom from internal stress. In order to keep the bath at constant temperature during plating, cooling coils made from 5/8" diameter polyethylene tube were installed. This proved adequate to handle the 160 watts of electrical power which are dissipated in the solution during normal plating, plus any heat generated by mechanical motion. The resultant shells can be cut apart with no visible change of curvature, showing the internal stresses are, indeed, small.

It has been found that 200 cc. of black-strap molasses in thirty gallons of Copper Fluoborate Solution will increase the linear region

of the stress-strain curve markedly. As a result, the material shows no measurable deviation from linearity up to 11,000 psi, and has a defined yield point (0.0001 offset) of about 17,000 psi (Fig. 12). The ultimate strength is about 65,000 psi.

In the previous section, the importance of uniform thickness was stressed. The rate of plating at a point on the cathode surface is governed, all things else being equal, by the electric field strength. In order to obtain uniformity in the shell thickness, therefore, the plating geometry must lead to a uniform field. The field between two concentric spheres is uniform. By making the anode spherical, and spacing it about 3/4" from the spherical cathode, (see Figs. 13 and 14) a uniform spherical field is obtained between the plates, except in a region near the edge. From parallel plate capacitor theory, it is known that this edge disturbance, or "bridging field", affects the uniformity of the field in a band near the edge whose characteristic width is the spacing between the plates. The wax form is 11" in diameter, while only the central 8" is used for the shell. By rejecting a 1 1/2" band at the edge, the thickness variations due to non-uniformity in the field are effectively eliminated.

In order to promote uniformity and smoothness, the shell is removed from the bath four times during plating, and carefully sanded. The anode is then rotated 90° with respect to the cathode, and the plating is resumed. By rotating the anode with respect to the cathode, imperfections in the plating system are randomized and thickness variations due to this source are minimized.

The bridging field at the edge tends to cause treeing of the plated material. This is suppressed with a plexiglass ring (see Fig. 13) which retards the flow of ions into this region and effectively prevents plating and therefore treeing. A plating current of 20 amps is normally used, which gives a current density of about 30 amps/sq. ft.

The machining of the wax is straightforward. The dish is turned in a lathe, and the spherical surface is cut by a tool which is pivoted at the desired spherical radius (Fig. 15). A two to one mixture of refined paraffin and Mobile Cerese 2305 wax has been found (Refs. 19 and 20) to have good machining characteristics, and can be cast free of bubbles. It adequately fulfilled the requirements of this job.

3.4 The Mounting Process

Once the shell has been electroformed, and the wax has been melted from it, it must be cleaned and mounted into rings for testing, without inducing edge moments, and without distorting the spherical shape. Clamping the shell between the rings was rejected for the reasons outlined in Section 3.2. Fixing the edge with a low melting point alloy (Ref. 19) was rejected because of the possibility of introducing thermal stress. Setting the edge into an epoxy cement which would harden at room temperature seemed like an ideal solution. Since a 0.005" to 0.015" void would be filled by the epoxy, it was required to have low shrinkage during hardening. "Devcon Type B Plastic Steel" fulfilled this requirement. In addition, it is easily softened and removed with acetone or alcohol, which facilitates re-use of the rings.

Residual wax is cleaned from the shell with benzene. In its free edge condition, the shell is very flexible, and can be readily distorted from the desired shape. It was evident, therefore, that the shell must be supported in the correct shape until the edge was clamped, in order to maintain close conformity to a spherical shape. A spherical dish 8 1/2" in diameter was machined from jig plate aluminum to support the shell. The shell itself is cut to an 8 7/8" diameter on the lathe while it is still supported by its wax form.

The 8 7/8" shell is centered in the dish and weighted with lead shot. The bottom ring is then glued to the shell, the excess glue is removed, more lead shot is added, and the assembly is allowed to harden (see Fig. 18). The overhang of the shell with respect to the dish prevents glue from seeping between them, and facilitates cleanup of the excess glue. Once the glue has set, the lead shot is removed and the ring-shell assembly is lifted from the dish. The shell is now rigid, due to the clamped edge support, so the upper ring can be glued in place without further support for the shell (see Fig. 19). Two pins are used to locate the rings concentrically. The upper and lower rings are held together by six bolts while the glue is drying, but shims are inserted between the rings to insure that the upper ring does not bear on the shell. A cap now closes off the upper half, and forms a pressure chamber. A valve is provided so that air can be bled from the system.

3.5 Testing Procedure.

A basic requirement for the testing program was a device to measure shell deflections as a function of radius. The requirements for this device were:

1. It should apply as little force as possible to the shell during measurement.
2. It should be able to quickly traverse a radius, and preferably also traverse in the theta direction, and measure deflections of a few percent of a shell thickness.

The device which was built is capable of repeating measurements to 0.0001". The absolute error, determined by traversing a precision flat, is better than $\pm$ 0.0002". The details are shown in Fig. 17 and 20. Unfortunately, the present device must be locked in place along a preselected radius, and cannot be moved in the θ direction during loading.

The location of a point on the surface of the shell is determined by a screw which sets the r coordinate, and a micrometer which measures the distance down to the shell from the traversing plane. A spring loaded point is brought into electrical contact with the shell, as determined by an ohmmeter. This system approaches the ideal of no force which is attained with electronic "measurement at a distance" gages such as the eddy current Bently gage (even these gages exert small electromagnetic forces of course), and at the same time maintains a very precise knowledge of the r, θ location of the measurement. Most of the electronic gages give an integrated average

distance to some small area, of order say $1/50$ in^2, while the point on the micrometer (Fig. 20) obviously integrates over an area several orders of magnitude smaller.

The shells were loaded with oil pressure. Since buckling pressures ranged from a few cm. of mercury to over 150 cm., both a water and a mercury manometer were provided to measure the pressures. The use of a manometer decreased the rigidity of the testing machine, and made the test condition a very poor approximation to either rigid displacement or dead weight testing. However, the testing machine makes no difference in the buckling load, if buckling occurs via the "classical criteria" assumed in the theory of Section II. The agreement between the buckling loads obtained in these tests and theoretical loads based on the classical criterion, plus the null result of Kaplan and Fung's (Ref. 7) experiments to detect a difference between air and oil load, tend to justify the assumption that the elasticity of the testing machine is of no consequence in these experiments.

3.6 Material Properties.

Three properties of the material are required for data reduction, namely, E(Young's Modulus), ν (Poisson's Ratio), and μ(Density). The density was used in the determination of thickness.

The modulus E was measured with a simple tension test. If a long strip of length ℓ and cross sectional area A is loaded in tension by a weight L, the modulus is related to the resultant change in length $\Delta \ell$ by the expression

$$E = \frac{\ell L}{A \Delta}$$

At 10,000 psi, which is the approximate stress limit for this linear relationship, $\frac{\Delta \ell}{\ell} \approx 6 \times 10^{-4}$. In order to make $\Delta \ell$ an easily measured quantity, therefore, it is important to make ℓ large, say of the order of 10^2 in.

Specimens 200" long of electroplated copper were obtained in the following manner. A cylinder 8" in diameter and 15" long was plated as described in reference 19. The shell, on its wax form, was then placed in the lathe, and cut with the threading mechanism into a 1/2" wide spiral. The cross sectional area of the spiral was determined by weighing the strip and using μ to find the volume. Upon dividing the volume by the length, the average cross sectional area was obtained. Marks 200" apart were scribed on the copper, and the motion of these points under load was recorded using two traveling microscopes. In this manner the stress-strain relationship of Fig. 12 was obtained, and E was calculated to be 16×10^6 lb/in^2. Several tests were made with different shells, and this value was found to vary $\pm$ 3 %/o from shell to shell. In view of this scatter, which appears to depend on plating conditions, it was thought to be desirable to develop a means of measuring E for each shell which was tested.

Strain gauges were fixed to a 200" specimen, in an effort to correlate strain measurements from this source with the optical method. Unfortunately, the strain gauge scatter was at least $\pm$ 5 %/o, ending any hope of using strain gauges to measure the strain.

Testing in an Instron machine, and using the head motion to determine strain, also proved to be hopeless. Machine deflections account for at least 25 ^{o}/o of the observed strain in a specimen 8" x 1/2" x 0.030", and these deflections proved to be highly nonlinear and non-repeatable, probably due to random motions in the bearings of the machine.

Because of these difficulties, the figure $E = 16.0 \pm 0.5 \times 10^6$ was accepted for all the shells which were tested.

Poisson's Ratio, ν, enters the expressions for q_{crit} and λ in the form $1 - \nu^2$. Since ν is constrained to fall between the limits $\nu = 0$ and $\nu = 0.5$, the determination of ν is not critical. In view of this, a handbook value was expected to be acceptable. A short survey, however, turned up published values of ν ranging from $\nu = 0.18$ to $\nu = 0.48$.

Strain gauges were attached to a tensile specimen in pairs, one longitudinal, and one transverse. The ratio of the strains was calculated, and values for ν were obtained in the range $\nu = 0.35$ to $\nu = 0.38$. This result justified comparing the experimental data to the $\nu = 1/3$ theoretical data published by Huang (Ref. 16).

The density of vacuo-distilled copper is given in handbooks as $\mu = 8.9326$ gm/cc at 20^{o}C (Kahlbaum, 1902). The electroplated copper was weighed in air, and immersed in water, and the calculated density was 8.9^{+}. Therefore the vacuo-distilled figure was used for data reduction.

3.7 Data Reduction

In addition to the material properties, the quantities R, t, b, and p_{crit} must be measured. The radius b is fixed by the rings, which were machined to a diameter of 8.000 ± 0.002. Thus b is known to a negligibly small 0.02 °/o. The buckling pressure p_{crit} was measured with either a water or a mercury manometer, to the nearest millimeter. The shells typically buckled at pressures greater than 500 mm of water, so p_{crit} was also determined to a fraction of a percent.

The thickness t, which is very critical in the data reduction, was calculated from the weight, the measured area and the density of the shell. However, the small errors inherent in this method do not reflect the true errors in t, which arise largely from the thickness variations of the shell and the roughness of the surface, as outlined in Section 3.2.

The spherical radius R, was determined from measurements which were made on the mounted shells, after the chamber was filled with oil, and just prior to the application of pressure. The traversing mechanism (Fig. 20) was set up along a diameter of the shell, and the distance between the traversing plane and the shell was measured at 17 stations. The spherical radius R was taken to be the radius of the circle which had the smallest least mean square deviation from these 17 data points.

The deviations from this "best circle" are shown in Figs. 21 and 22 for typical shells. In order to test the consistency of the

spherical radius obtained by this method, the measurements were repeated along a second diameter for several of the shells. The value of spherical radius obtained from the two sets of data was found to agree to better than 1 part in 10^3 in all cases.

IV. TEST RESULTS

Buckling tests were performed on shells with nominal spherical radii of 40" and 20". All of the shells were tested in rings whose radius was 4.0". In order to limit the membrane buckling stress

$$\sigma_{crit} = \frac{Et}{\sqrt{3(1-\nu^2)}\,R}\, q_{crit}$$

to values within the linear region of the plated copper ($\sigma_{crit} < 11,000$ psi), the restriction $t < 0.045$ was adopted. As $t \rightarrow 0.0$, the buckling load $p_{crit} \rightarrow 0.0$, so a lower limit on thickness is reached, below which the present handling and testing techniques are not adequate. A second limiting factor is the initial imperfection of the shell, which tends to remain constant in magnitude, and thus to grow in comparison to the thickness, as thickness decreases. In these experiments the lower practical limit for t was in the range 0.005" to 0.0010". In this range and below, the buckling data became sporadic, and relatively low values were recorded for some of the shells which were tested. Values of q_{crit} as low as $q_{crit} = 0.45$ were found for two 20" shells whose thicknesses were 0.0048 and 0.0073 for example.

Within these constraints it was possible to make shells with values of λ in the range $5.5 < \lambda < 20$. The 40" shells cover the range $5.5 < \lambda < 12$, while the 20" shells fall in the range $10 < \lambda < 20$. The agreement between the data in the region where similar values of λ were tested was fair (Fig. 23). The 40" data tended to fall below the 20" data near $\lambda = 12$. The thinness of the 40" shells probably accounts for the difficulty.

The rise of the shells can be calculated from the equation

$$h = R(1 - \cos\phi) = R(1 - \sqrt{1 - b^2/R^2}) \approx \frac{b^2}{2R}$$

For the two types of shells which were tested, the values $h_{40''} \approx 0.2''$ and $h_{20''} \approx 0.4''$ are obtained. Thus, both types of shells fulfill the "shallowness assumption" $h/b < 1/8$, and can properly be classed as shallow spherical shells.

Since the buckling loads calculated by Huang (Ref. 16) using numerical methods agree with those of Section II, which were obtained by Galerkin's method, within the range of λ where the approximations of Section II are valid, the buckling loads of Huang are used in the subsequent comparison between theory and experiment.

The initial imperfections for the shells, along an arbitrarily selected diameter are shown in Figs. 21 and 22. The buckling pressures as a function of λ are shown in Fig. 23.

Deflection vs. radius measurements were made along an arbitrarily selected diameter, as a function of load. These measurements are shown for typical shells in Figs. 24-33 inclusive. The deflection vs. load behavior according to the approximate theory of Section II is shown for shells for which $\lambda < 12$. The agreement is quite good, while the inadequacy of the assumed deflection shape is evident as $\lambda \rightarrow 12$.

V. CONCLUDING REMARKS

The wide variance between the present experimental buckling loads and previous data lends support to the thesis that small differences between experimental and theoretical conditions can lead to large differences in buckling load. In particular, the uncertainties introduced by variations in thickness and improper boundary conditions should be emphasized. On the other hand, the agreement with the theory of Huang indicates that the classical static criterion of buckling may be adequate. In particular, artificial buckling criterion such as the "energy criterion" of Tsien are not required to explain these experiments.

The recent theoretical results of Weinitschke (Ref. 15) are in striking contrast to the present result. Although the same governing differential equations are used, no agreement between his asymmetrical buckling loads (Fig. 4) and the present theory or experiments can be found. The agreement between his theory, and previous experiments, appears to be fortuitous, since the stability curve has been computed for the asymmetrical buckling of perfect shells, while the low values which were previously found for buckling loads now appear to have been the result of imperfections in the experiments. Recent calculations by Thurston (Ref. 22), in which the effect of symmetrical imperfections on buckling load is considered, substantiate this opinion.

The present work raises one interesting point with regard to Huang's (Ref. 16) results. For $\lambda < 10$, both the present theory and experiment support the existence of $n = 2$ and $n = 3$ asymmetrical

buckling. However, for $\lambda < 10$, the experimental results lie above the stability curve of Huang (Fig. 23), and may indicate a return to symmetrical buckling. The present theory is not valid in this region of course. However, the $n = 4$, and $n = 5$ mode solutions begin to occur below the snap buckling load for values of λ as low as $\lambda = 7$ in Huang's theory (Fig. 4). No solutions for $n = 5$ or $n = 6$ were found in the present theory (Figs. 8 - 11 inclusive).

This observation may simply reflect inadequacies in the present work. On the other hand, the $n > 4$ instabilities which Huang has found may be in error.

The variation of the stability curve with ν has not been pointed out before. Some authors have presented curves for a stated value of ν, while others have presented curves without mentioning the value of ν which was used in the calculations. The 20 % variation from this effect (Figs. 8 - 11 inclusive) will become significant as the experiments improve.

In conclusion, it appears that some of the questions which have shrouded the problem of the buckling of shells have at last been answered. Agreement between theory and experiment has been obtained using time honored concepts of buckling. The approach to more complicated problems seems clear. The nonlinear equations governing the precise shape of the shell must be investigated for snap buckling points. The boundary conditions must be carefully specified. In addition, the linear equations governing admissible perturbations

around the large deflection equilibrium positions must be investigated to determine bifurcation buckling points. Diligent adherence to this program may well clear up the mystery which has surrounded certain shell buckling problems.

REFERENCES

1. Fung, Y. C. and Sechler, E. E.: "Instability of Thin Elastic Shells", Structural Mechanics, Proc. of First Symposium on Naval Structural Mechanics, pp. 115-167, Pergamon Press (1960).

2. Thompson, J. M. T.: "Basic Principles in the General Theory of Elastic Stability", Journal of the Mechanics and Physics of Solids, Vol. 11, pp. 13-20, Pergamon Press (1963).

3. Ziegler, H.: "On the Concept of Elastic Stability", Advances in Applied Mechanics, Vol. IV, p. 351, Academic Press (1956).

4. Hoff, N. J., and Bruce, V. G.: "Dynamic Analysis of the Buckling of Laterally Loaded Flat Arches", PIBAL Rep. 191, Contract Nonr-26700, Office of Naval Research and Polytechnic Institute of Brooklyn (1951).

5. von Karman, T. and Tsien, H. S.: "The Buckling of Spherical Shells by External Pressure", Journal of the Aeronautical Sciences, Vol. 9, No. 10, pp. 373-384 (1942).

6. Feodosiev, V. I.: "Calculation of Thin Clicking Membranes", Prikladnaia Matematika i Mekhanika, Vol. X, p. 295 (1946).

7. Kaplan, A. and Fung, Y. C.: "A Nonlinear Theory of the Bending and Buckling of Thin Elastic Shallow Spherical Shells", NACA Technical Note 3212 (1954).

8. Archer, R. R.: "Stability Limits for a Clamped Spherical Shell Segment under Uniform Pressure", Quarterly of Applied Mathematics, Vol. XV, p. 355-366, (1958).

9. Weinitschke, H. J.: "On the Nonlinear Theory of Shallow Spherical Shells", Journal of the Society for Industrial and and Applied Mathematics, Vol. 6, p. 209 (1958).

10. Budiansky, B.: "Buckling of Clamped Shallow Spherical Shells" Proceedings of the Symposium on the Theory of Thin Elastic Shells, North Holland Publisning Company, pp. 64-94 (1950).

11. Thurston, G. A.: "A Numerical Solution of the Nonlinear Equations for Axisymmetric Bending of Shallow Spherical Shells", Journal of Applied Mechanics, Vol. 28, pp. 557-568 (1961).

12. Budiansky, B. and Weinitschke, H.: "On Axisymmetrical Buckling of Clamped Shallow Spherical Shells", Journal of the Aeronautical Sciences (Readers Forum), Vol. 27, pp 545-546 (1960).

13. Grigolyuk, E. I.: "On the Unsymmetrical Snapping of Shells of Revolution". Proceedings of the Symposium on the Theory of Thin Elastic Shells, North Holland Publishing Company, pp. 112-121 (1960).

14. Gjelsvik, A. and Bodner, S. R.: "The Non-Symmetrical Snap Buckling of the Clamped Spherical Cap". Technical Report No. 30, Engineering Division, Brown University (1962).

15. Weinitschke, H. J.: "Asymmetric Buckling of Clamped Spherical Shells", Collected Papers on Instability of Shell Structures, NASA TN D-1510, pp. 481-490 (1962).

16. Huang, Nai-Chien: "Unsymmetrical Buckling of Shallow Spherical Shells", American Institute of Aeronautics and Astronautics Journal, Vol. I, No. 4, p. 945 (1963).

17. Homewood, R. H., Brine, A. C., and Johnson, A. E.: "Experimental Investigation of the Buckling Instability of Monocoque Shells", SESA Paper No. 547, Vol. 18, No. 1, pp. 88-96 (1961).

18. Bellinfante, R. J., "Buckling of Spherical Caps under Uniform External Pressure", Douglas Aircraft Company Report No. SM-38938 (1962).

19. Babcock, C. D.: "The Buckling of Cylindrical Shells with an Initial Imperfection under Axial Compression Loading", Ph. D. Thesis, California Institute of Technology (1962).

20. Thompson, J. M. T.: "Making of Thin Metal Shells for Model Stress Analysis", Journal Mech. Eng. Sciences, Vol. 2, No. 2, pp. 105-108 (1960).

21. Gray, A. G.: Modern Electroplating, John Wiley and Sons, Inc. New York (1953).

22. Thurston, G. A.: "Comparison of Experimental and Theoretical Buckling Pressures for Spherical Caps", Collected Papers on Instability of Shell Structures", NASA TN D-1510, pp. 515-522 (1962).

23. Timoshenko. S.: "Theory of Elastic Stability", First Edition, McGraw and Hill, pp. 491-497 (1936).

APPENDIX A

The problem of calculating the classical buckling load of a complete sphere is considered in detail in reference 23, for the case of a symmetrical buckling mode. In terms of the parameters

$$\alpha = \frac{D(1 - \nu^2)}{R^2 E t_s}$$

$$\phi = \frac{p R(1 - \nu^2)}{2Et_s}$$

where

$$D = \frac{Et_b^3}{12(1 - \nu^2)}$$

the lowest critical buckling load is shown to be given by the condition

$$\phi = 2\sqrt{(1 - \nu^2)\alpha} - 6\nu\alpha$$

Thus

$$p_{crit} = \frac{2Et_s}{R(1 - \nu^2)} \left[2\sqrt{(1 - \nu^2)\alpha} - 6\nu\alpha \right]$$

If the distinction between t_b and t_s is maintained the expression

$$p_{crit} = \frac{2Et_s}{R(1-\nu^2)} \left[\frac{1}{R}\sqrt{\frac{t_b^3(1-\nu^2)}{3\,t_s}} - 6\,\nu\,\frac{t_b^3}{12\,R^2 t_s} \right]$$

is obtained for the buckling pressure. For thin spherical shells, the second term in the brackets can be ignored compared to the first and the buckling load can be written

$$p_{crit} = \frac{2\,E\,t_b^{3/2}\,t_s^{1/2}}{R^2\sqrt{3(1-\nu^2)}}$$

TABLE I

COEFFICIENTS OF THE SYMMETRICAL EQUATIONS (Eq. 12) FOR VARIOUS VALUES OF POISSON'S RATIO

	$\nu = 0$			$\nu = 1/4$		
	Eq. 1	Eq. 2	Eq. 3	Eq. 1	Eq. 2	Eq. 3
A_1	-5.814	-1.699	1.644	-6.869	-2.460	1.644
A_2	-5.099	-29.25	-5.406	-7.380	-34.57	-7.870
A_3	4.934	-5.406	-53.57	4.934	-7.870	-63.07
A_4	-6.327	-81.54	-21.94	-9.369	-98.43	-31.80
A_5	-29.25	-18.98	-18.93	-34.57	-29.11	-22.48
A_6	-18.93	-65.82	-244.9	-22.48	-95.39	-294.4
A_7	6.692	-50.10	-398.9	6.692	-72.28	-484.4
A_8	-53.57	-11.27	20.08	-63.07	-18.12	20.08
A_9	-11.27	-244.9	-150.3	-18.12	-294.4	-216.8
A_{10}	36.53	25.28	5.431	44.06	33.12	9.463
A_{11}	71.79	171.8	128.4	87.92	222.5	164.3
A_{12}	109.6	190.8	331.9	132.2	247.6	440.8
A_{13}	50.57	143.6	51.76	66.25	175.8	69.29
A_{14}	10.86	51.76	219.1	18.93	69.29	264.3
A_{15}	51.76	256.9	381.5	69.29	328.6	495.2
A_{16}	-3686.	-3283.	-1015.	-3686.	-3283.	-1015.
A_{17}	-52.84	-71.66	-56.62	-64.79	-91.75	-75.80
A_{18}	-3283.	-45710.	-32400.	-3283.	-45710.	-32400.
A_{19}	-71.66	-126.7	-107.4	-91.75	-160.4	-139.7
A_{20}	-1015.	-32400.	-215700.	-1015.	-32400.	-215700.
A_{21}	-56.62	-107.4	-117.6	-75.80	-139.7	-148.4
A_{22}	1189.	2000.	1910.	1189.	2000.	1910.

TABLE I (Cont'd)

COEFFICIENTS OF THE SYMMETRICAL EQUATIONS (Eq. 12) FOR VARIOUS VALUES OF POISSON'S RATIO

	$\nu = 1/3$			$\nu = 1/2$		
	Eq. 1	Eq. 2	Eq. 3	Eq. 1	Eq. 2	Eq. 3
A_1	-7.397	-2.840	1.644	-8.980	-3.981	1.644
A_2	-8.521	-37.23	-9.102	-11.94	-45.20	-12.80
A_3	4.934	-9.102	-67.82	4.934	-12.80	-82.06
A_4	-10.89	-106.9	-36.72	-15.45	-132.2	-51.51
A_5	-37.23	-32.67	-24.26	-45.20	-46.36	-29.58
A_6	-24.26	-110.2	-319.2	-29.58	-154.5	-393.4
A_7	6.692	-83.36	-527.2	6.692	-116.6	-655.4
A_8	-67.82	-21.54	20.08	-82.06	-31.81	20.08
A_9	-21.54	-319.2	-250.1	-31.81	-393.4	-349.9
A_{10}	47.83	37.04	11.48	59.13	48.80	17.53
A_{11}	95.97	247.8	182.2	120.2	323.8	235.9
A_{12}	143.4	276.0	495.3	177.4	361.2	658.5
A_{13}	74.09	192.0	78.06	97.61	240.3	104.3
A_{14}	22.96	78.06	286.9	35.05	104.3	354.7
A_{15}	78.06	364.4	552.0	104.4	471.9	722.4
A_{16}	-3686.	-3283.	-1015.	-3686.	-3283.	-1015.
A_{17}	-70.76	-101.8	-85.39	-88.68	-131.9	-114.2
A_{18}	-3283.	-45710.	-32400.	-3283.	-45710.	-32400.
A_{19}	-101.8	-177.3	-155.8	-131.9	-228.0	-204.2
A_{20}	-1015.	-32400.	-215700.	-1015.	-32400.	-215700.
A_{21}	-85.39	-155.8	-163.8	-114.2	-204.2	-210.0
A_{22}	1189.	2000.	1910.	1189.	2000.	1910.

TABLE II

COEFFICIENTS OF ASYMMETRICAL EQUATIONS (Eq. 13) FOR N = 1 → 6 AND VARIOUS VALUES OF POISSON' RATIO

$\nu = 0$

	N = 1	N = 2	N = 3	N = 4	N = 5	N = 6
B_1	-3.188	-4.812	-6.989	-10.04	-13.98	-18.82
B_2	-5.983	-6.555	-14.18	-25.06	-38.86	-55.63
B_3	-0.4504	9.750	18.23	25.72	33.37	41.51
B_4	-12.18	-36.49	-51.24	-66.98	-84.53	-104.0
B_5	-11.62	-34.01	-58.27	-87.64	-125.8	-173.3
B_6	-21.96	-49.93	-99.10	-154.0	-212.2	-273.1
B_7	15.79	19.82	30.20	46.03	66.96	92.81
B_8	26.42	56.02	87.70	126.8	175.2	233.3
B_9	18.38	23.57	42.78	69.11	101.5	139.8
B_{10}	-8.793	-8.311	-8.034	-7.877	-7.787	-7.733
B_{11}	-4807.	-9614.	-30440.	-86520.	-204800.	-419800.

TABLE II (Cont'd)

COEFFICIENTS OF ASYMMETRICAL EQUATIONS (Eq. 13) FOR N = 1 ⟶ 6 AND VARIOUS VALUES OF POISSON'S RATIO

$\nu = 1/4$

	N = 1	N = 2	N = 3	N = 4	N = 5	N = 6
B_1	-3.749	-5.639	-8.587	-12.69	-17.97	-24.42
B_2	-6.882	-8.582	-16.76	-28.88	-44.53	-63.62
B_3	-0.5580	9.416	17.74	25.58	33.44	41.67
B_4	-14.45	-40.19	-58.33	-78.07	-100.7	-126.4
B_5	-14.35	-37.83	-66.52	-101.2	-145.3	-199.9
B_6	-26.84	-58.18	-114.0	-178.7	-248.9	-324.3
B_7	18.54	24.37	38.13	58.80	85.95	199.4
B_8	31.18	64.61	101.8	148.8	207.4	278.2
B_9	22.84	31.52	56.48	90.50	132.7	183.0
B_{10}	-9.215	-8.559	-8.180	-7.967	-7.844	-7.770
B_{11}	-4807.	-9614.	-30440.	-86520.	-204800.	-419800.

TABLE II (Cont'd)

COEFFICIENTS OF ASYMMETRICAL EQUATIONS (Eq. 13) FOR N = 1⟶6 AND VARIOUS VALUES OF POISSON'S RATIO

$\nu = 1/3$

	N = 1	N = 2	N = 3	N = 4	N = 5	N = 6
B_1	-4.025	-6.088	-9.412	-14.04	-19.98	-27.22
B_2	-7.315	-9.426	-17.98	-30.79	-47.38	-67.62
B_3	-0.598	9.002	17.65	25.59	33.52	41.75
B_4	-15.57	-42.18	-61.87	-83.59	-108.7	-137.7
B_5	-15.68	-40.04	-70.75	-107.8	-154.9	-213.2
B_6	-29.26	-62.45	-121.7	-191.2	-267.4	-349.8
B_7	19.89	26.64	42.11	65.20	95.46	132.7
B_8	33.49	68.80	108.8	159.8	223.5	300.7
B_9	25.02	35.42	63.22	101.1	148.2	204.5
B_{10}	-9.374	-8.652	-8.235	-8.000	-7.865	-7.784
B_{11}	-4807.	-9614.	-30440.	-86520.	-204800.	-419800.

TABLE II (Cont'd)

COEFFICIENTS OF ASYMMETRICAL EQUATIONS (Eq. 13) FOR N = 1—→6 AND VARIOUS VALUES OF POISSON'S RATIO

$\nu = 1/2$

	N = 1	N = 2	N = 3	N = 4	N = 5	N = 6
B_1	-4.847	-7.481	-11.92	-18.09	-26.00	-35.64
B_2	-8.574	-11.74	-21.60	-36.52	-55.94	-79.67
B_3	-0.6871	8.772	17.57	25.71	33.72	41.96
B_4	-18.88	-48.22	-72.40	-100.0	-132.9	-171.3
B_5	-19.61	-46.91	-83.38	-127.7	-183.7	-252.8
B_6	-36.52	-75.44	-144.7	-228.4	-322.4	-426.2
B_7	23.86	33.51	54.09	84.42	124.0	172.7
B_8	40.29	81.11	129.6	192.5	271.8	368.0
B_9	31.45	46.95	83.24	132.7	194.6	269.1
B_{10}	-9.722	-8.856	-8.356	-8.075	-7.912	-7.815
B_{11}	-4807.	-9614.	-30440.	-86520.	-204800.	-419800.

TABLE III

SUMMARY OF BUCKLING TESTS

Shell	R inches	$t \times 10^3$ inches	λ	RMS* roughness convex surface	RMS* roughness concave surface	p_{crit} (cm.Hg)	$q_{crit.}$
1	40.94	16.8	8.69	40	35	11.2	0.65
2	40.85	9.4	11.62	40	40	3.34	0.62
3	40.58	20.0	8.00	30	110	17.2	0.69
4	39.49	32.3	6.38	50	35	48.0	0.70
5	39.21	9.2	12.02	60	30	3.49	0.63
6	39.92	40.3	5.68			71.7	0.69
7	19.83	13.1	14.14	40	70	40.1	0.90
8	19.74	10.4	15.88	40	70	21.1	0.74
9	19.87	16.9	12.43			50.0	0.68
10	19.69	12.7	14.42	40	50	34.7	0.82
11	19.44	15.5	13.13	30	35	56.3	0.87
12	19.54	8.9	17.26			17.5	0.83
13	19.58	26.3	10.04	30	30	138.9	0.76
14	19.48	10.3	16.07	35	40	24.0	0.84
15	19.44	21.2	11.21	25	20	98.0	0.81
16	19.50	8.3	17.88	25	15	15.5	0.83
17	19.42	6.5	20.32	25	15	8.1	0.72
18	38.59	11.5	10.83	20	20	5.9	0.66
19	37.61	10.0	11.73	30	10	4.73	0.65
20	39.55	13.6	9.84	30	25	8.6	0.72
21	39.14	20.5	8.04	35	20	20.0	0.71
22	39.39	9.6	11.71	8	25	4.43	0.73

*inches $\times 10^6$

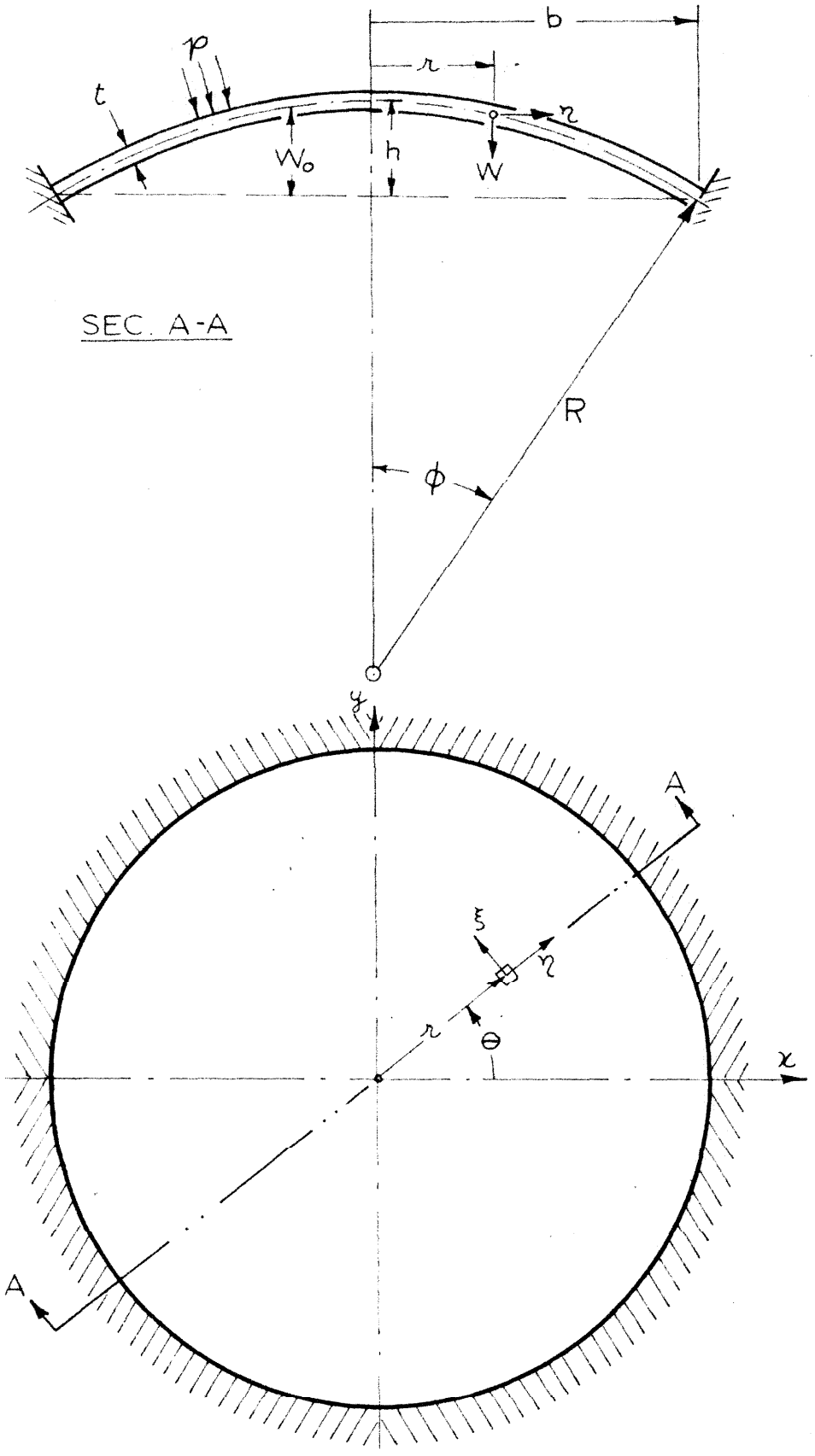

FIGURE 1: GEOMETRY

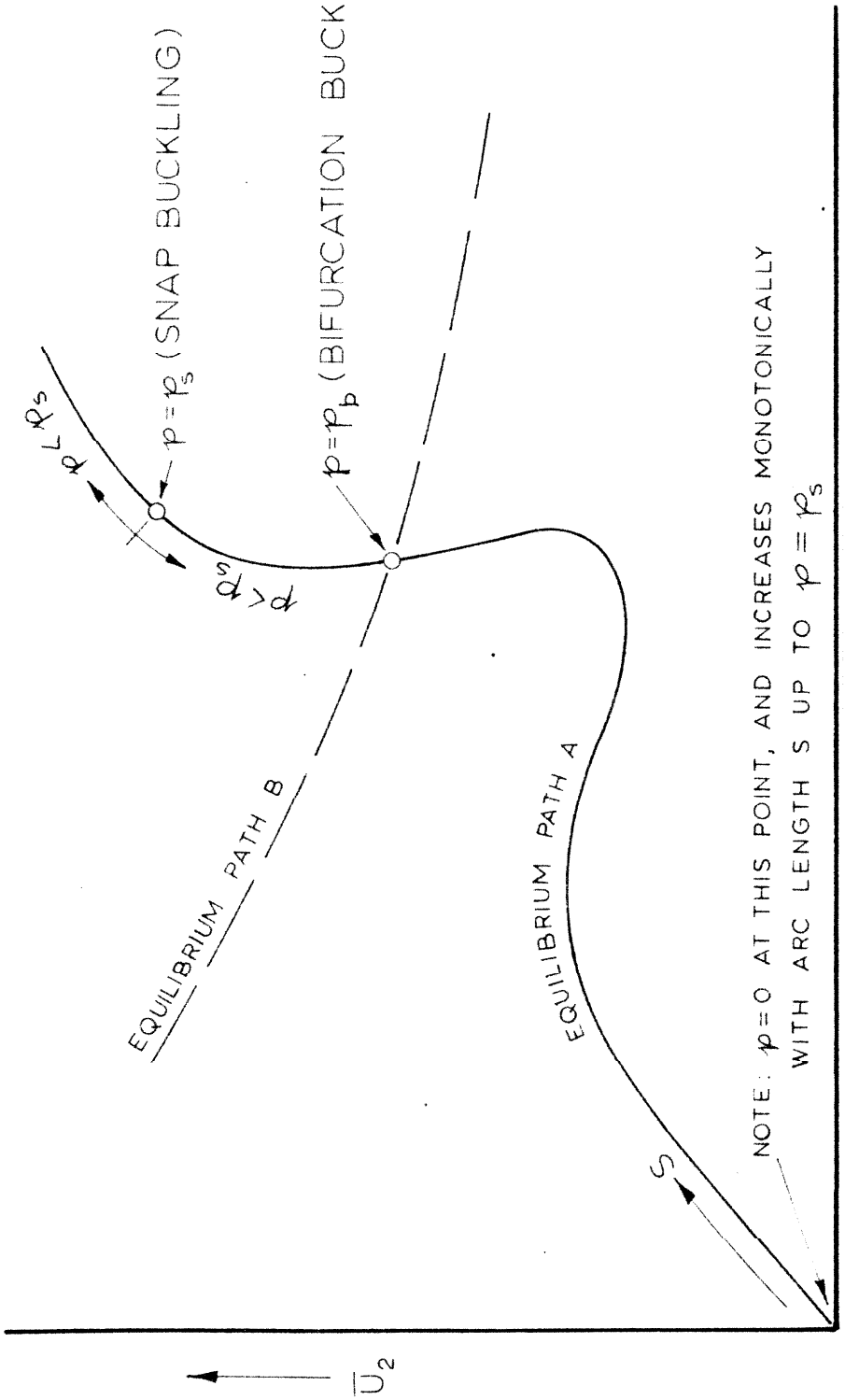

FIGURE 2a: TYPICAL EQUILIBRIUM PATHS IN CONFIGURATION SPACE FOR THE CASE N = 2

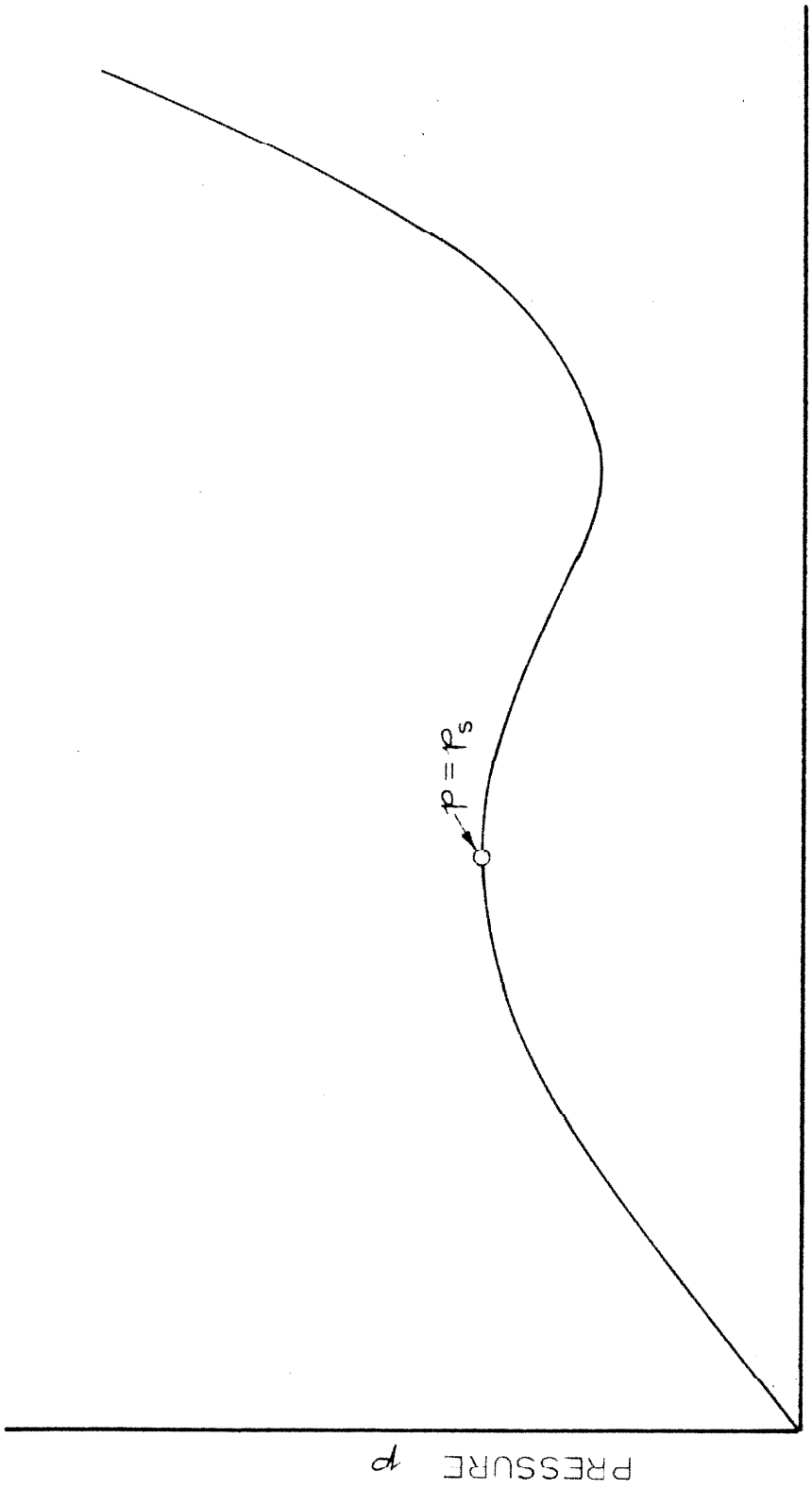

FIGURE 2b: PRESSURE VS. ARC LENGTH FOR PATH A OF FIGURE 2a

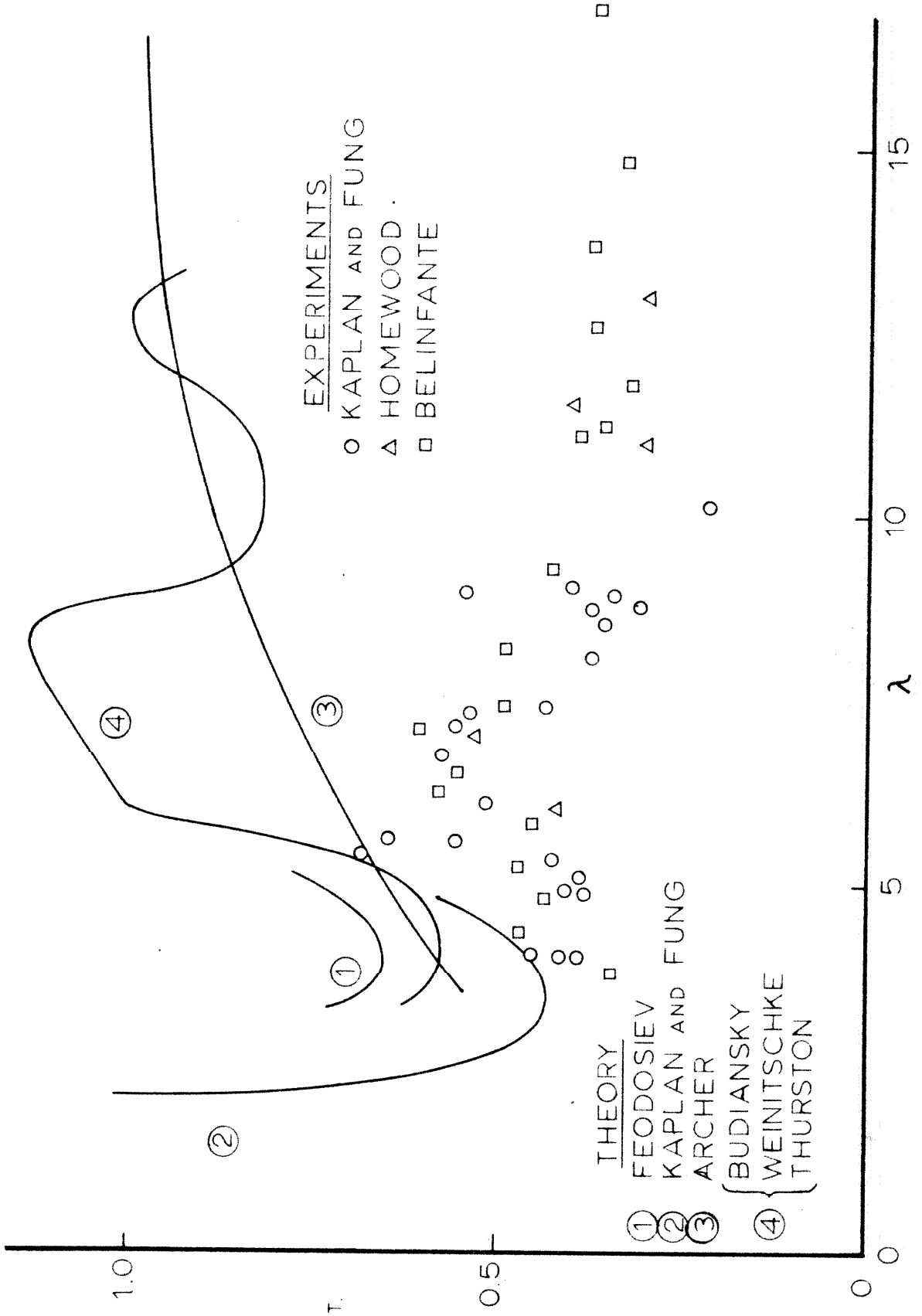

FIGURE 3: EARLY RESULTS

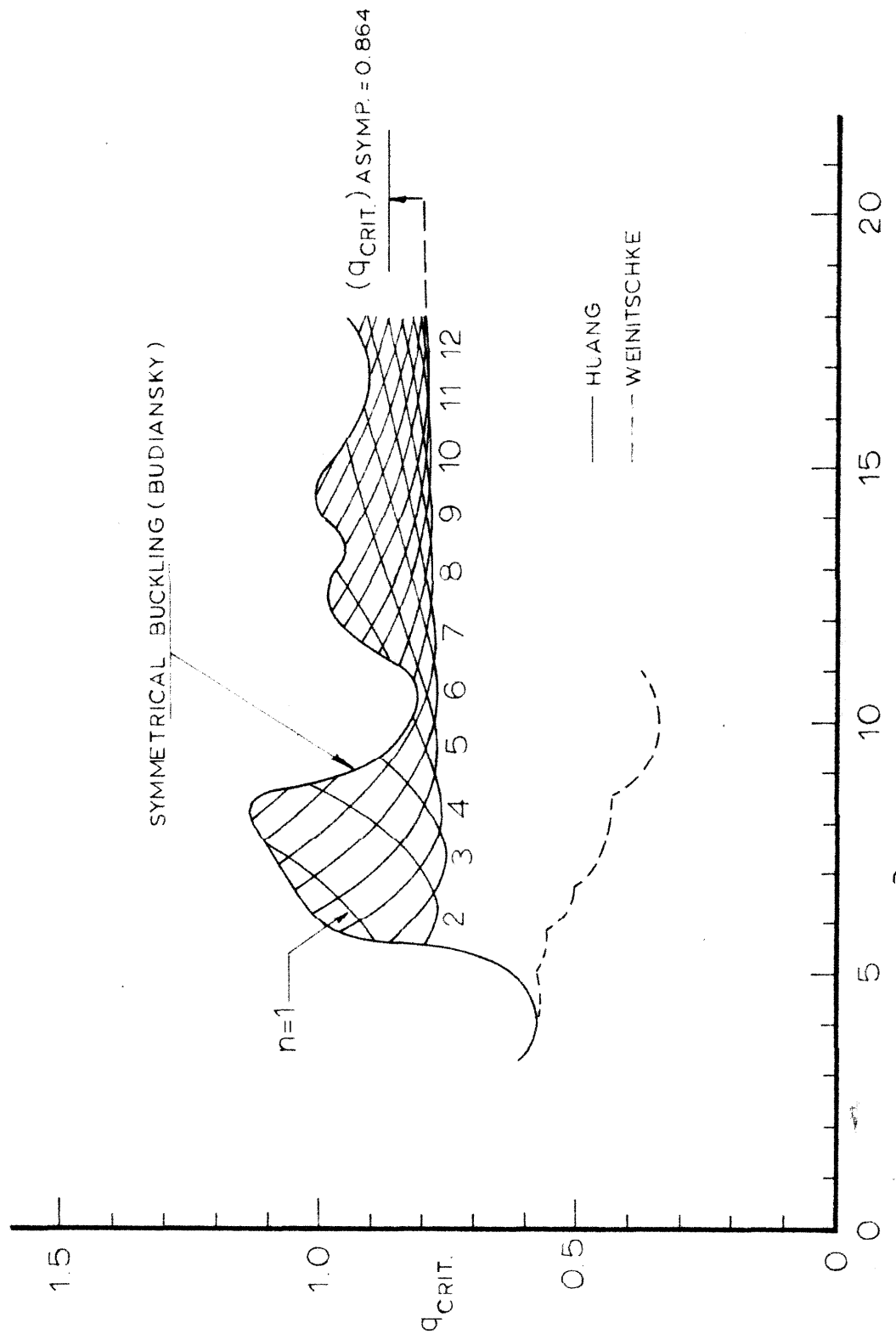

FIGURE 4: RECENT THEORETICAL RESULTS FOR ASYMMETRICAL BUCKLING

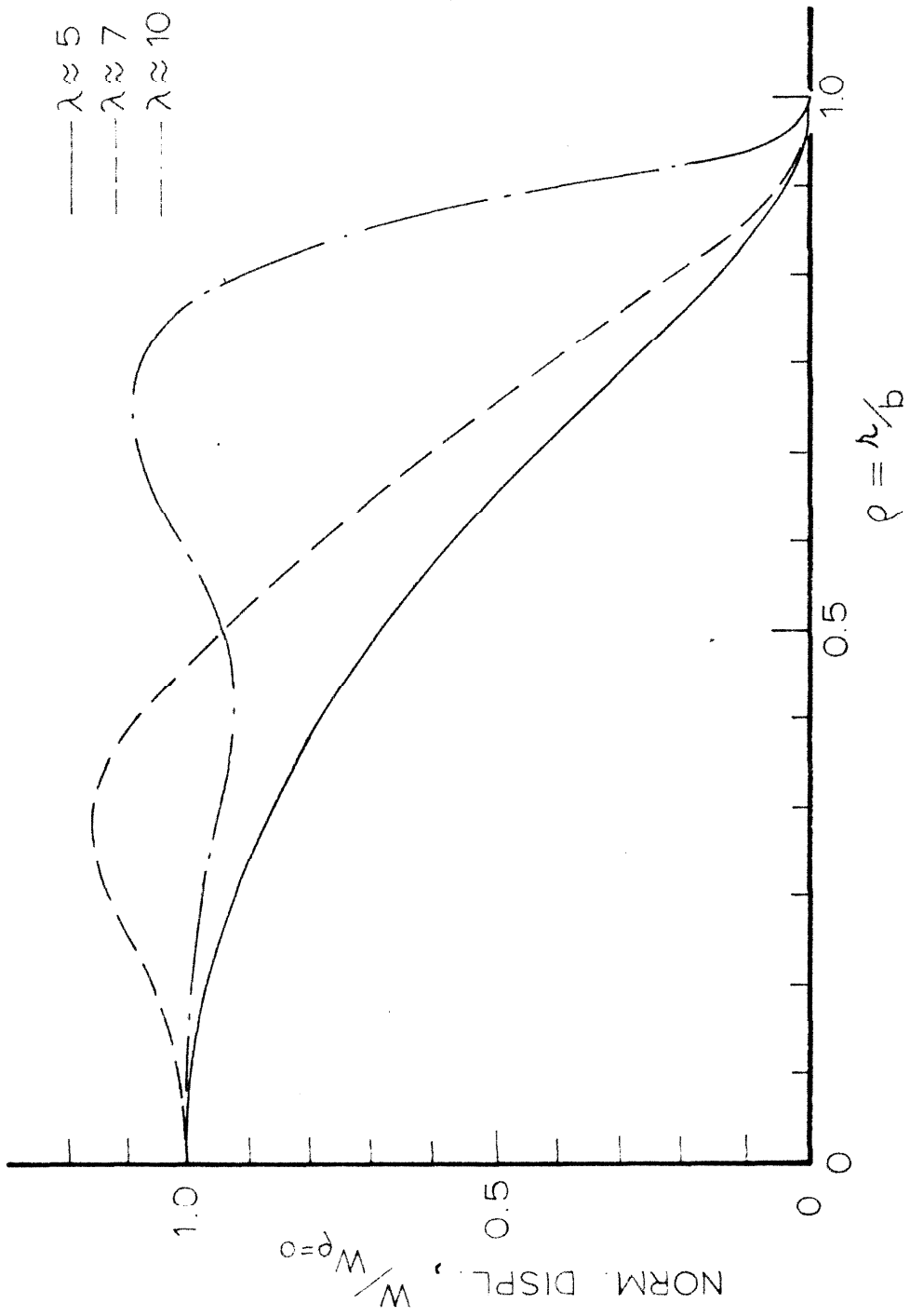

FIGURE 5. VARIATION OF DISPLACEMENT MODE WITH λ

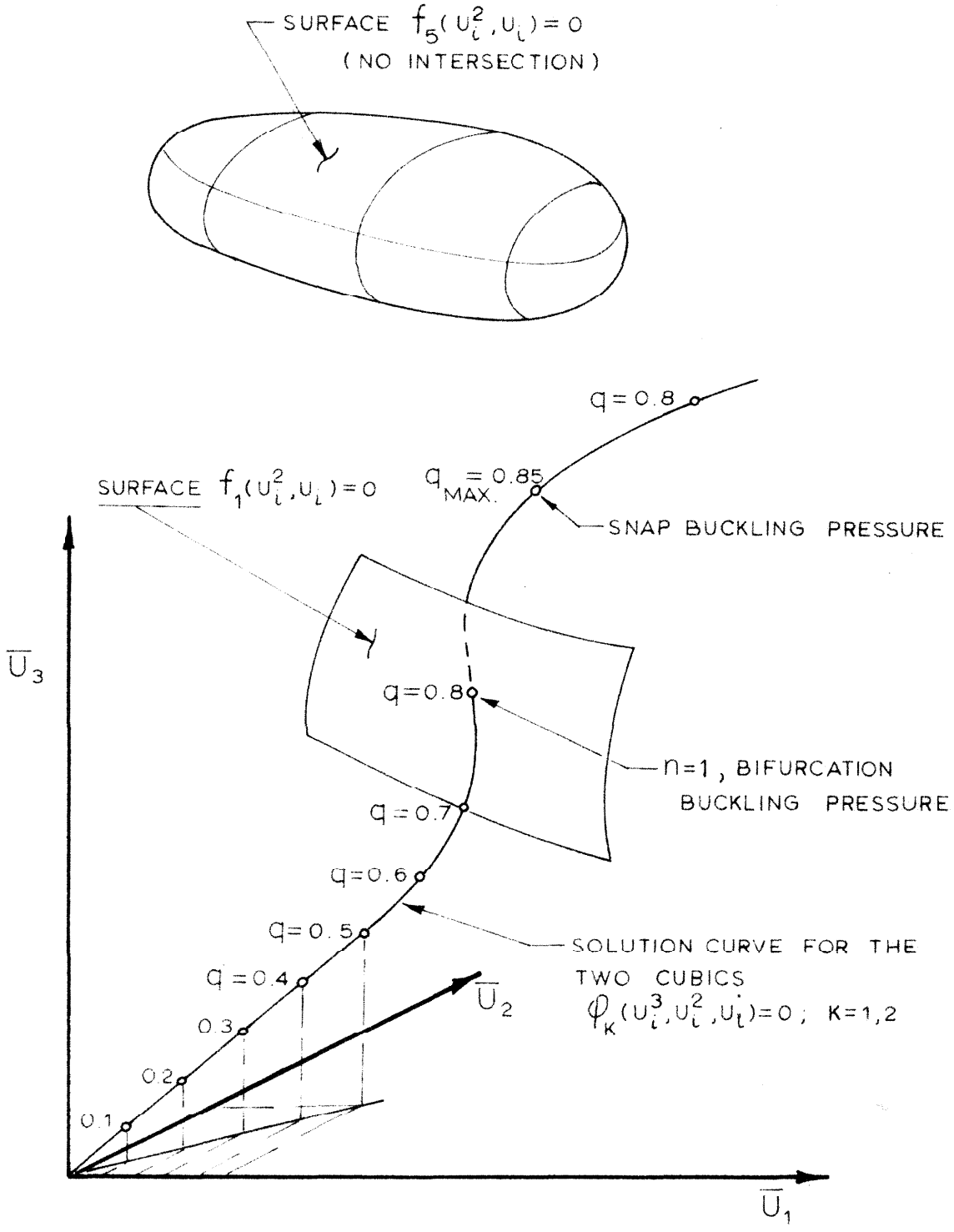

FIGURE 6: EQUILIBRIUM PATH IN CONFIGURATION SPACE

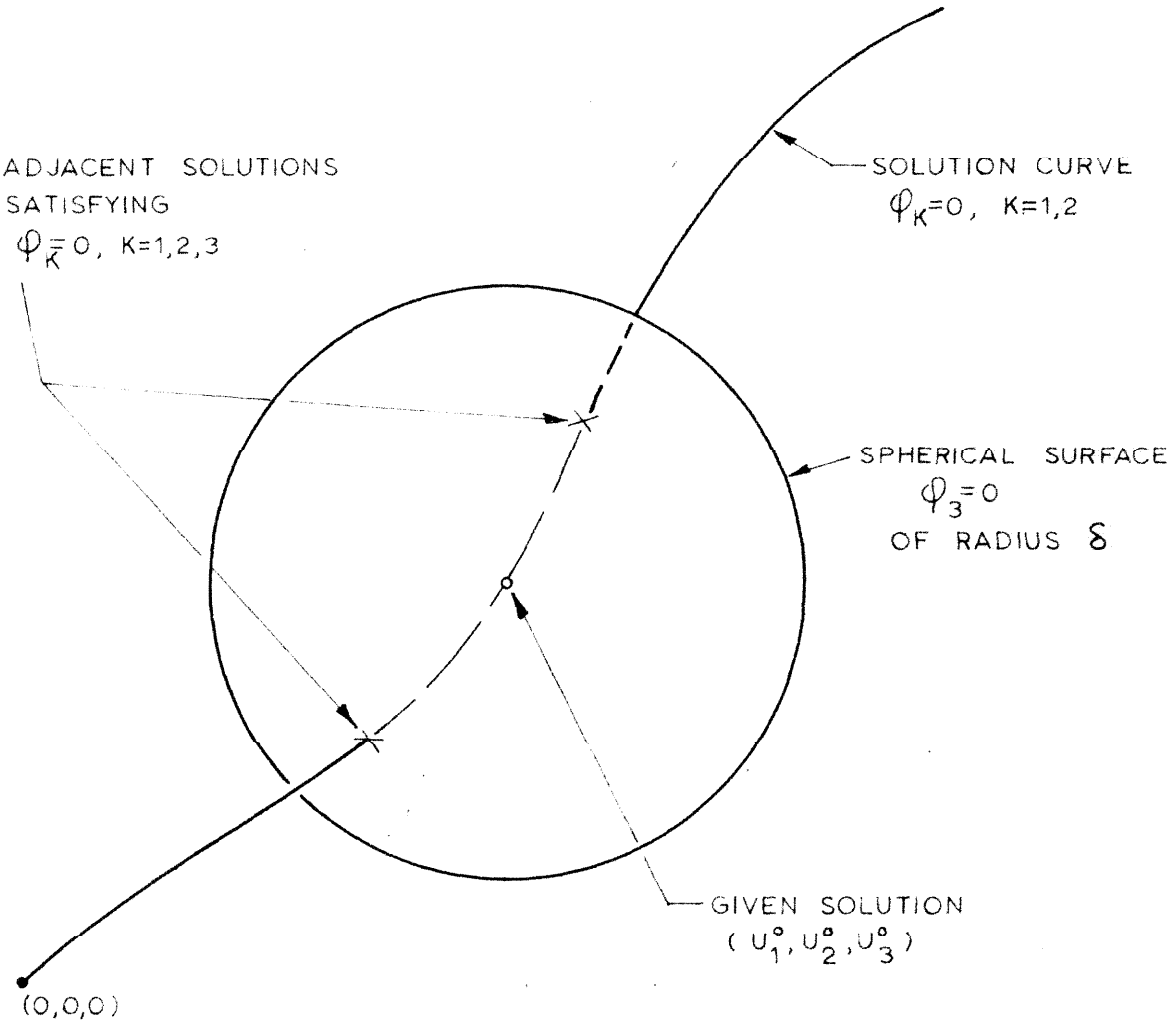

FIGURE 7: EXTENDING THE SOLUTION IN CONFIGURATION SPACE

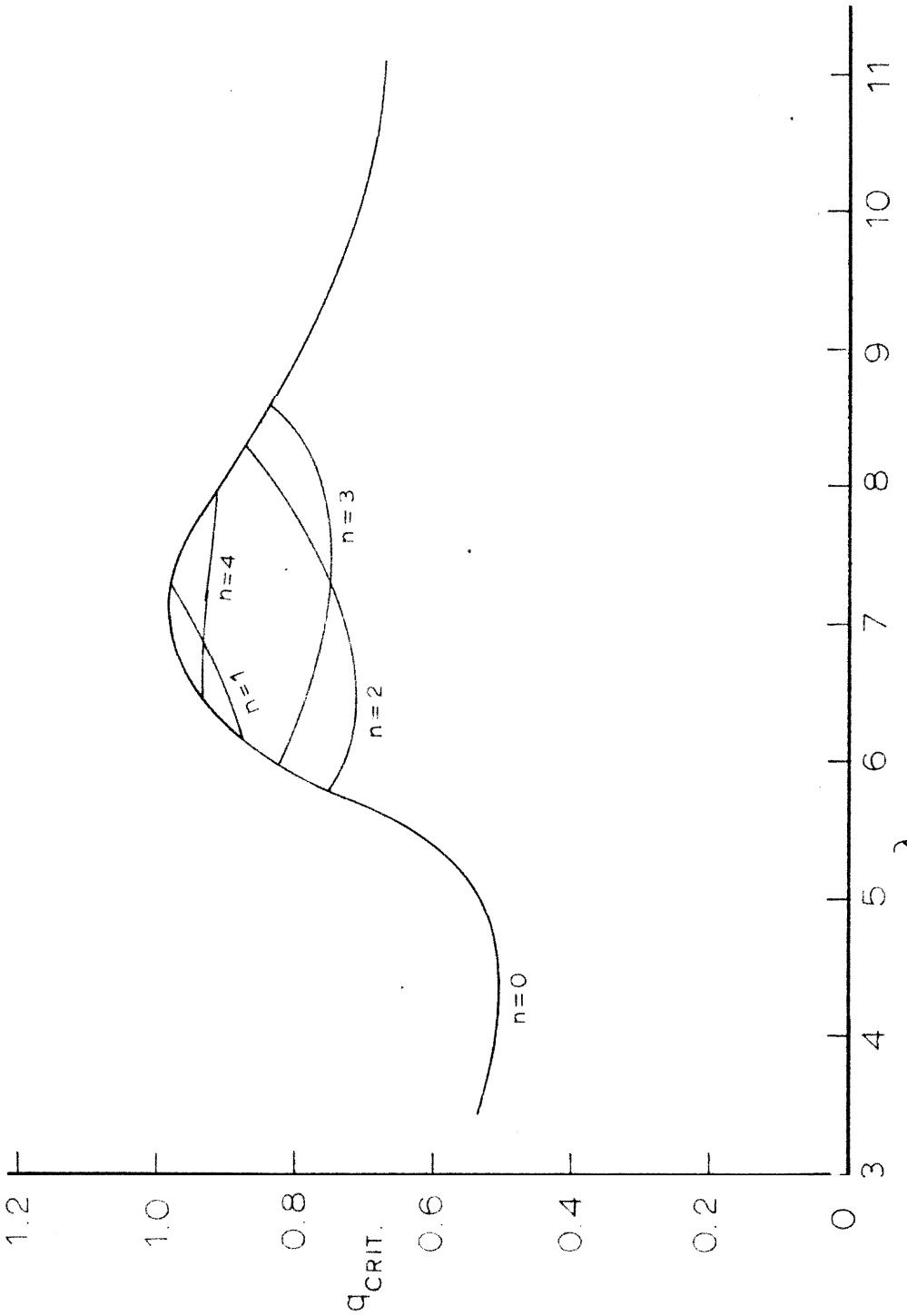

FIGURE 8: THEORETICAL RESULTS, $\nu = 0$

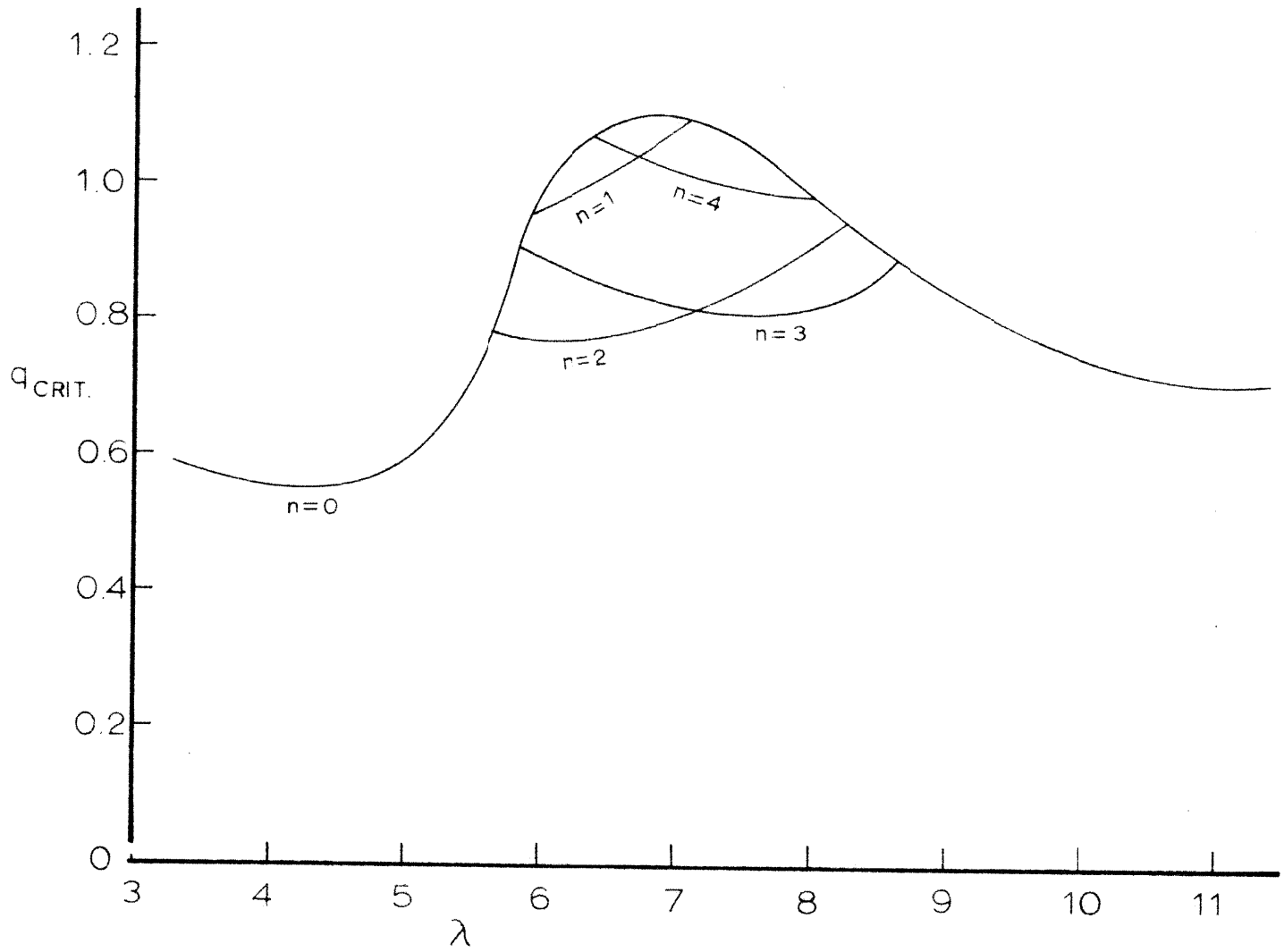

FIGURE 9: THEORETICAL RESULTS, $\nu = 1/4$

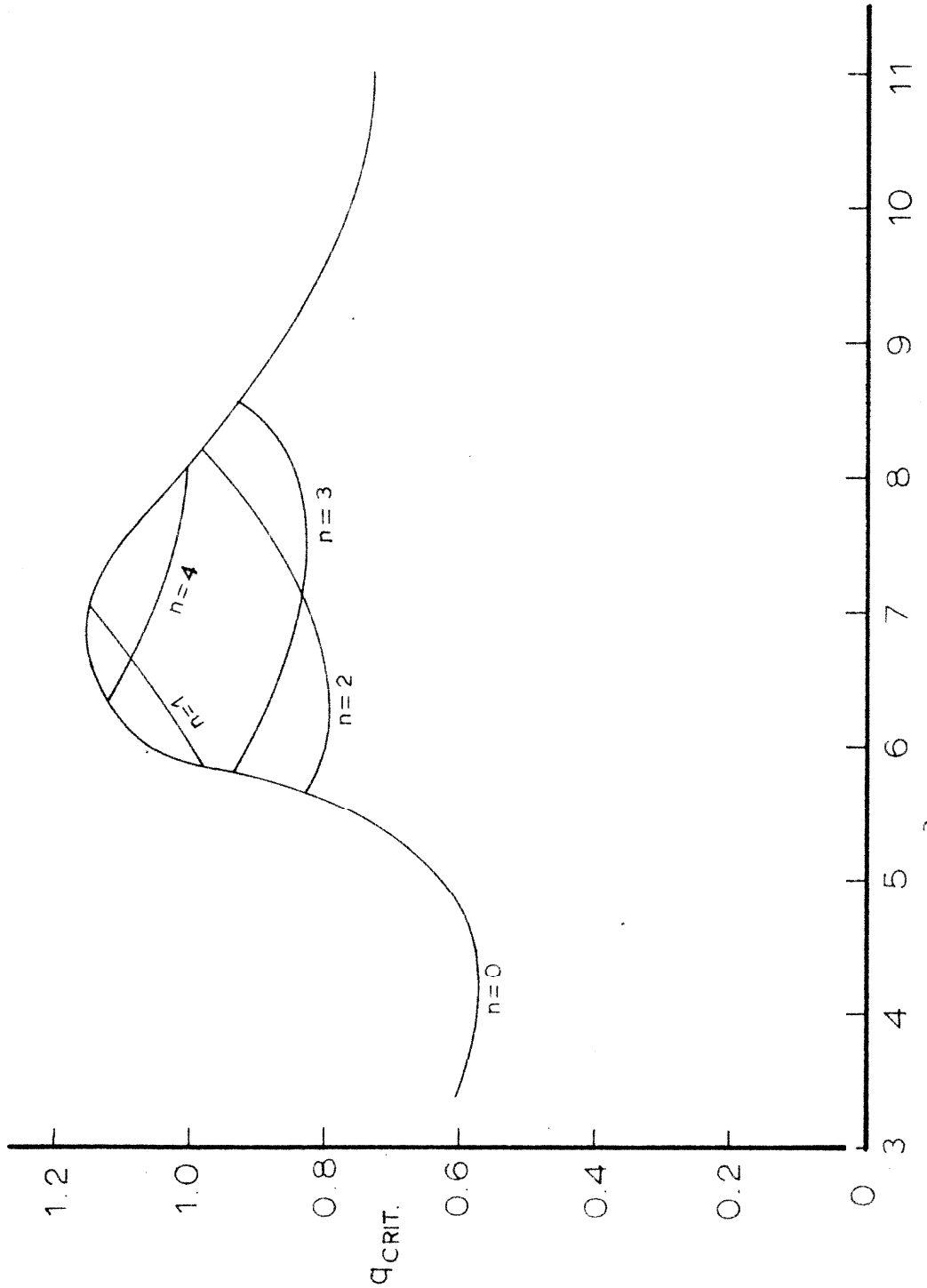

FIGURE 10: THEORETICAL RESULTS, $\nu = 1/3$

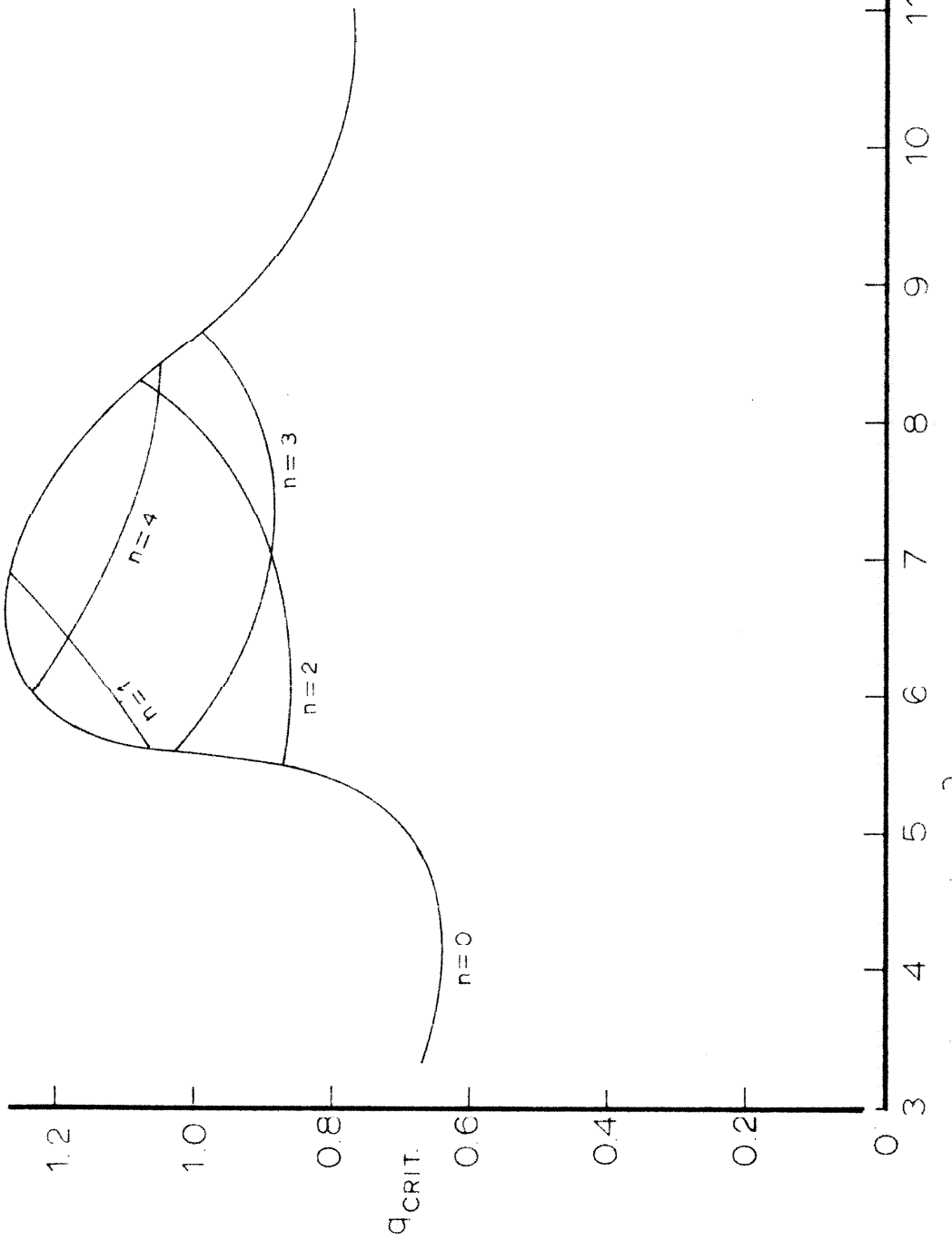

FIGURE 11: THEORETICAL RESULTS, $\nu = 1/2$

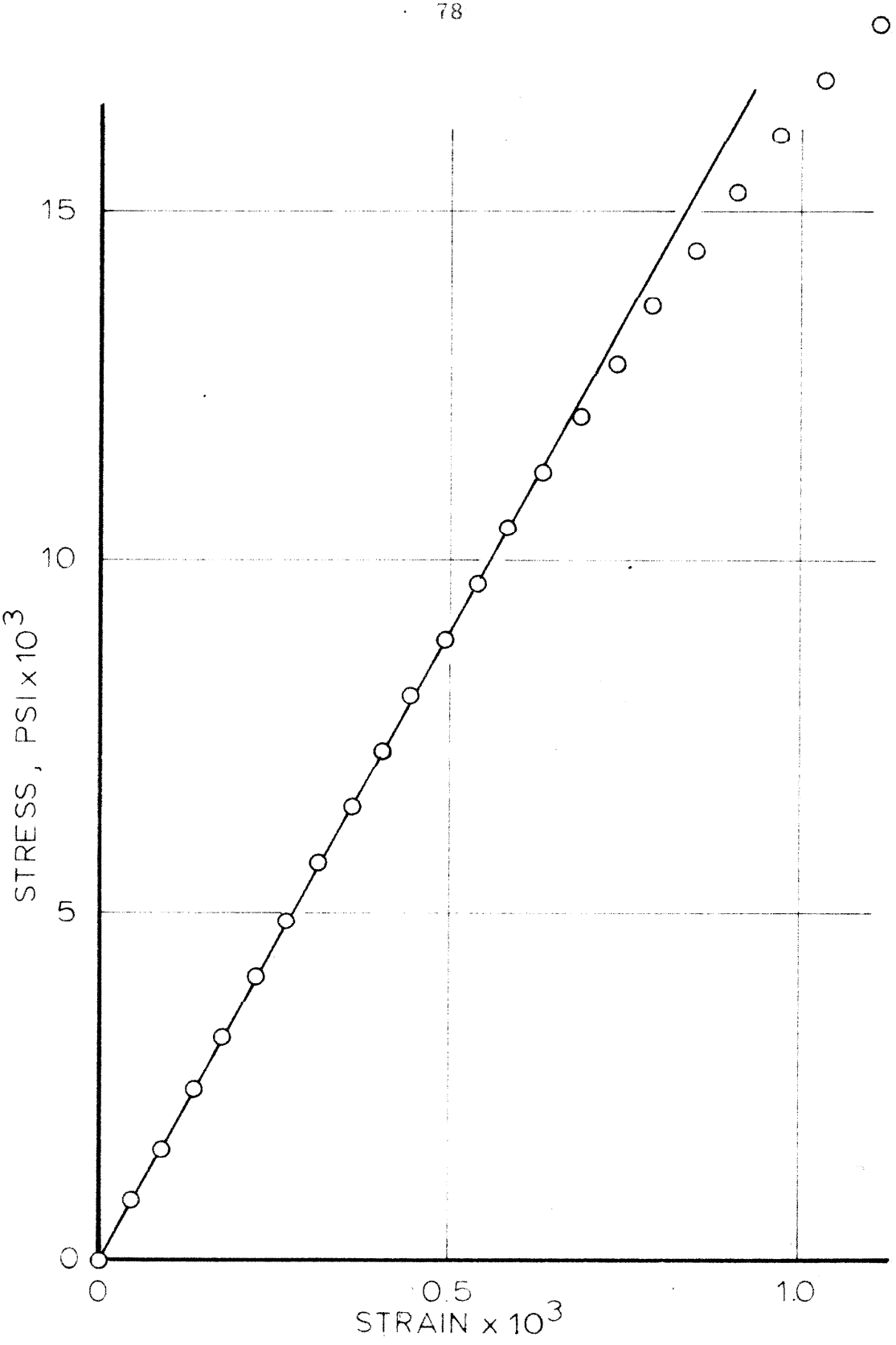

FIGURE 12: TYPICAL STRESS VS. STRAIN FOR PLATED COPPER

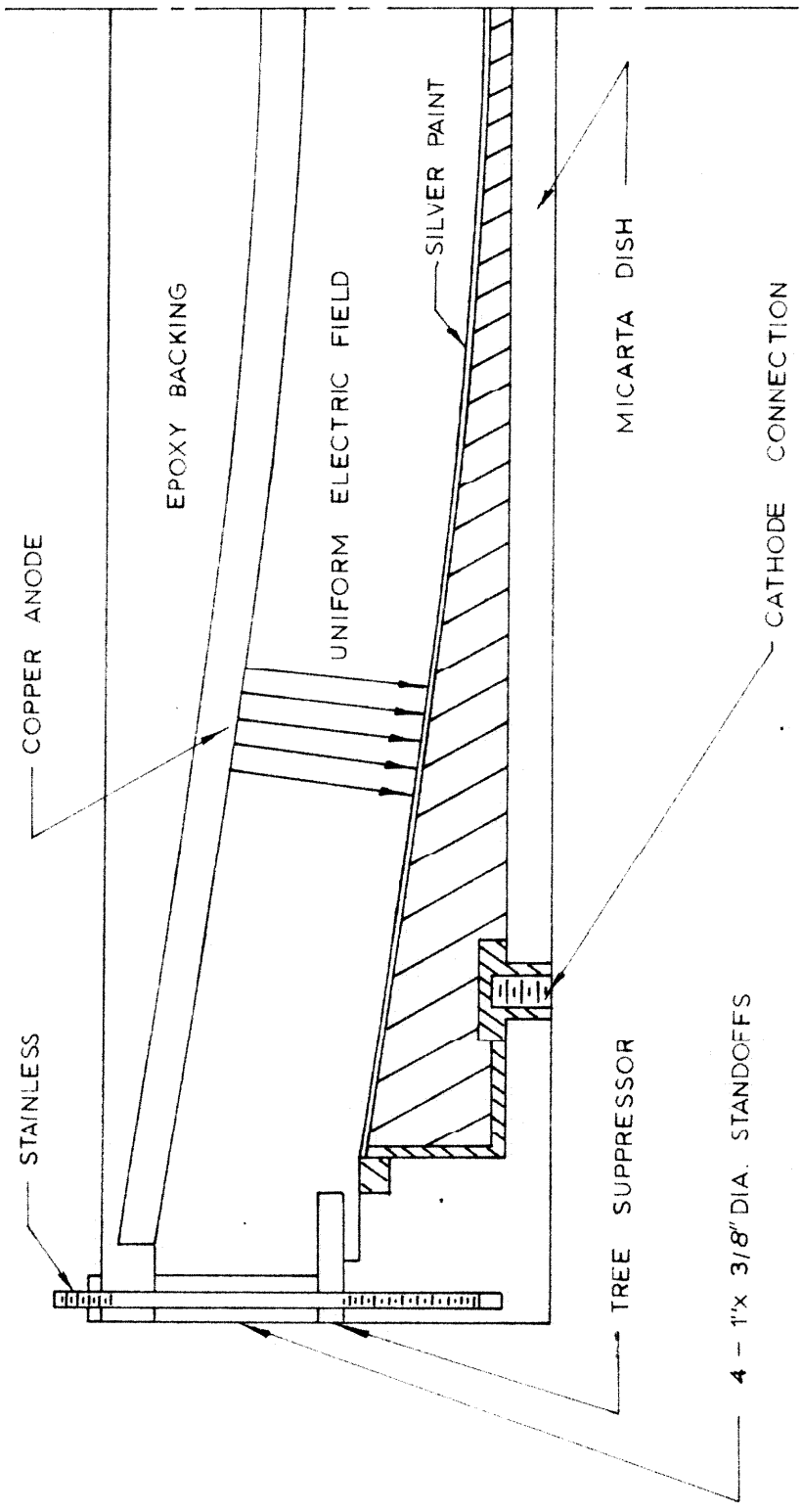

FIGURE 13: DETAIL OF WAX FORM AND ANODE ASSEMBLED FOR PLATING

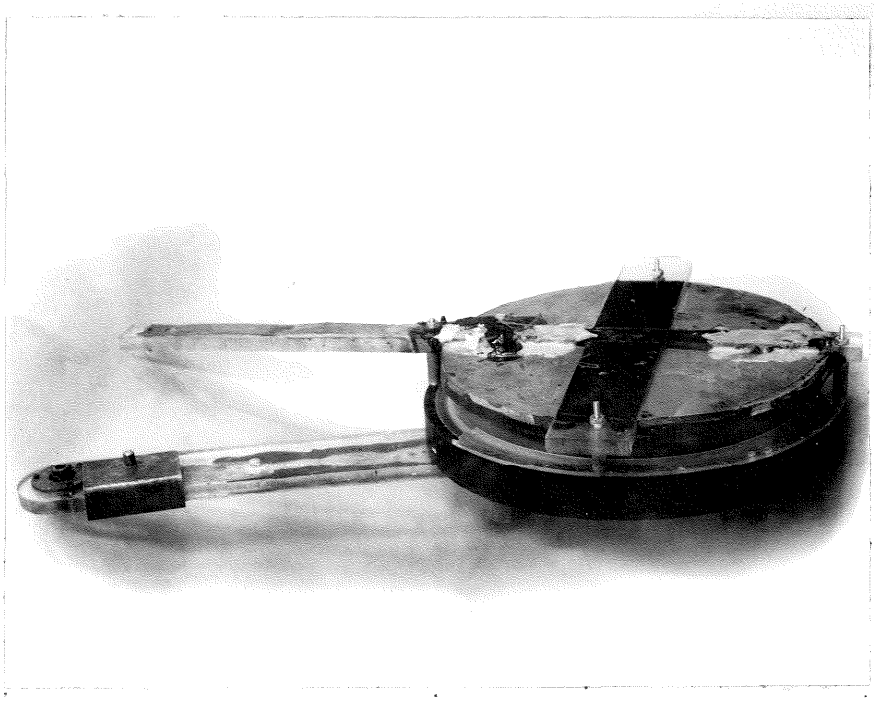

Figure 14: Wax Form and Anode Assembly Ready for Plating

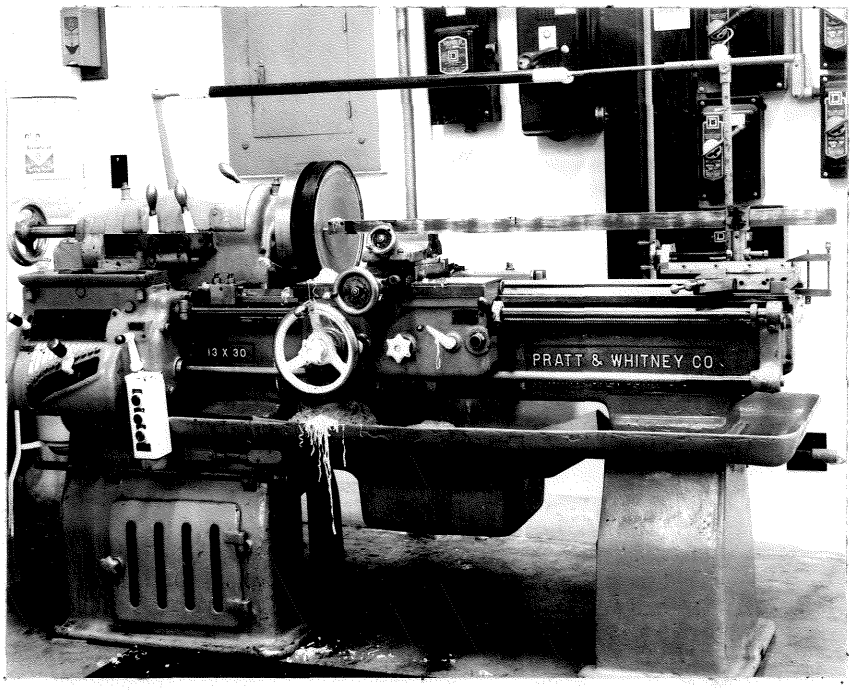

Figure 15: Machining the Wax Form

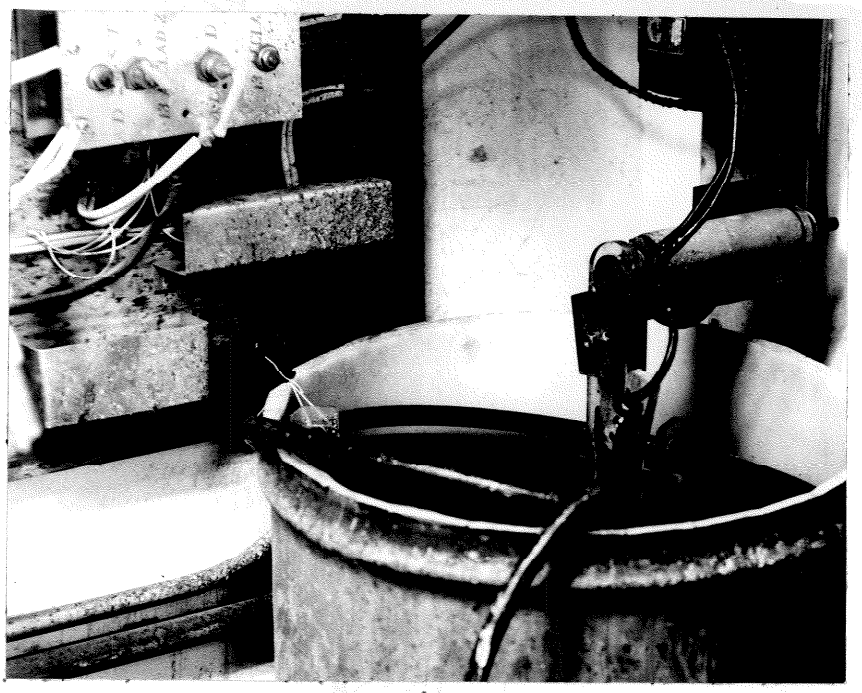

Figure 16: Plating Installation

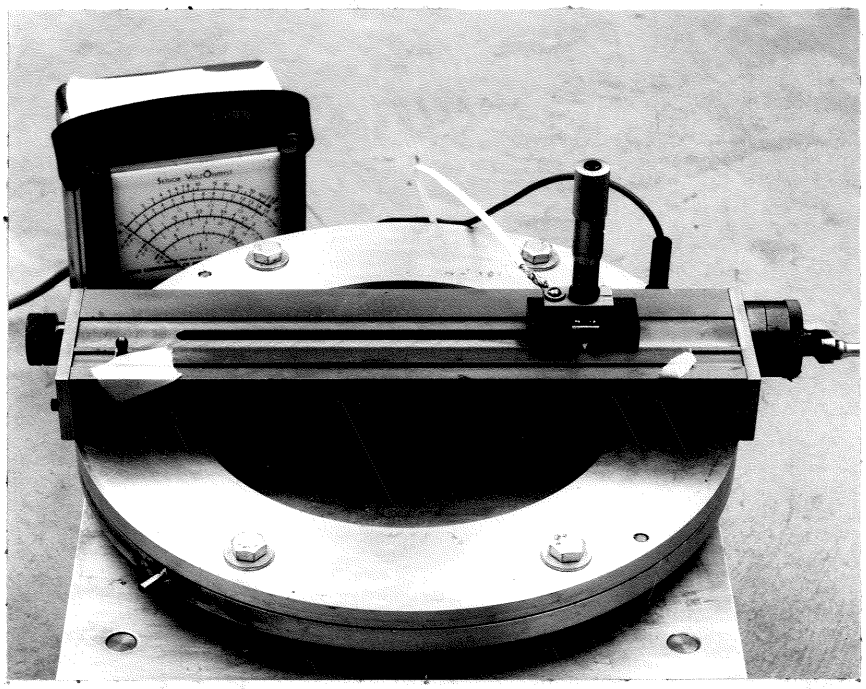

Figure 17: Shell, Mounted in Rings, Ready for Testing

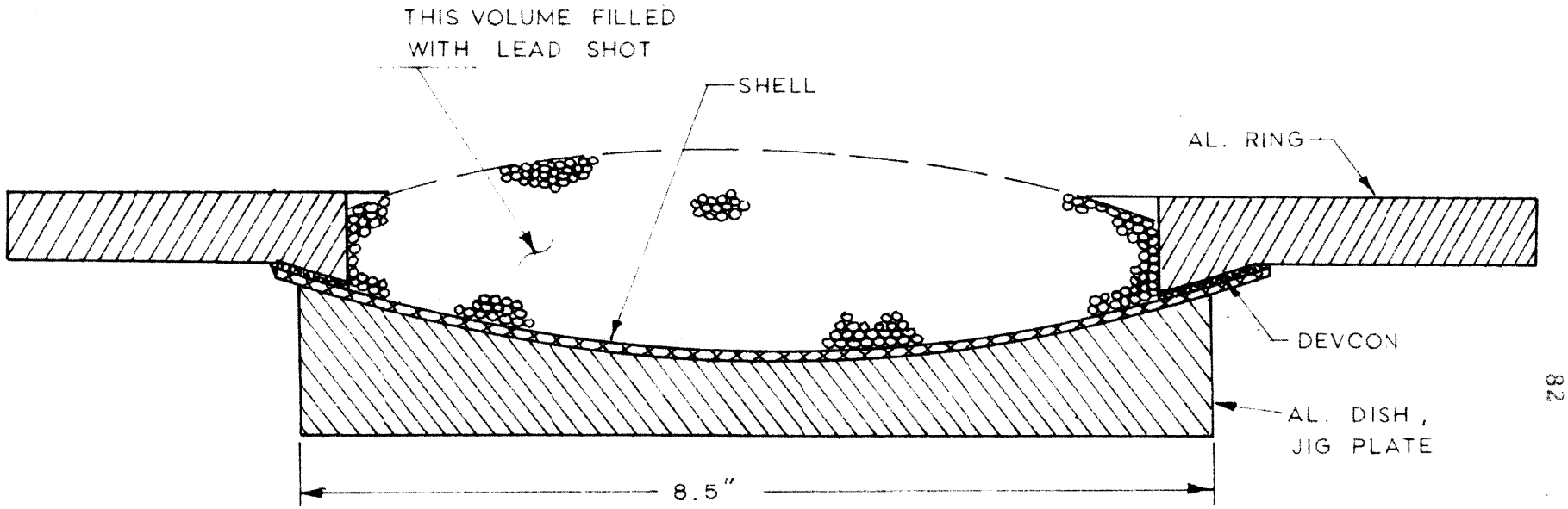

FIGURE 18: DETAIL OF ASSEMBLY OF SHELL AND RING

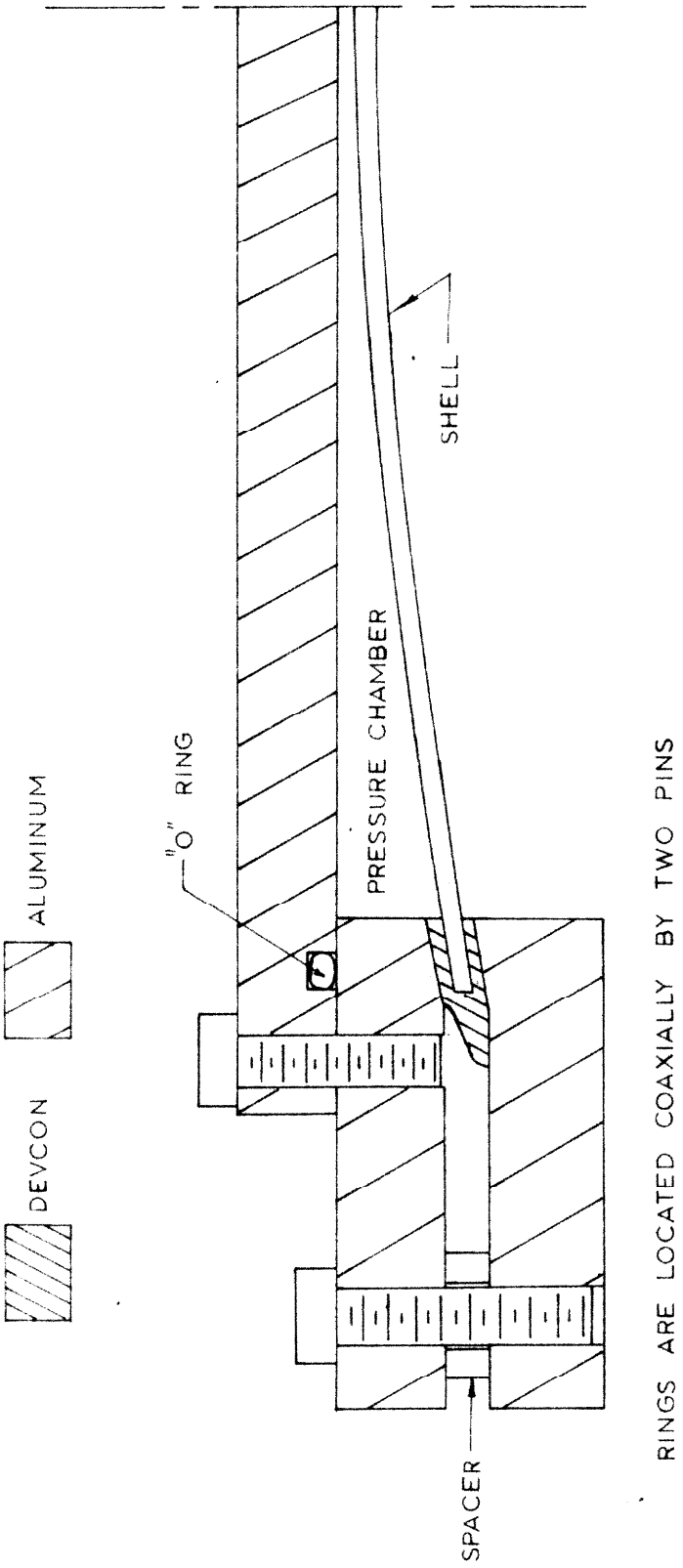

FIGURE 19. DETAIL OF CLAMPING RINGS

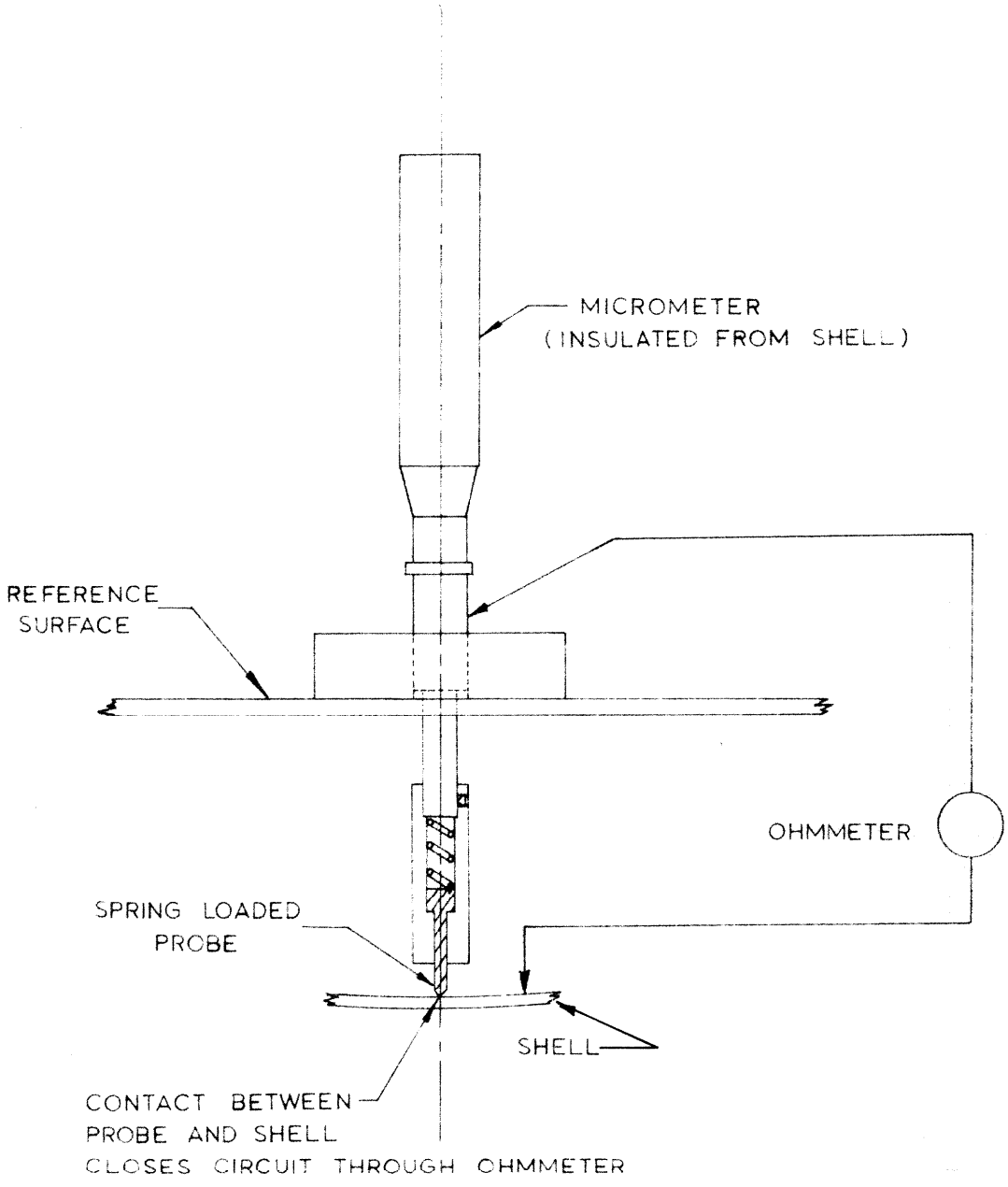

FIGURE 20: DETAIL OF DEFLECTION MEASURING EQUIPMENT

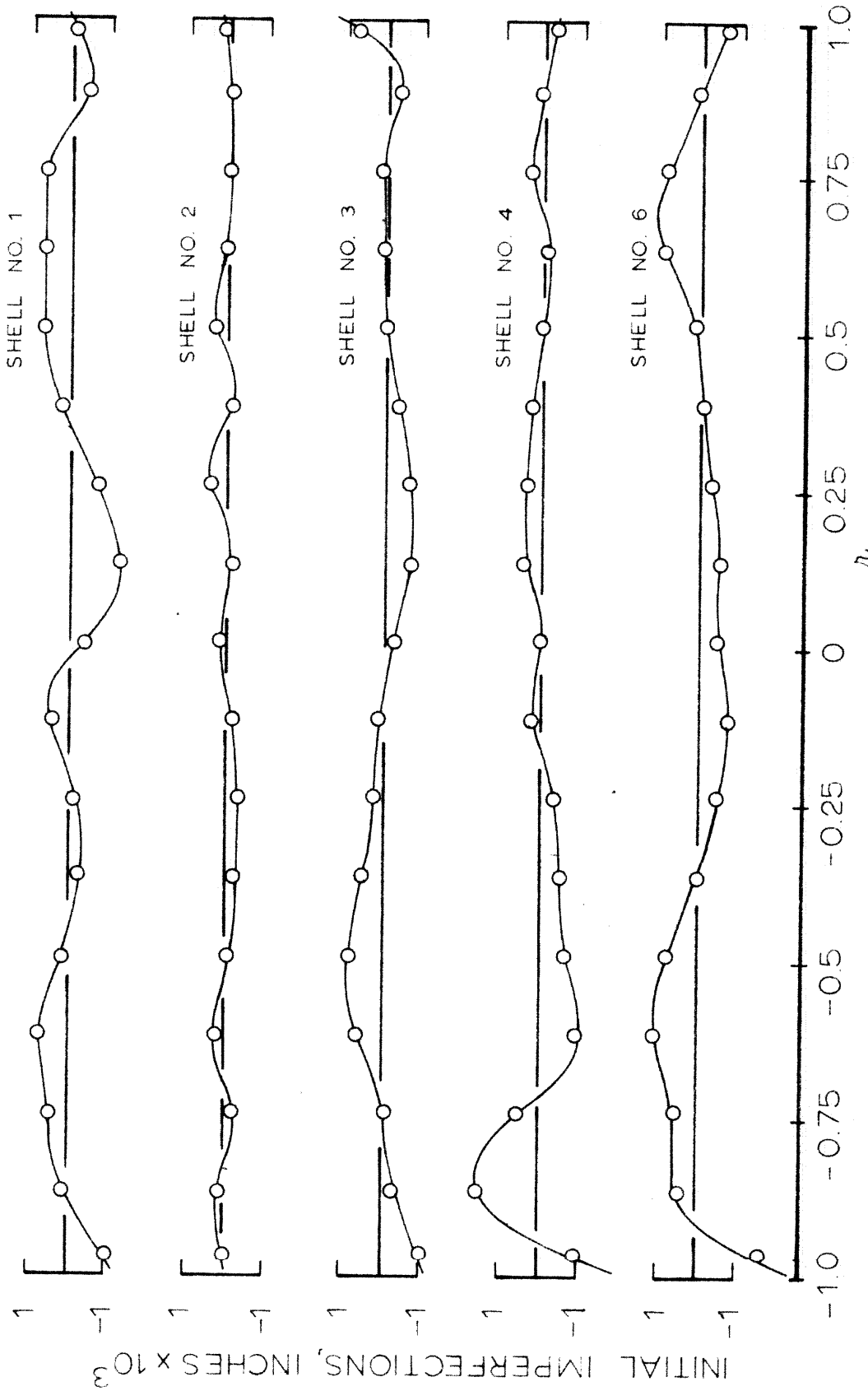

FIGURE 21: INITIAL IMPERFECTIONS

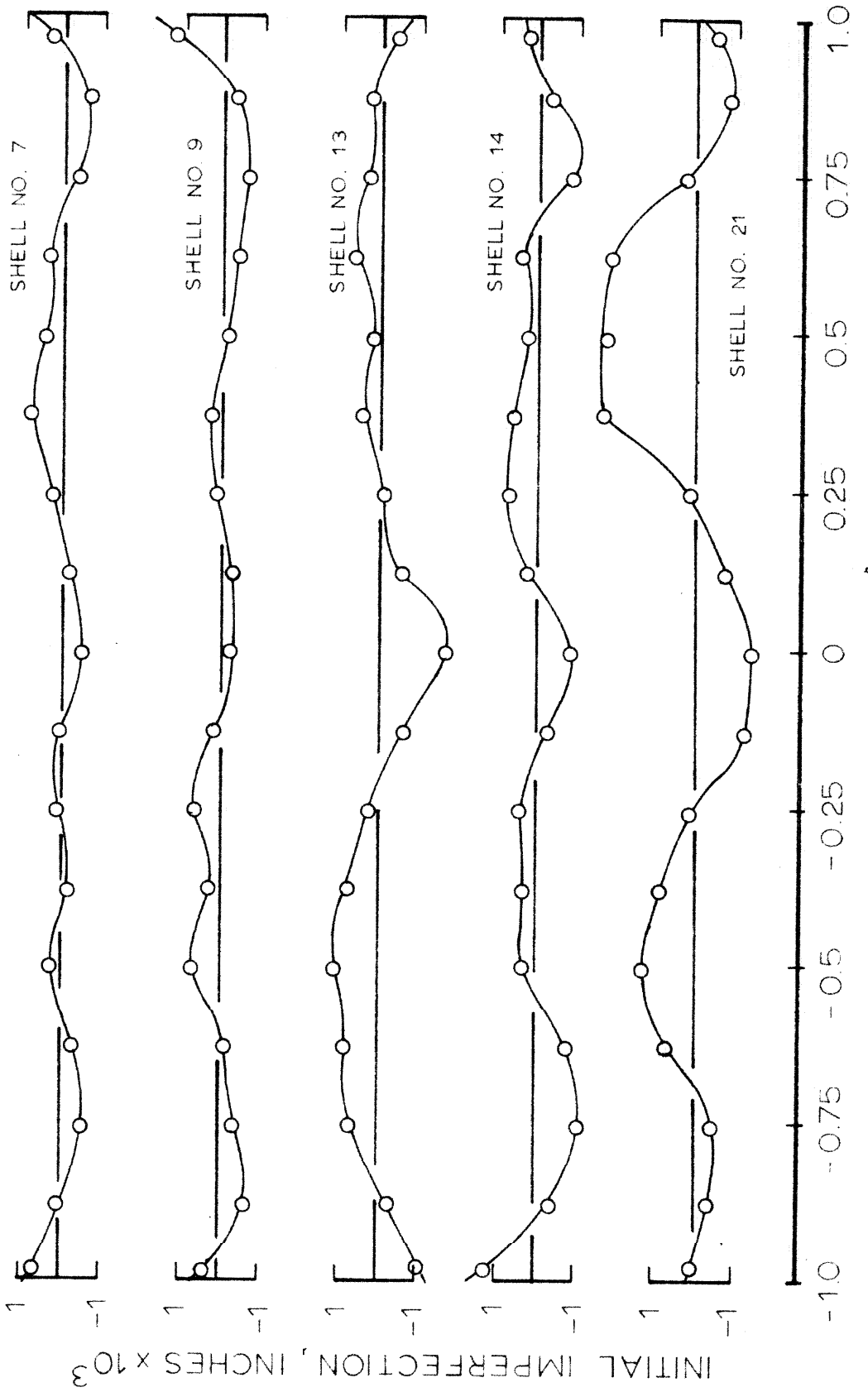

FIGURE 22: INITIAL IMPERFECTIONS

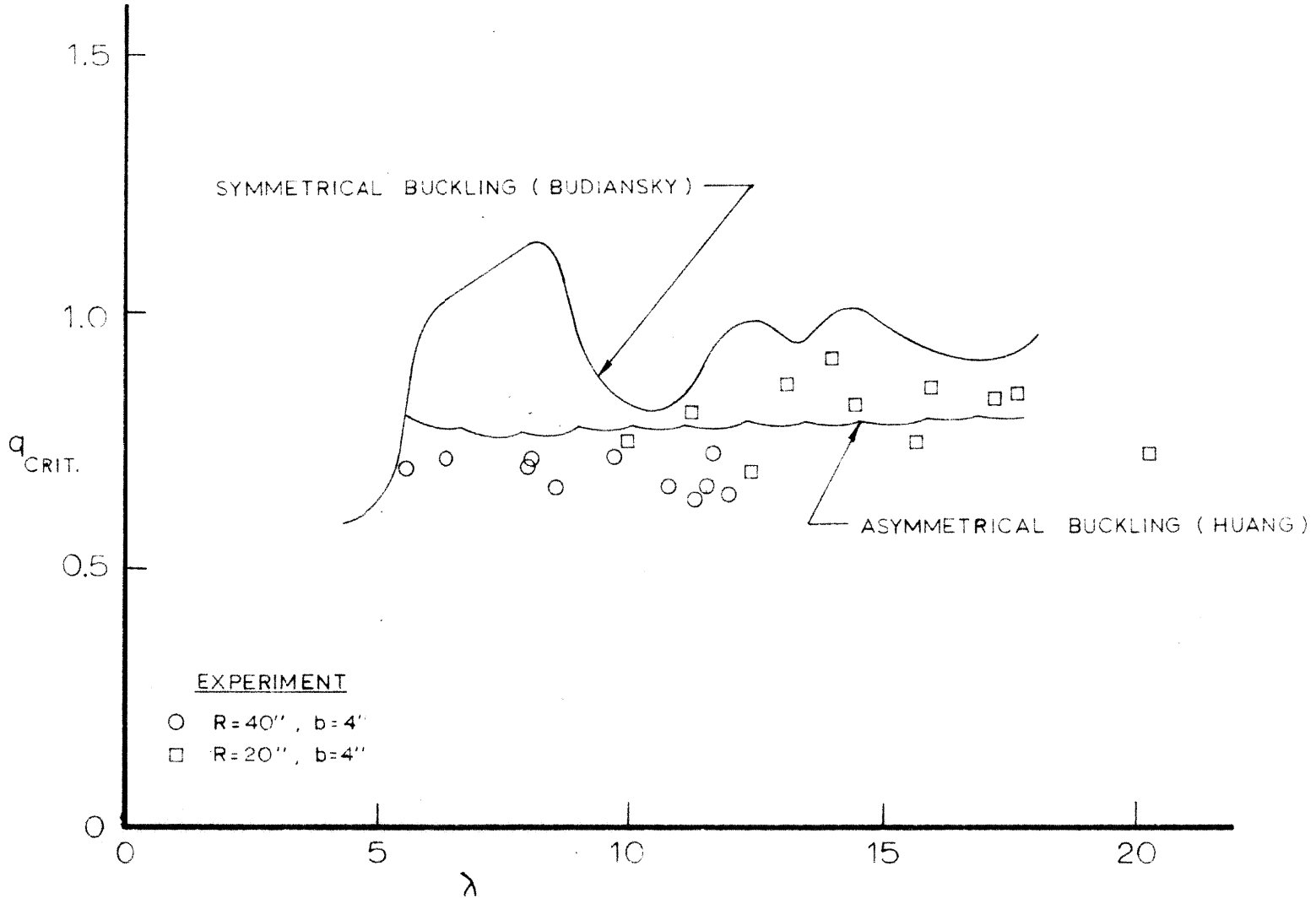

FIGURE 23: SUMMARY OF EXPERIMENTAL RESULTS

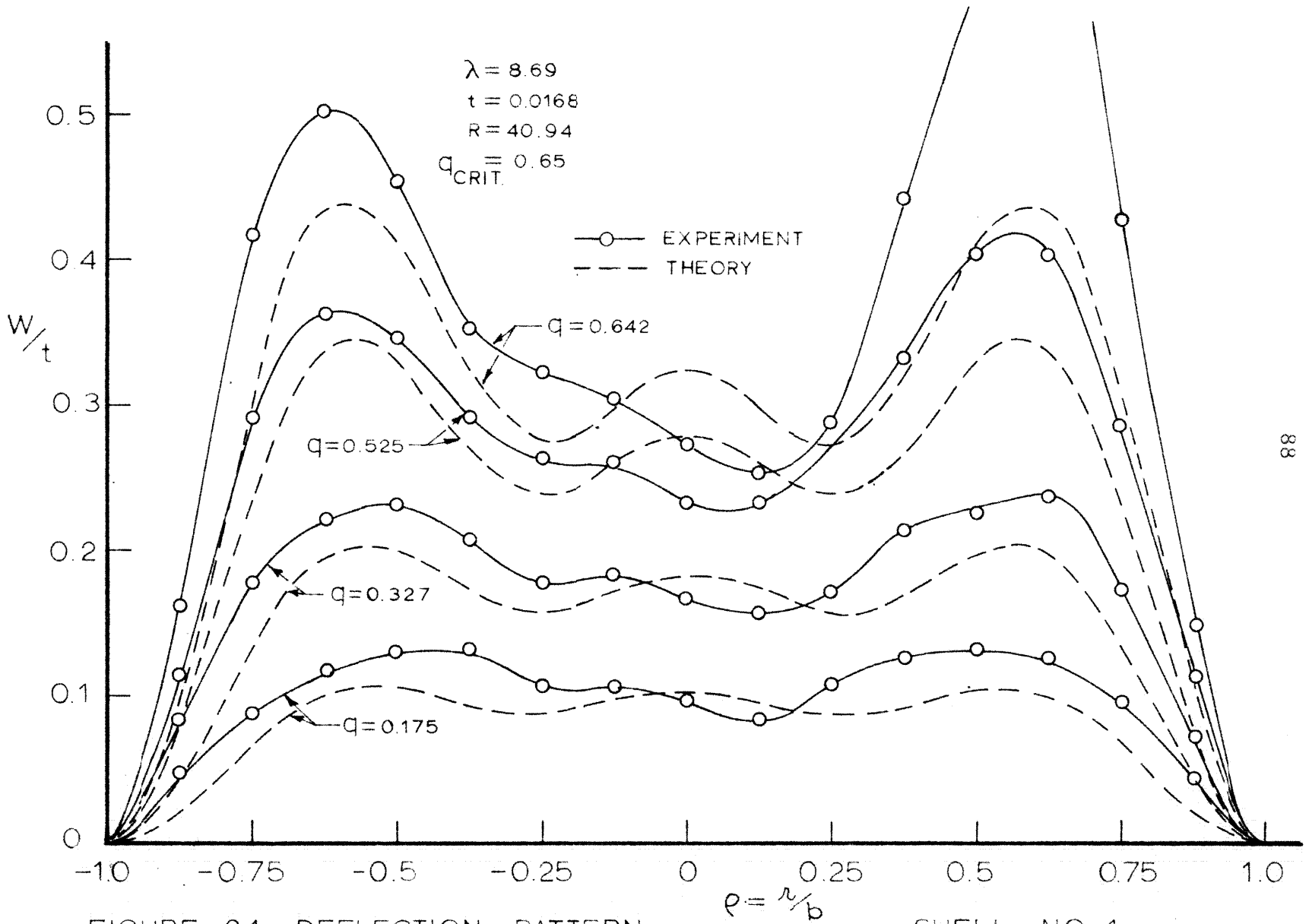

FIGURE 24: DEFLECTION PATTERN, SHELL NO. 1

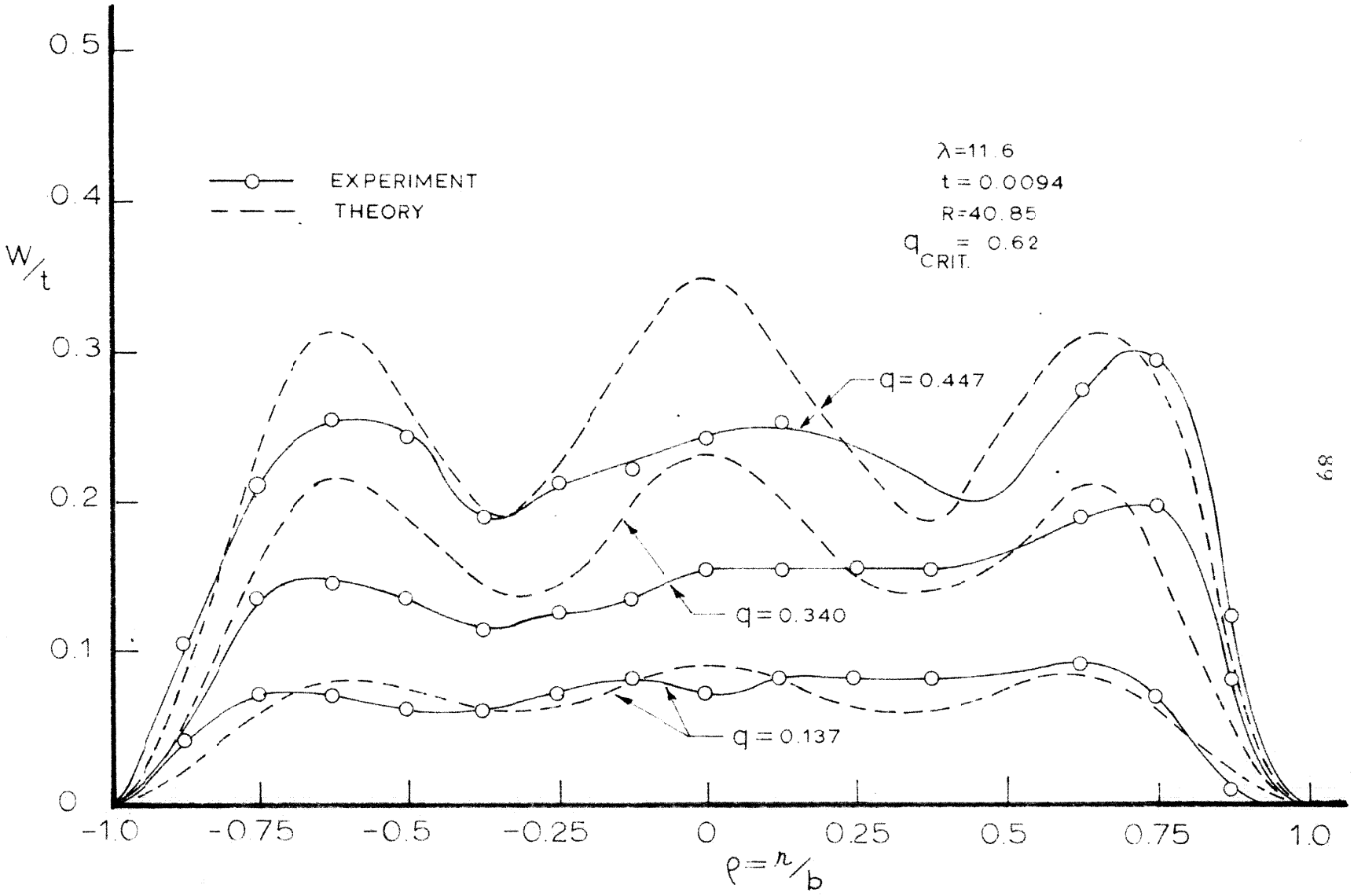

FIGURE 25: DEFLECTION PATTERN, SHELL NO. 2

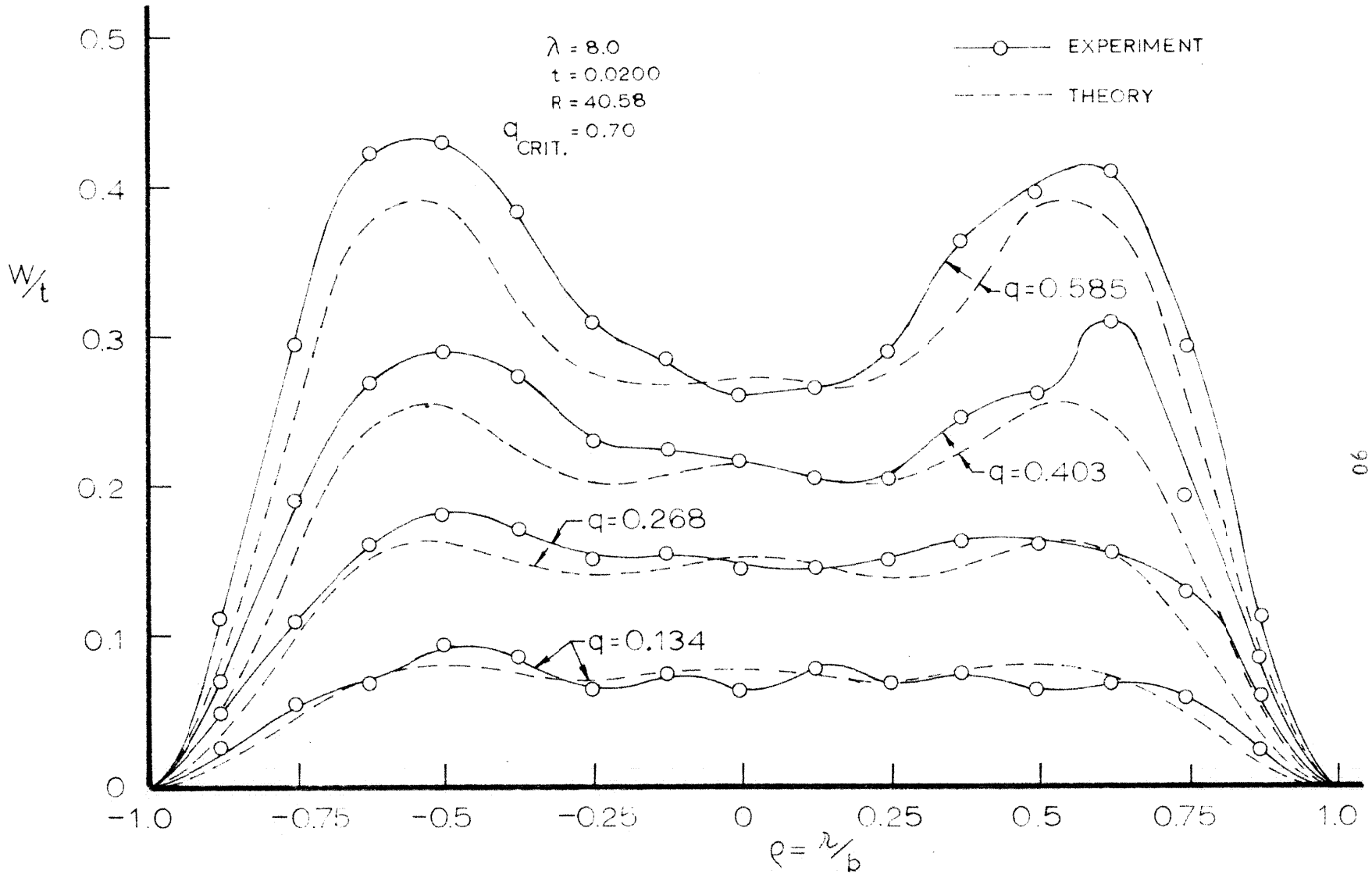

FIGURE 26: DEFLECTION PATTERN, SHELL NO. 3

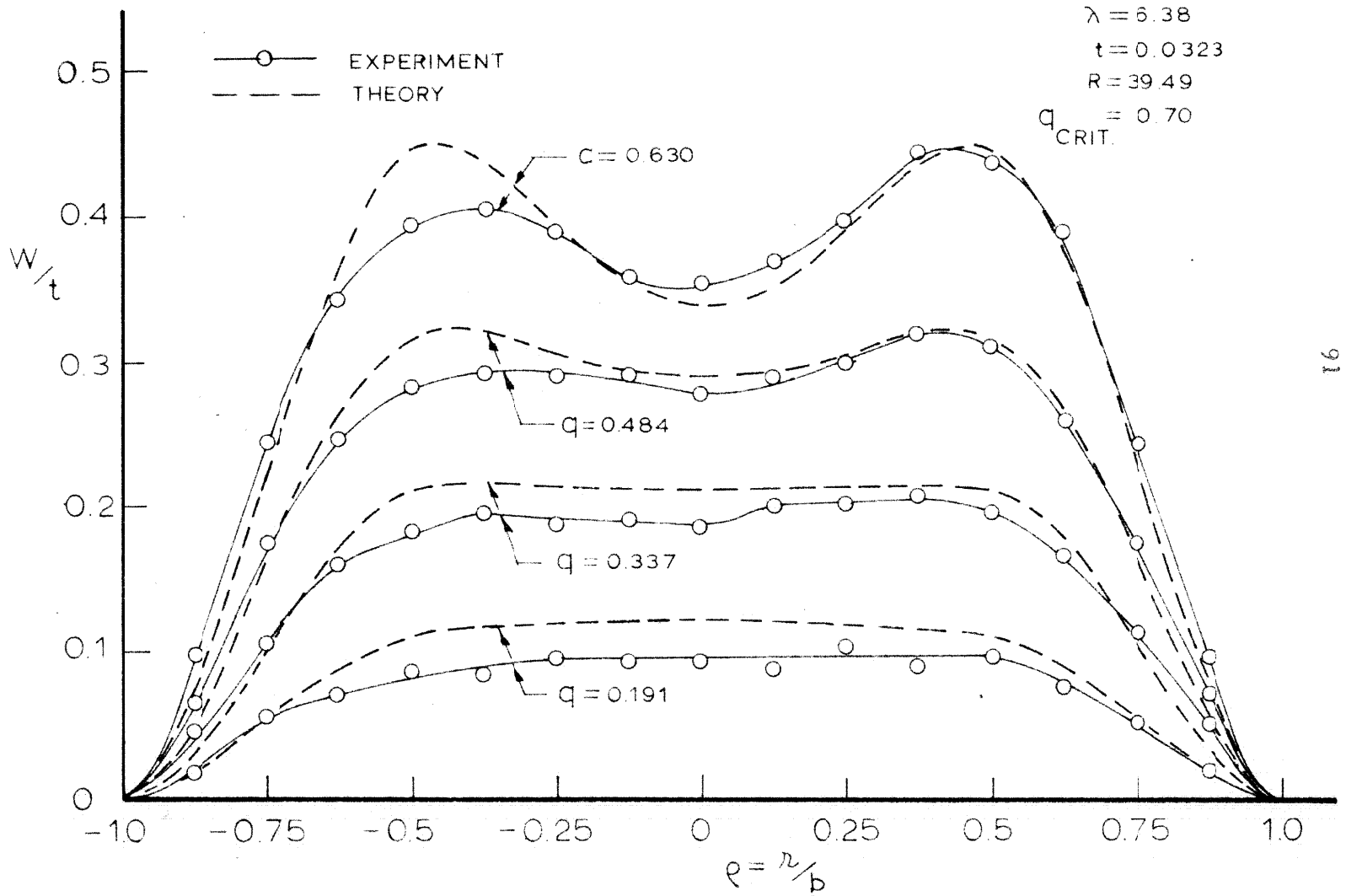

FIGURE 27: DEFLECTION PATTERN, SHELL NO. 4

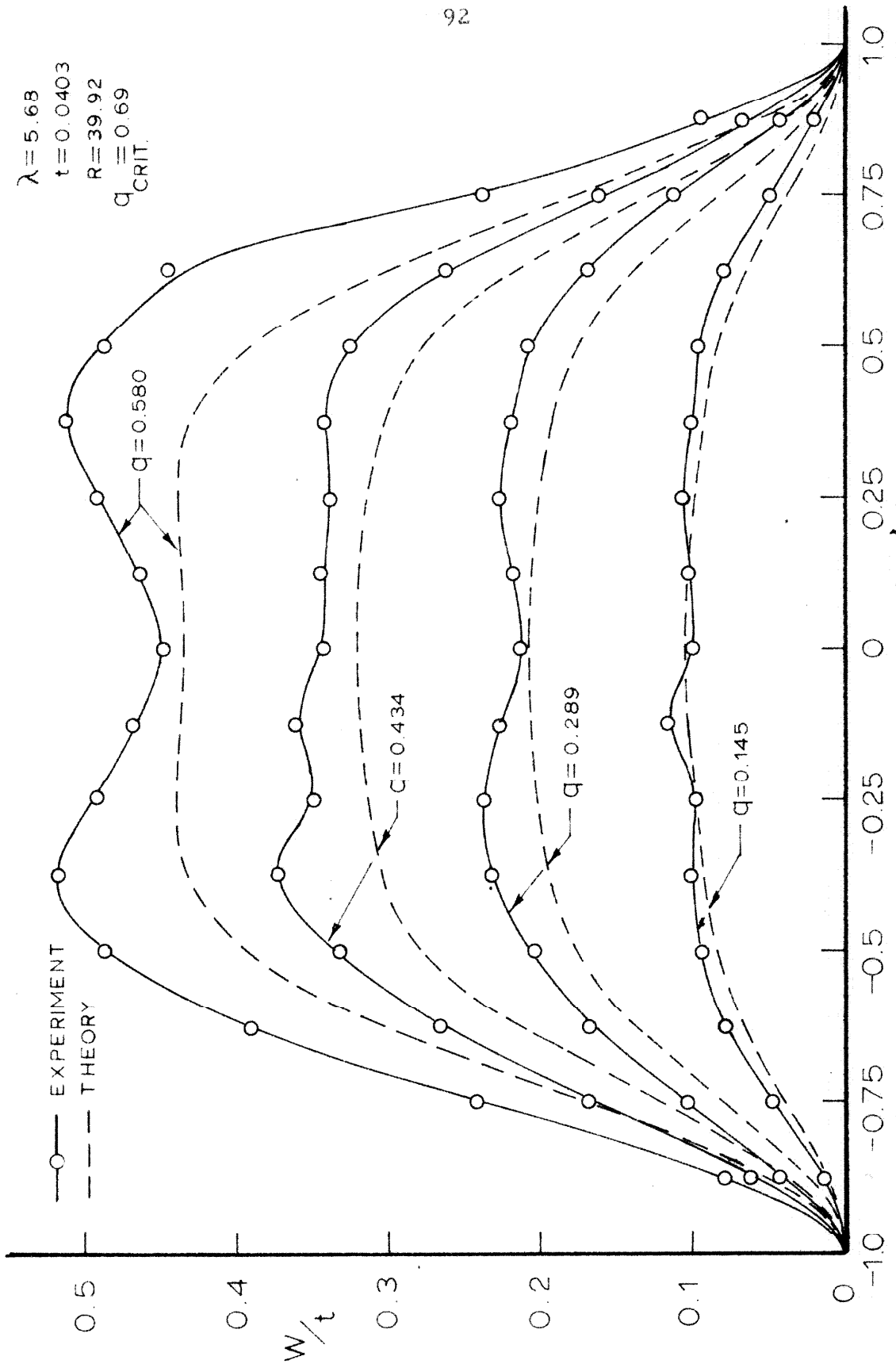

FIGURE 28: DEFLECTION PATTERN, SHELL NO. 6

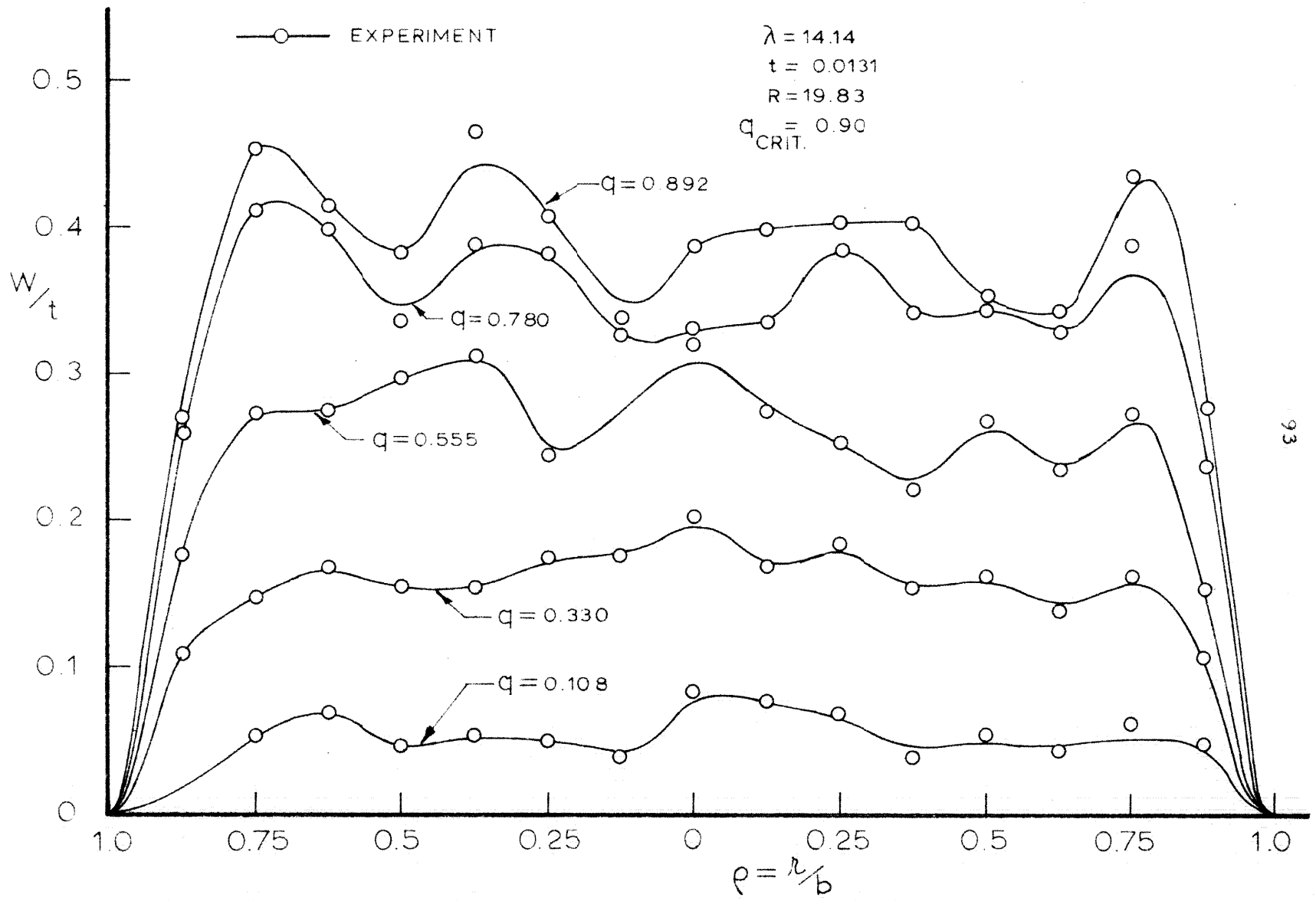

FIGURE 29: DEFLECTION PATTERN, SHELL NO. 7

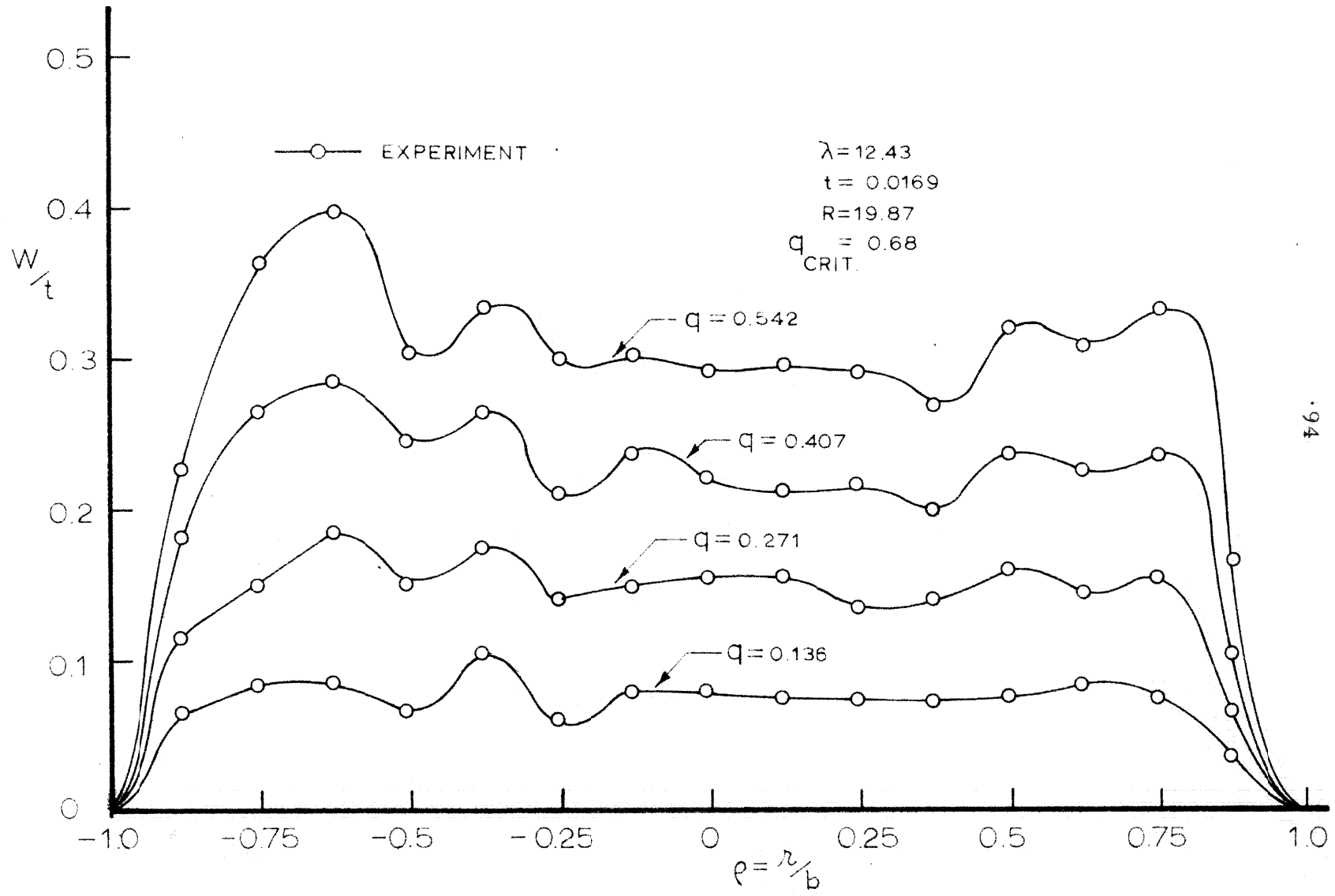

FIGURE 30: DEFLECTION PATTERN, SHELL NO. 9

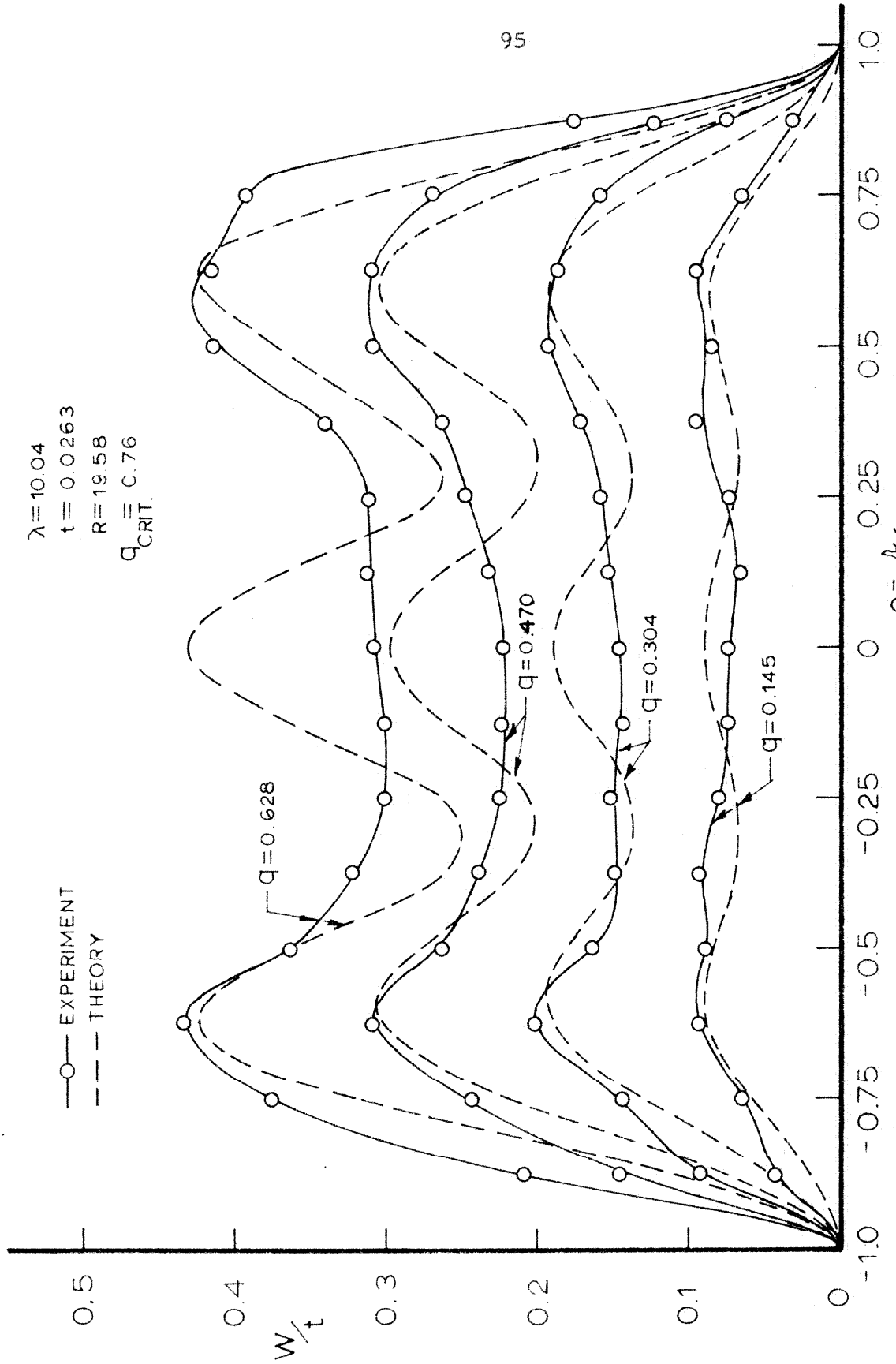

FIGURE 31: DEFLECTION PATTERN, SHELL NO. 13

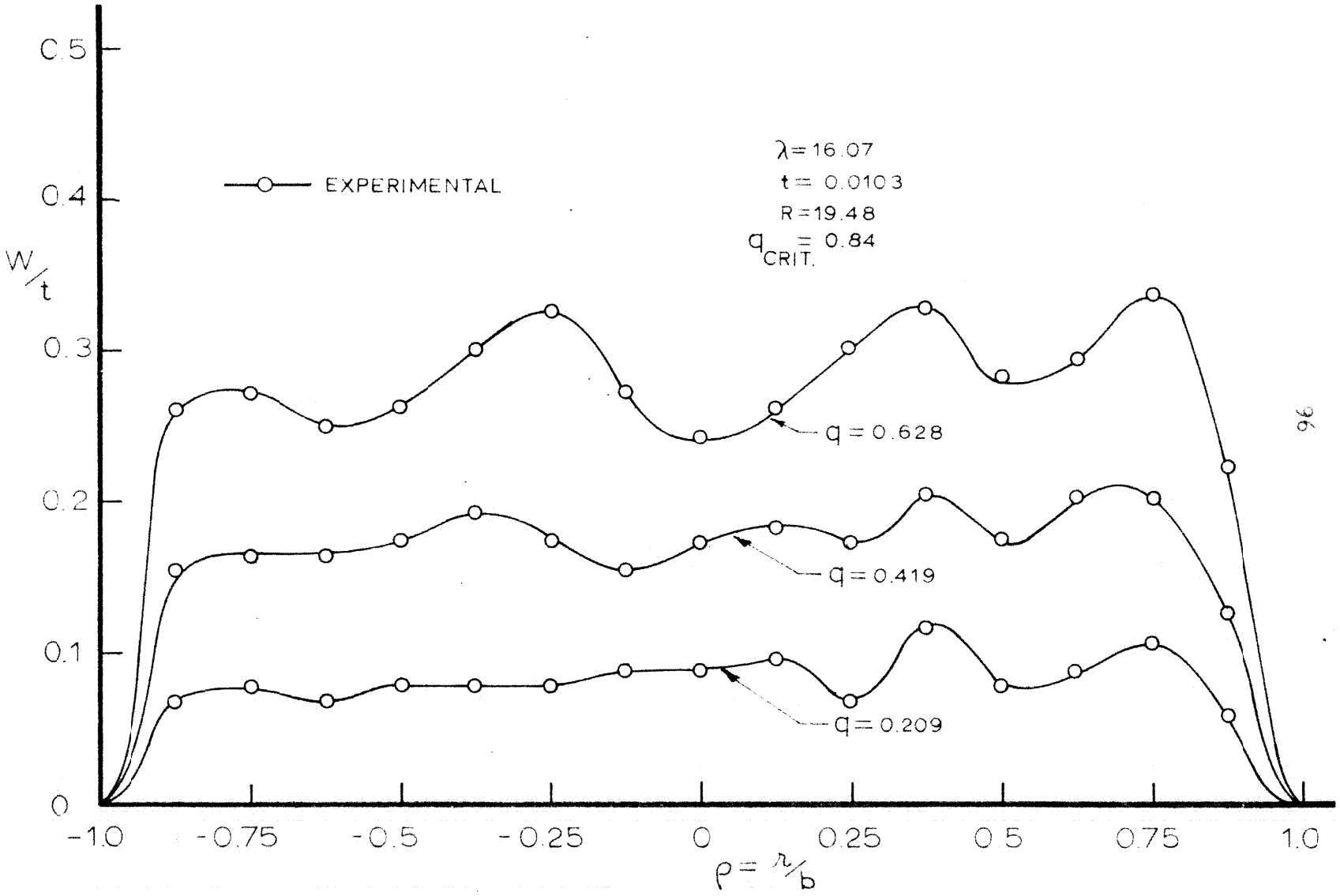

FIGURE 32 : DEFLECTION PATTERN, SHELL NO. 14

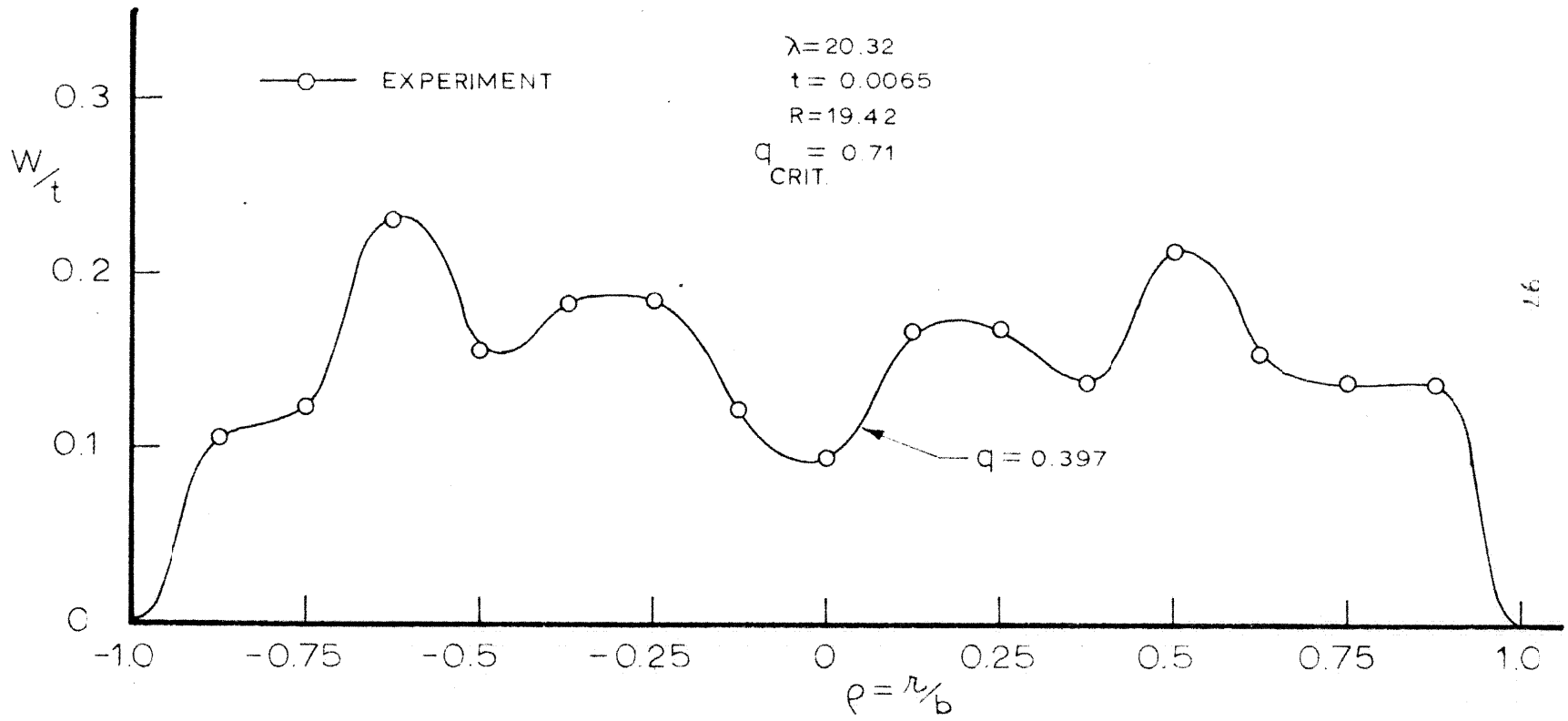

FIGURE 33: DEFLECTION PATTERN, SHELL NO. 17